RESEARCH ARTICLE SUMMARY

COSMOCHEMISTRY

Macromolecular organic matter in samples of the asteroid (162173) Ryugu

Hikaru Yabuta* ***et al.***

INTRODUCTION: Organic compounds in asteroids and comets contain information about the early history of the Solar System. They could also have delivered organic material to early Earth. The Hayabusa2 spacecraft visited the carbonaceous asteroid Ryugu and collected samples of its surface materials, which were brought to Earth in December 2020.

RATIONALE: We investigated the macromolecular organic matter in the Ryugu samples, measuring its elemental, isotopic, and functional group compositions along with its small-scale structures and morphologies. Analytical methods used included spectro-microscopies, electron microscopy, and isotopic microscopy. We examined intact Ryugu grains and insoluble carbonaceous residues isolated by acid treatment of the Ryugu samples.

RESULTS: Organic matter is abundant in the Ryugu grains, distributed as submicrometer-sized organic grains and as organic matter dispersed in matrix. The Ryugu organic matter consists of aromatic carbons, aliphatic carbons, ketones, and carboxyls. The functional group compositions are consistent with those of insoluble organic matter (IOM) from primitive carbonaceous CI (Ivuna-type) and CM (Mighei-type) chondritic meteorites. Those meteorites experienced aqueous alteration (reactions with liquid water) on their parent bodies, which implies that the Ryugu organic material was also modified by aqueous alteration on the asteroid parent body.

The functional group distributions of the Ryugu organic matter vary on submicrometer scales in ways that relate to the morphologies: nanoparticulate and/or nanoglobular regions are aromatic-rich, whereas organic matter associated with Mg-rich phyllosilicate matrix and carbonates is IOM-like or occurs as diffuse carbon. The observed macromolecular diversity provides further evidence that the organics were modified by aqueous alteration on Ryugu's parent body. The diffuse carbon is similar to clay-bound organic matter that occurs in CI chondrites and the ungrouped C2-type meteorite Tagish Lake. No graphite-like material was found, which indicates that the Ryugu organic matter was not subjected to heating events on the parent body.

The bulk hydrogen and nitrogen isotopic ratios of the Ryugu grains are between the bulk values of CI chondrites and the IOM in CI chondrites. Some carbonaceous grains showed extreme deuterium (D) and/or nitrogen-15 (^{15}N) enrichments or depletions. These indicate an origin in the interstellar medium or presolar nebula. The bulk hydrogen isotopic ratios of insoluble carbonaceous residues from the Ryugu samples are lower than those in CI and CM chondrites. The range of D enrichments are consistent with the ranges of CI, CM, and Tagish Lake chondrites. The nitrogen isotopic ratios of the IOM from Ryugu samples were close to those in CI chondrites.

CONCLUSION: The organic matter in Ryugu probably consists of primordial materials that formed during (or before) the early stages of the Solar System's formation, which were later modified by heterogeneous aqueous alteration on Ryugu's parent body asteroid. Although the surface of Ryugu is exposed to solar wind, impacts, and heating by sunlight, the macromolecular organics in the surface grains of Ryugu are similar in their chemical, isotopic, and morphological compositions to those seen in primitive carbonaceous chondrites. The properties of Ryugu's organic matter could explain the low albedo of the asteroid's surface. ■

The complete list of authors and their affiliations is available in the full article online.
*Corresponding author. Email: hyabuta@hiroshima-u.ac.jp
Cite this article as H. Yabuta *et al.*, *Science* **379**, eabn9057 (2023). DOI: 10.1126/science.abn9057

READ THE FULL ARTICLE AT https://doi.org/10.1126/science.abn9057

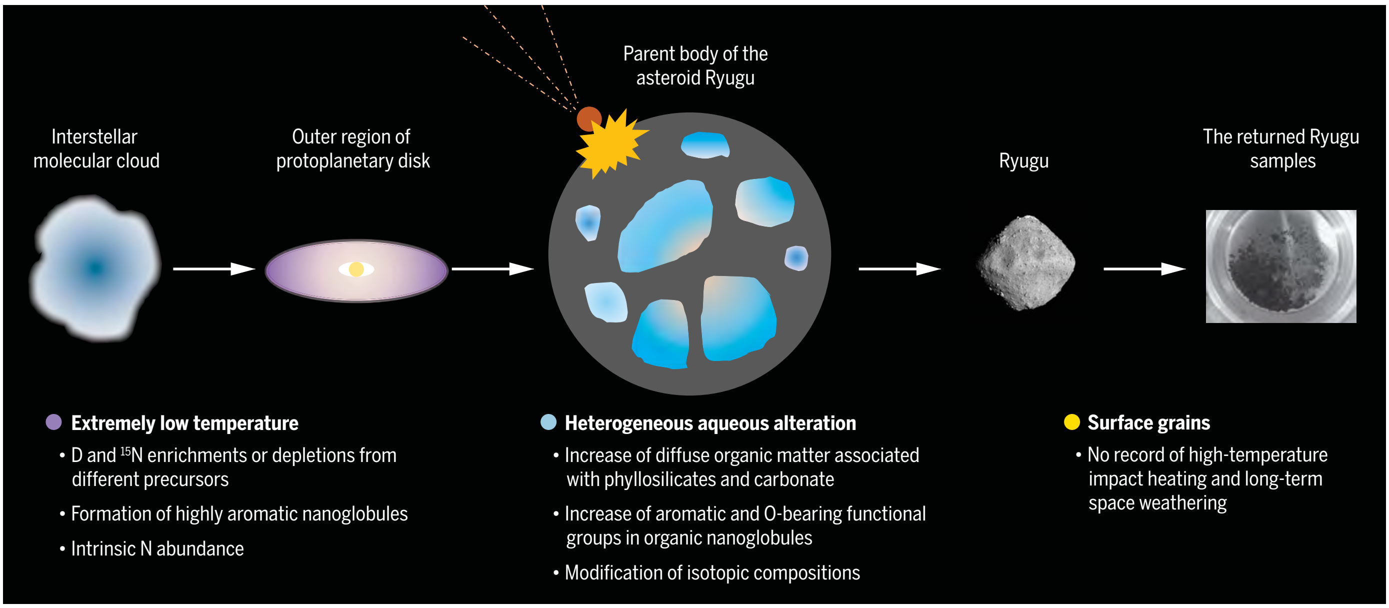

Chemical evolution of macromolecular organic matter in samples of asteroid Ryugu. Organic matter formed in the interstellar medium or in the outer region of the protoplanetary disk that formed the Solar System. It was then incorporated into a planetesimal—Ryugu's parent body—where it experienced varying degrees of reactions with liquid water. An impact ejected material from the parent body, which reassembled to form Ryugu. Samples were brought to Earth by Hayabusa2.

CREDIT: HIROSHIMA UNIVERSITY, JAXA, UNIVERSITY OF TOKYO, KOCHI UNIVERSITY, RI

RESEARCH ARTICLE

COSMOCHEMISTRY

Macromolecular organic matter in samples of the asteroid (162173) Ryugu

Hikaru Yabuta[1]*†, George D. Cody[2], Cécile Engrand[3], Yoko Kebukawa[4], Bradley De Gregorio[5], Lydie Bonal[6], Laurent Remusat[7], Rhonda Stroud[5]‡, Eric Quirico[6], Larry Nittler[2]§, Minako Hashiguchi[8], Mutsumi Komatsu[9,10], Taiga Okumura[11], Jérémie Mathurin[12], Emmanuel Dartois[13], Jean Duprat[7], Yoshio Takahashi[11,14], Yasuo Takeichi[14], David Kilcoyne[15]¶, Shohei Yamashita[14], Alexandre Dazzi[12], Ariane Deniset-Besseau[12], Scott Sandford[16], Zita Martins[17], Yusuke Tamenori[18], Takuji Ohigashi[19], Hiroki Suga[18], Daisuke Wakabayashi[14], Maximilien Verdier-Paoletti[7], Smail Mostefaoui[7], Gilles Montagnac[20], Jens Barosch[2], Kanami Kamide[1], Miho Shigenaka[1], Laure Bejach[3], Megumi Matsumoto[21], Yuma Enokido[21], Takaaki Noguchi[22], Hisayoshi Yurimoto[23], Tomoki Nakamura[21], Ryuji Okazaki[24], Hiroshi Naraoka[24], Kanako Sakamoto[25], Harold C. Connolly Jr.[26], Dante S. Lauretta[27], Masanao Abe[25,28], Tatsuaki Okada[25,29], Toru Yada[25], Masahiro Nishimura[25], Kasumi Yogata[25], Aiko Nakato[25], Miwa Yoshitake[25], Ayako Iwamae[30], Shizuho Furuya[11], Kentaro Hatakeda[30], Akiko Miyazaki[25], Hiromichi Soejima[30], Yuya Hitomi[30], Kazuya Kumagai[30], Tomohiro Usui[25], Tasuku Hayashi[25], Daiki Yamamoto[25], Ryota Fukai[25], Seiji Sugita[11,31], Kohei Kitazato[32], Naru Hirata[32], Rie Honda[33], Tomokatsu Morota[11], Eri Tatsumi[34], Naoya Sakatani[35], Noriyuki Namiki[28,36], Koji Matsumoto[28,36], Rina Noguchi[37], Koji Wada[31], Hiroki Senshu[31], Kazunori Ogawa[38], Yasuhiro Yokota[25], Yoshiaki Ishihara[38], Yuri Shimaki[25], Manabu Yamada[31], Chikatoshi Honda[32], Tatsuhiro Michikami[39], Moe Matsuoka[40], Naoyuki Hirata[41], Masahiko Arakawa[41], Chisato Okamoto[41]¶, Masateru Ishiguro[42], Ralf Jaumann[43], Jean-Pierre Bibring[44], Matthias Grott[45], Stefan Schröder[46], Katharina Otto[1,45], Cedric Pilorget[44,47], Nicole Schmitz[45], Jens Biele[48], Tra-Mi Ho[49], Aurélie Moussi-Soffys[50], Akira Miura[25], Hirotomo Noda[28,36], Tetsuya Yamada[25], Keisuke Yoshihara[25], Kosuke Kawahara[25], Hitoshi Ikeda[25], Yukio Yamamoto[25], Kei Shirai[41], Shota Kikuchi[31,36], Naoko Ogawa[25], Hiroshi Takeuchi[25,28], Go Ono[51], Yuya Mimasu[25], Kent Yoshikawa[51], Yuto Takei[25], Atsushi Fujii[25], Yu-ichi Iijima[25]¶, Satoru Nakazawa[25], Satoshi Hosoda[25], Takahiro Iwata[25,28], Masahiko Hayakawa[25], Hirotaka Sawada[38], Hajime Yano[25,28], Ryudo Tsukizaki[25], Masanobu Ozaki[25,28], Fuyuto Terui[52], Satoshi Tanaka[25,28], Masaki Fujimoto[25], Makoto Yoshikawa[25,28], Takanao Saiki[25], Shogo Tachibana[11,25], Sei-ichiro Watanabe[8], Yuichi Tsuda[25]

Samples of the carbonaceous asteroid (162173) Ryugu were collected and brought to Earth by the Hayabusa2 spacecraft. We investigated the macromolecular organic matter in Ryugu samples and found that it contains aromatic and aliphatic carbon, ketone, and carboxyl functional groups. The spectroscopic features of the organic matter are consistent with those in chemically primitive carbonaceous chondrite meteorites that experienced parent-body aqueous alteration (reactions with liquid water). The morphology of the organic carbon includes nanoglobules and diffuse carbon associated with phyllosilicate and carbonate minerals. Deuterium and/or nitrogen-15 enrichments indicate that the organic matter formed in a cold molecular cloud or the presolar nebula. The diversity of the organic matter indicates variable levels of aqueous alteration on Ryugu's parent body.

Organic compounds in asteroids and comets were produced and modified within the presolar molecular cloud, the protoplanetary disk, during the formation of planetesimals in the early Solar System and their subsequent evolution. Delivery of extraterrestrial organic compounds might have contributed to the habitability of terrestrial planets, including Earth. Analysis of pristine samples collected from primitive small bodies (asteroids and comets) could provide information on how organic compounds were formed and modified in space and which organic compounds were supplied to early Earth. Macromolecular organic matter, a dark, complex acid-insoluble organic matter (IOM), accounts for most carbon in primitive carbonaceous chondrite meteorites.

The Hayabusa2 asteroid sample return mission visited the carbonaceous (C-type) asteroid (162173) Ryugu. The mission goals included investigating the origin and evolution of organic compounds in the early Solar System (*1*). Remote sensing and lander observations showed that Ryugu is a dark, rubble-pile asteroid that contains hydrated minerals on its surface (*2*–*4*) and indicated a relationship between C-type asteroids and carbonaceous chondrites (*3*, *4*). The average albedo of Ryugu is consistent with the thermally metamorphosed subgroups of the CI1 and CM2 meteorites (*3*, *4*). CI1 meteorites are Ivuna-type carbonaceous chondrites of petrologic type 1 (extensively altered by aqueous fluids on the parent asteroid), and CM2 meteorites are Mighei-type carbonaceous chondrites of petrologic type 2 (moderately aqueously altered). Spectral and thermal inertia variations indicated that Ryugu consists of boulders that experienced different degrees of thermal and space weathering processes (*5*–*7*), derived from a much larger parent body and potentially additional materials from different asteroids (*8*).

The Hayabusa2 spacecraft collected the surface material from two touchdown sites on Ryugu and returned them to Earth on 6 December 2020. The Ryugu samples exhibit near-infrared absorption features as a result of OH and carbonate and/or organic C-H bonds, at 2.7 and 3.4 μm respectively (*9*, *10*), which indicates that the Ryugu samples are similar to CI carbonaceous chondrites (*9*).

We sought to determine the distributions and chemical characteristics of macromolecular organic matter in the Ryugu samples. We therefore measured the elemental, isotopic, and functional group compositions, structures, and textures of organic macromolecules from the Ryugu samples. The analytical procedures included micro–Fourier transform infrared (FTIR) spectroscopy, micro-Raman spectroscopy, synchrotron-based scanning transmission x-ray microscopy (STXM), x-ray absorption near-edge structure (XANES), scanning transmission electron microscopy (STEM) coupled with electron energy-loss spectroscopy (EELS) and energy-dispersive x-ray spectroscopy (EDS), atomic force microscope–based infrared (AFM-IR) spectroscopy, and nanometer-scale secondary ion mass spectrometry (NanoSIMS) (*11*). The analytical workflow (fig. S1) was designed to optimize the use of these complementary techniques.

The samples we used were selected aggregates stored in collection chamber A (from the first touchdown) and collection chamber C (from the second touchdown) of the spacecraft sample catcher (*12*) (table S1). We studied (i) intact grains (taken from aggregates designated A0108 and C0109), ranging from 200 to 900 μm in size per particle, and (ii) insoluble carbonaceous residues (fig. S2) isolated by acid treatment of Ryugu aggregates (designated A0106 and C0107). Each of these samples was split into several subsamples for analysis with different techniques (table S1).

Structural properties of macromolecular organic matter

To characterize the macromolecular structures of organic matter in Ryugu, we applied micro-Raman spectroscopy. Two peaks, identified as the D-band (~1350 cm^{-1}) and G-band (~1580 cm^{-1}) of polyaromatic molecular structures (*13*), are present in the Raman spectra of A0108 and C0109 (Fig. 1A and fig. S3A). The spectral features are broad, indicating lattice disorder in the organic macromolecules, and are superimposed on a fluorescence background. The numerical values of the derived spectral parameters of the D- and G-bands, such as their full widths at half maximum ($FWHM_{-D}$ and $FWHM_{-G}$, respectively), peak positions (ω_D and ω_G), and intensity ratio (I_D/I_G), are similar for all grains examined from the two aggregates (Fig. 1, B to D, and fig. S3, B to D).

The macromolecular structures of organic matter in meteorites reflect the thermal histories of the meteorite parent bodies (*13*–*16*). To evaluate the thermal history of Ryugu, we compared the Raman parameters measured from the Ryugu samples with those measured from meteorites (Fig. 1, B to D, and fig. S3, B to D). The closest matches to Ryugu are the primitive CI1 and CM2 carbonaceous chondrites. The Ryugu samples are distinct from carbonaceous chondrites of petrologic type 3 (thermally metamorphosed) (Fig. 1B) and from the thermally metamorphosed subgroup of CM2, such as the Jbilet Winselwan meteorite (Fig. 1, C and D), and other ungrouped carbonaceous chondrites of petrologic type 2 (C2), such as the Wisconsin Range (WIS) 91600 and Pecora Escarpment (PCA) 02012 meteorites (Fig. 1, C and D). This indicates that the Ryugu samples A0108 and C0109 did not experience long-duration radiogenic thermal metamorphism on their parent bodies, as petrologic type 3 chondrites did (*17*), or impact-induced, short-duration heating, as experienced by some petrologic type 2 chondrites (*18*).

Functional group compositions

We used micro-FTIR spectroscopy to characterize the organic molecules and minerals. The FTIR spectra of the Ryugu grains show bands due to organic aliphatic C-H stretching (3000 to 2800 cm^{-1}, 3.33 to 3.57 μm), aromatic C=C stretching (~1600 cm^{-1}, ~6.25 μm), and carbonyl C=O stretching modes (~1700 cm^{-1}, ~5.88 μm), as well as bands due to mineral Si-O stretching (~1000 cm^{-1}, ~10.00 μm), structural OH stretching of phyllosilicates (~3680 cm^{-1}, ~2.72 μm), and the ν3 stretching mode of carbonates (~1435 cm^{-1}, ~6.97 μm) (Fig. 2A). The spectra also contain bands from interlayer water, of varying intensities, contributing at ~3300 cm^{-1} (~3.03 μm; stretching) and 1640 cm^{-1} (6.10 μm; bending). Part of this water is intrinsic to the Ryugu grains, and part can be attributed to water adsorbed on the grains under atmospheric conditions.

These absorption bands are commonly observed in unheated, aqueously altered carbonaceous chondrites (*19*, *20*), whereas organic features are weaker in thermally metamorphosed CM chondrites, such as the Jbilet Winselwan meteorite (Fig. 2A). The spectral shape of the OH band in the Ryugu samples is characteristic of Mg-rich phyllosilicates, which have been observed in CI chondrites as saponite and serpentine (*21*, *22*). There were large spectral heterogeneities among the Ryugu grains, but there is no obvious difference in the spectral variations observed between samples from chambers A and C. Compared with CI chondrites, the sulfate S=O stretching band (~1100 to 1200 cm^{-1}, ~9.09 to 8.33 μm) is absent from the spectra of Ryugu samples. The absence of sulfates is consistent with other elemental and mineralogical measurements of Ryugu samples (*23*, *24*). Sulfate can be produced by oxidation of sulfides during terrestrial weathering of the meteorites (*25*), so the lack of sulfate indicates that the Ryugu samples are pristine (*23*).

The shapes of the FTIR spectra of the grains are consistent with the reflectance spectra of Ryugu's surface acquired by the Hayabusa2 spacecraft (*4*). The OH band and aliphatic C-H band features in our absorption spectra are similar to reflectance spectra of other Ryugu samples (*9*), but we find lower intensities of aliphatic C-H peaks.

The FTIR spectra of insoluble carbonaceous residues obtained from our Ryugu samples show similar functional groups to those of the intact Ryugu grains (Fig. 2B). The aliphatic C-H stretching band (3000 to 2800 cm^{-1}, 3.33 to 3.57 μm) from the carbonaceous residue from Ryugu is more intense than those of IOM from meteorites (*26*, *27*). The peak intensity ratios of CH_2 to CH_3 (I_{CH2}/I_{CH3}) of the Ryugu residues are 1.9, whereas those of IOMs in Murchison and Ivuna meteorites are 1.2 and 1.3, respectively. Because I_{CH2}/I_{CH3} ratios are proportional to the molar ratios of CH_2 to CH_3 (CH_2/CH_3), we infer the CH_2/CH_3 ratios of the residue, which are higher than those of meteoritic IOMs. This could indicate that Ryugu's organic matter contains longer aliphatic chains, or aliphatic chains with a higher degree of cross-linking. The Ryugu carbonaceous residue also exhibits an absorption band of C=O (~1670 cm^{-1}, ~5.99 μm), which is not seen in meteoritic IOMs. We assign this C=O band to unsaturated ketones, aldehydes, or amides.

Chemical and morphological variations

Macromolecular diversity

We used synchrotron-based STXM, with spatial resolution of 30 to 50 nm, to produce

[1]Department of Earth and Planetary Systems Science, Hiroshima University, Hiroshima 739-8526, Japan. [2]Earth and Planets Laboratory, Carnegie Institution for Science, Washington, DC 20015, USA. [3]Laboratoire de Physique des 2 Infinis Irène Joliot-Curie, Université Paris-Saclay, Centre National de la Recherche Scientifique, 91405 Orsay, France. [4]Faculty of Engineering, Yokohama National University, Yokohama 240-8501, Japan. [5]Materials Science and Technology Division, US Naval Research Laboratory, Washington, DC 20375, USA. [6]Institut de Planétologie et d'Astrophysique, Université Grenoble Alpes, 38000 Grenoble, France. [7]Institut de Mineralogie, Physique des Materiaux et Cosmochimie, Museum National d'Histoire Naturelle, Centre National de la Recherche Scientifique, Sorbonne Université, 75231 Paris, France. [8]Graduate School of Environmental Studies, Nagoya University, Nagoya 464-8601, Japan. [9]Center for University-Wide Education, Saitama Prefectural University, Saitama 343-8540, Japan. [10]Department of Earth Sciences, Waseda University, Tokyo 169-8050, Japan. [11]Department of Earth and Planetary Science, The University of Tokyo, Tokyo 113-0033, Japan. [12]Institut Chimie Physique, Université Paris-Saclay, Centre National de la Recherche Scientifique, 91405 Orsay, France. [13]Institut des Sciences Moléculaires d'Orsay, Université Paris-Saclay, Centre National de la Recherche Scientifique, 91405 Orsay, France. [14]Institute of Materials Structure Science, High Energy Accelerator Research Organization, Tsukuba 305-0801, Japan. [15]Advanced Light Source, Lawrence Berkeley National Laboratory, Berkeley, CA 94720, USA. [16]NASA Ames Research Center, Moffett Field, CA 94035, USA. [17]Centro de Química Estrutural, Institute of Molecular Sciences and Department of Chemical Engineering, Instituto Superior Técnico, Universidade de Lisboa, Lisboa 1049-001, Portugal. [18]Japan Synchrotron Radiation Research Institute, Hyogo 679-5198, Japan. [19]Institute for Molecular Science, UVSOR Synchrotron Facility, Okazaki 444-8585, Japan. [20]École normale supérieure de Lyon, University Lyon 1, 69342 Lyon, France. [21]Department of Earth Science, Tohoku University, Sendai 980-8578, Japan. [22]Department of Earth and Planetary Sciences, Kyoto University, Kyoto 606-8502, Japan. [23]Department of Earth and Planetary Sciences, Hokkaido University, Sapporo 060-0810, Japan. [24]Department of Earth and Planetary Sciences, Kyushu University, Fukuoka 819-0395, Japan. [25]Institute of Space and Astronautical Science, Japan Aerospace Exploration Agency (JAXA), Sagamihara 252-5210, Japan. [26]Department of Geology, School of Earth and Environment, Rowan University, Glassboro, NJ 08028, USA. [27]Lunar and Planetary Laboratory, University of Arizona, Tucson, AZ 85721, USA. [28]School of Physical Sciences, The Graduate University for Advanced Studies, Hayama 240-0193, Japan. [29]Department of Chemistry, The University of Tokyo, Tokyo 113-0033, Japan. [30]Marine Works Japan Ltd., Yokosuka 237-0063, Japan. [31]Planetary Exploration Research Center, Chiba Institute of Technology, Narashino 275-0016, Japan. [32]Aizu Research Cluster for Space Science, University of Aizu, Aizu-Wakamatsu 965-8580, Japan. [33]Center of Data Science, Ehime University, Matsuyama 790-8577, Japan. [34]Instituto de Astrofísica de Canarias, University of La Laguna, Tenerife E-38205, Spain. [35]Department of Physics, Rikkyo University, Tokyo 171-8501, Japan. [36]Research of Interior Structure and Evolution of Solar System Bodies, National Astronomical Observatory of Japan, Mitaka 181-8588, Japan. [37]Faculty of Science, Niigata University, Niigata 950-2181, Japan. [38]JAXA Space Exploration Center, JAXA, Sagamihara 252-5210, Japan. [39]Faculty of Engineering, Kindai University, Higashi-Hiroshima 739-2116, Japan. [40]Geological Survey of Japan, National Institute of Advanced Industrial Science and Technology, Tsukuba 305-8567, Japan. [41]Department of Planetology, Kobe University, Kobe 657-8501, Japan. [42]Department of Physics and Astronomy, Seoul National University, Seoul 08826, Republic of Korea. [43]Freie Universität Berlin, Institute of Geological Sciences, Planetary Sciences and Remote Sensing, Berlin 12249, Germany. [44]Institut d'Astrophysique Spatiale, Université Paris-Saclay, Centre National de la Recherche Scientifique, 91405 Orsay, France. [45]Institute of Planetary Research, German Aerospace Center, Berlin 12489, Germany. [46]Department of Computer Science, Electrical and Space Engineering, Luleå University of Technology, 98128 Kiruna, Sweden. [47]Institut Universitaire de France, 75005 Paris, France. [48]Microgravity User Support Centre, German Aerospace Center, Cologne 53147, Germany. [49]Institute of Space Systems, German Aerospace Center, Bremen 28359, Germany. [50]Centre National d'Études Spatiales, 31401 Toulouse, France. [51]Research and Development Directorate, JAXA, Sagamihara 252-5210, Japan. [52]Department of Mechanical Engineering, Kanagawa Institute of Technology, Atsugi 243-0292, Japan.
***Corresponding author. Email: hyabuta@hiroshima-u.ac.jp**
†Present address: International Institute for Sustainability with Knotted Chiral Meta Matter, Hiroshima University, Hiroshima 739-8526, Japan.
‡Present address: Buseck Center for Meteorite Studies, Arizona State University, Tempe, AZ 85827, USA.
§Present address: School of Earth and Space Exploration, Arizona State University, Tempe, AZ 85827, USA. ¶Deceased.

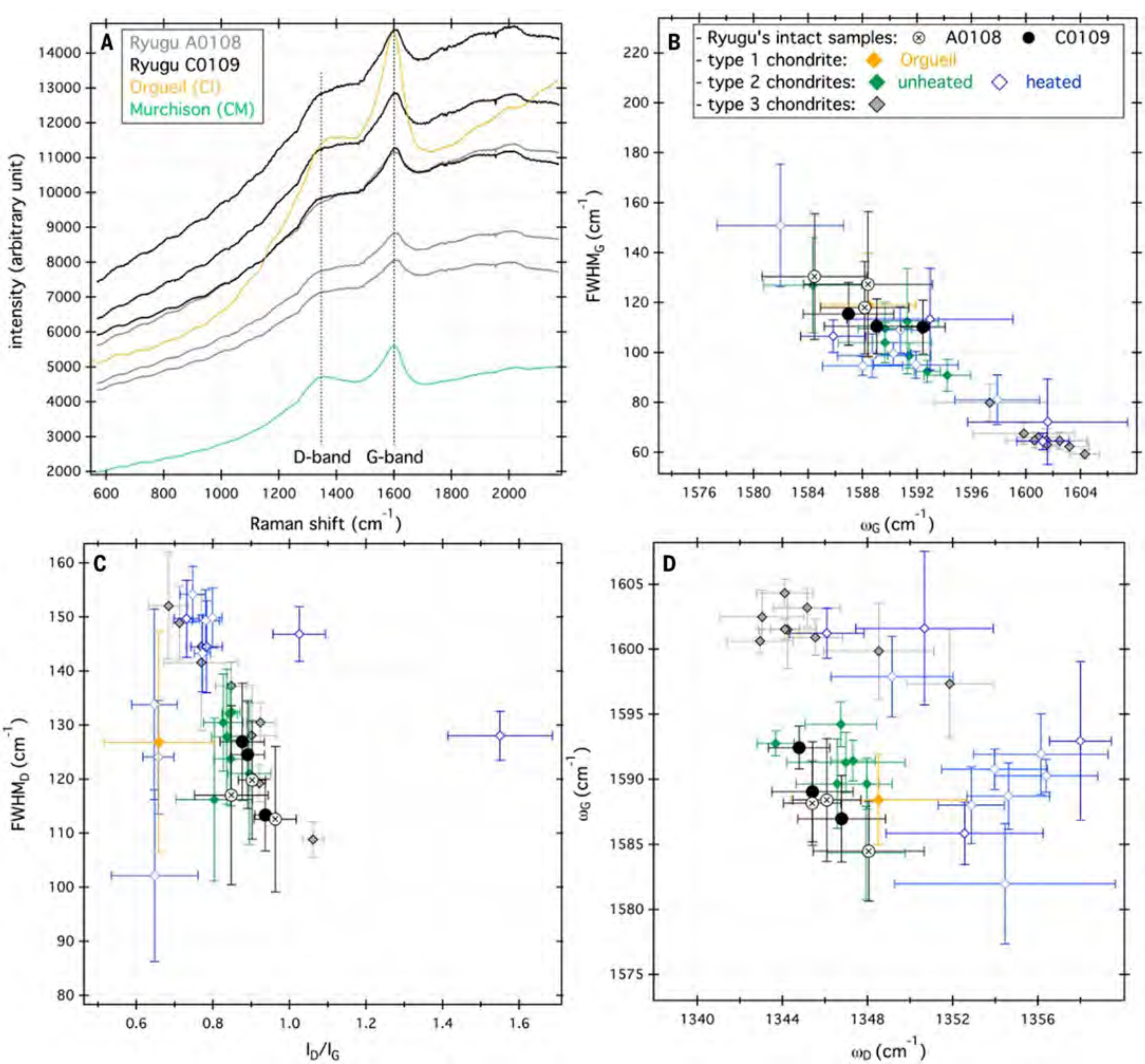

Fig. 1. Raman spectra and spectral parameters: Comparison between Ryugu samples and chondrites. (**A**) Average Raman spectra of Ryugu grains from chamber A (samples A0108-6, -10, and -18) (in gray) and chamber C (samples C0109-5, -9, and -12) (in black) compared with the meteorites Murchison (CM; green) and Orgueil (CI; yellow). All spectra were acquired in the same analytical conditions (*11*). (**B** to **D**) Average spectral parameters (error bars show standard deviations) determined from the Raman spectra: $FWHM_G$ as a function of ω_G (B); $FWHM_D$ as a function of I_D/I_G (C); and ω_G as a function of ω_D (D). Data are for individual grains from chamber A (open circles) and chamber C (black filled circles) compared with petrologic type 1 (Orgueil; orange diamond), unheated petrologic type 2 chondrites (green filled diamonds), heated petrologic type 2 chondrites (open blue diamonds), and petrologic type 3 chondrites (filled gray diamonds) (*11*). Petrologic type 2 chondrites were classified (*16*) as unheated (e.g., Murchison, Nogoya, and Tarda) or heated (e.g., Jbilet Winselwan and WIS 91600).

elemental x-ray maps and XANES spectra. Carbon x-ray maps (Fig. 3, A and B) show discrete grains of organic material with sizes of ~200 nm. X-ray absorption by carbon atoms is also present in the phyllosilicate matrix at low levels but nearly ubiquitously (Fig. 3B). Carbon-XANES spectra of the discrete grains show three major peaks, resulting from aromatic carbon (C=C, 285 eV), aromatic ketone (C=C-C=O, 286.7 eV), and carboxyl (COOH, 288.5 eV) functional groups (Fig. 3E), which have been observed in primitive extraterrestrial carbonaceous matter, such as carbonaceous chondrites (*28*, *29*) and their extracted IOMs (*30*), interplanetary dust particles (IDPs) (*31*), dust particles from Comet Wild 2 (*32*), and Antarctic micrometeorites (AMMs) (*33*). Some spectra of fine-grained matrices in the Ryugu samples contain an additional peak at 290.4 eV, which corresponds to a 1s-π* transition of carbonate groups—e.g., in calcite and other carbonate minerals. However, our matrix XANES spectra containing this feature lack extended x-ray absorption fine structure

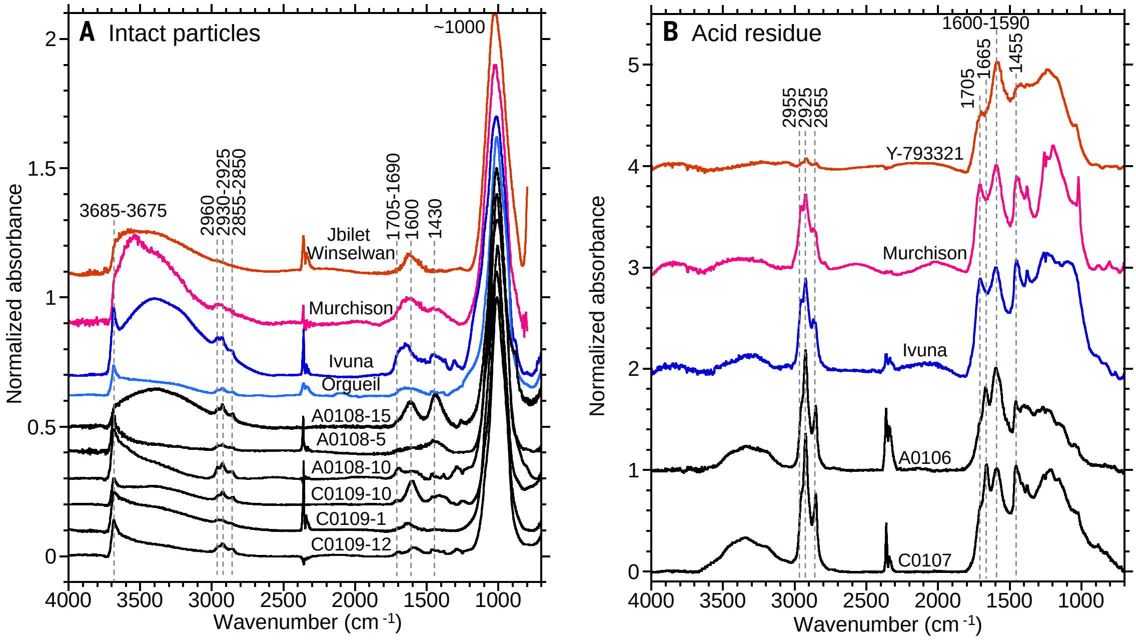

Fig. 2. Micro-FTIR spectra of Ryugu samples compared with chondrites. (**A**) Infrared transmission spectra (*11*) of six Ryugu grains from the aggregates A0108 and C0109 (black), heated CM chondrite (Jbilet Winselwan) (red), unheated CM Murchison (pink), and two CI chondrites Orgueil (light blue) and Ivuna (dark blue). All the spectra were baseline-corrected using spline curves and normalized by the peak height of the band at ~1000 cm^{-1} (~10.00 μm). Dashed lines indicate identified bands: silicate OH and SiO at 3685 to 3675 cm^{-1} (2.71 to 2.72 μm) and ~1000 cm^{-1} (~10.00 μm); aliphatic C-H bands at 2960 cm^{-1} (3.38 μm; CH_3 asymmetric stretching), 2930 to 2925 cm^{-1} (3.41 to 3.42 μm; CH_2 asymmetric stretching), 2855 to 2850 cm^{-1} (3.50 to 3.51 μm; CH_3 and CH_2 symmetric stretching), 1460 cm^{-1} (6.85 μm), and 1380 cm^{-1} (7.25 μm; bending); and other organic features at 1705 to 1690 cm^{-1} (5.87 to 5.92 μm; C=O) and ~1600 cm^{-1} (~6.25 μm; aromatic with some water bending mode contribution). Some spectra show a peak at ~1430 cm^{-1} (~6.99 μm) due to carbonates. A broad water stretching band at ~3400 cm^{-1} (~2.94 μm) is observed, which is weaker in samples that were measured at 60°C or higher temperatures. The peaks at 2360 cm^{-1} (4.24 μm) are due to atmospheric CO_2. The A0108-5 and C0109-1 Ryugu grains and the Murchison and Ivuna meteorites were measured at 60°C under N_2 flow. The Jbilet Winselwan meteorite was measured at 80°C under N_2 flow. The A0108-10 and C0109-12 Ryugu grains were measured at 80°C under vacuum. The Orgueil meteorite was measured at 130°C under vacuum. (**B**) Same as (A), but for insoluble carbonaceous residues from the Ryugu samples (A0106 and C0107) compared with IOM from the heated CM meteorite Y-793321 (*16*), the CM Murchison (*27*), and the CI meteorite Ivuna (*27*). The spectra were the averages of main fractions of A0106 and C0107, respectively, after baseline-correction using spline curves and normalization by the peak height of the aromatic C=C band at ~1600 cm^{-1} (~6.25 μm).

(EXAFS) features at higher energies (294 to 304 eV), indicating that the carbonate is not in a crystalline structure so is more likely to be molecular carbonate. A similar carbonate feature has previously been reported in clay-bound carbon from extensively hydrated carbonaceous chondrites, Ivuna (CI1), Orgueil (CI1), and Tagish Lake (C2) (*34*), and in diffuse carbon (organic matter) in the fine-grained matrices of Renazzo (CR2; a Renazzo-type carbonaceous chondrite of petrologic type 2), Murchison (CM2), and Orgueil (*28*).

We classify the STXM spectra of Ryugu organic matter on the basis of spectral shape similarities into four representative types: (i) highly aromatic (~25% of individual carbon grains), (ii) aromatic (~35% of individual grains), (iii) IOM-like (~40% of individual grains), and (iv) diffuse carbon associated with a molecular carbonate peak (Fig. 3E). Aromatic spectra show higher ratios of aromatic carbon to aromatic ketone compared with IOM-like spectra, whereas highly aromatic spectra show a broader peak for aromatic carbon, indicating increased diversity of aromatic structures. The frequency distributions of these classes were similar for both chamber A and C samples. We find a relationship between the morphology of organic matter and XANES spectral shape, with particulate and nanoglobular regions having more frequent aromatic or highly aromatic XANES spectra, whereas organic matter dispersed in the matrix more commonly has IOM-like or diffuse carbon spectra. These observations indicate that the molecular functional groups present are influenced by aqueous processing on the asteroid parent body. We did not find any evidence of long-duration thermal metamorphism, such as the 1s-σ* exciton (291.6 eV) peak of graphite or other graphitized carbon materials (*35*).

Similar characteristics are found for the insoluble carbonaceous residues from Ryugu. Average carbon-XANES spectra have IOM-like spectral shapes but with more prominent aromatic C=C, ketone, and carboxyl peaks compared with IOM from Orgueil and Murchison (Fig. 3E). Several hollow and solid organic nanoglobules are apparent in the x-ray absorption images (Fig. 3, C and D), which we confirmed using TEM imaging (Fig. 4, A and B). Their XANES spectra were either IOM-like, aromatic, or highly aromatic (Fig. 3E). The 290.4-eV carbonate feature was not observed in the insoluble carbonaceous residue, perhaps because this organic phase was incorporated into phyllosilicate interlayers and so was removed or destroyed during the acid-extraction process.

Nitrogen-XANES spectra (fig. S4A) of the Ryugu intact grains and insoluble residue did not show clear absorption peaks, indicating low abundances of N-rich Ryugu organics. This is consistent with carbonaceous chondrites, where N-rich particles are only occasionally observed (*32*). Oxygen-XANES spectra (fig. S4B) of Ryugu organic matter often contain a peak at ~531.3 eV, corresponding to carbonyl C=O bonds in the ketone and carboxyl functional groups (*36*). The peak intensity of the carbonyl absorption, relative to the main oxygen 1s-σ* peak in Ryugu, is similar to that of aqueously altered carbonaceous chondrites. We cannot determine whether these carbonyl functional groups are also present in the phyllosilicate-bound diffuse organic matter because its oxygen-XANES spectrum is dominated by the surrounding phyllosilicate.

Nanoscale morphologies

We performed TEM and STEM-EELS-EDS analysis (Fig. 4) on ultrathin sections of particles and carbonaceous residues, including from some of the same sections we analyzed

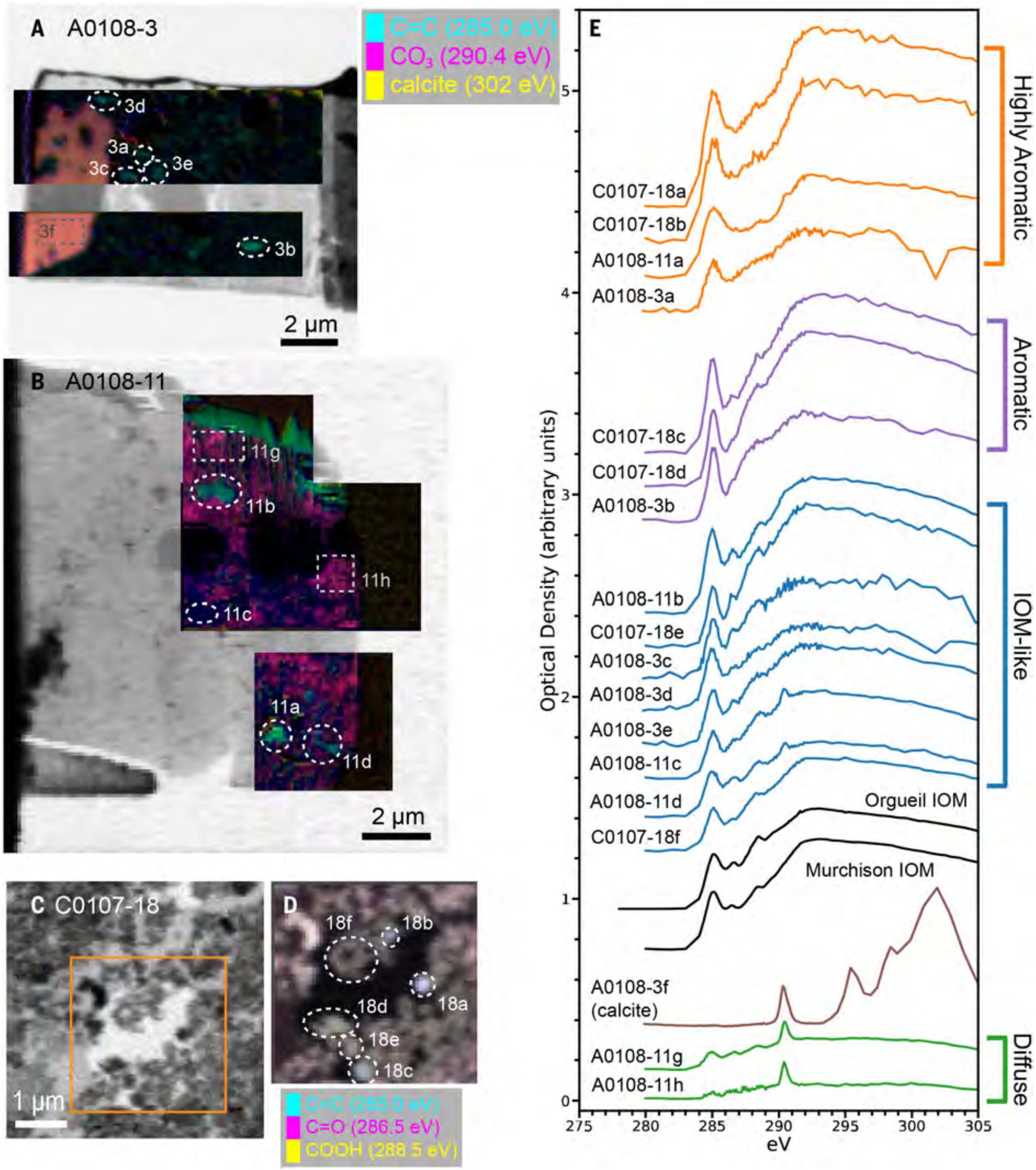

Fig. 3. STXM elemental maps and carbon-XANES spectra of Ryugu samples. (**A** and **B**) STXM grayscale images of FIB sections extracted from the Ryugu grains A0108-3, observed at 520 eV (A), and A0108-11, observed at 390 eV (B) (*11*). In both panels, color overlays on both FIB sections are false-color maps of x-ray absorptions due to aromatic C (cyan), carbonate functional groups (magenta), and calcite minerals (yellow). Dashed circles and boxes indicate regions measured for (E). (**C**) STXM image at 290 eV of insoluble carbonaceous residue from Ryugu sample C0107-18. The orange box shows the region in (D). (**D**) X-ray absorption map of aromatic carbon (cyan), ketones (magenta), and carboxyl (yellow) functional groups. Circled features are solid nanoglobules except for feature 18f, which is a cluster of typical Ryugu IOM. (**E**) Carbon-XANES spectra for carbonaceous grains and matrix regions identified in (A), (B), and (D). IOM from the meteorites Orgueil and Murchison (black) are shown for comparison (*11*).

previously with STXM. The two most abundant organic microstructures are nanoglobules (Fig. 4, A and B) and diffuse carbon mixed with phyllosilicates—i.e., clay-bound carbon (Fig. 4, C and E). Other microstructures include dense, irregularly shaped particles (Fig. 4B); diffuse organic matter trapped in vesicles in carbonate grains (Fig. 4, D and F); and organic matter coatings on sulfide grains. The presence of organic matter associated with Mg-rich phyllosilicates and carbonates, which likely formed through aqueous alteration (*24*), implies that much of the organic material was altered by low-temperature, aqueous processing on Ryugu's parent body. However, we also find nanodiamonds associated with amorphous organic carbon, which probably formed in the interstellar medium or the Solar System's protoplanetary

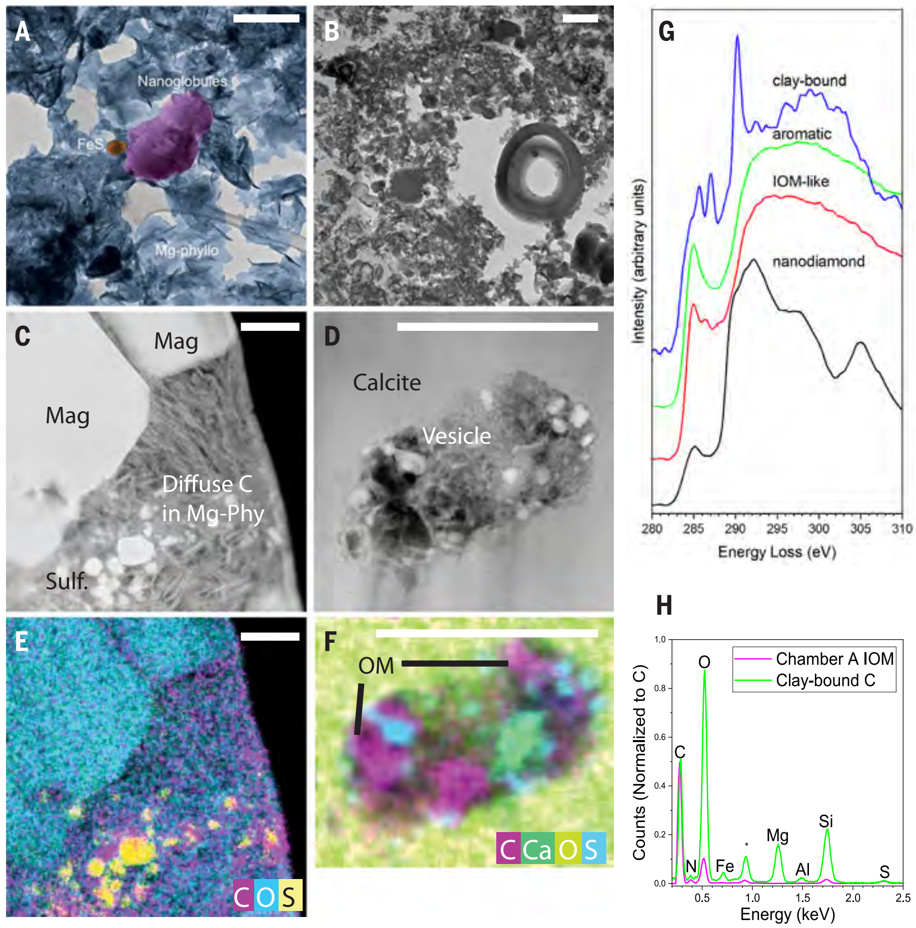

Fig. 4. STEM-EELS-EDS analysis of Ryugu samples. All scale bars are 500 nm. (**A**) False-color bright-field TEM image of the ultrathin section of C0109-11, indicating nanoglobules (magenta), Mg-phyllosilicates (blue), and FeS (orange). (**B**) Bright-field TEM image of insoluble organic residue from a microtome slice of sample C0107, showing hollow and solid nanoglobules and fluffy materials. (**C**) High-angle annular dark field (HAADF) STEM image of a FIB section of A0108-11 (region 11h in Fig. 3B) showing two magnetite grains (labeled Mag) adjacent to carbon-bearing Mg-rich phyllosilicates (Mg-phy) with Fe and Ni sulfide nanoparticles (Sulf). (**D**) HAADF STEM image of a vesicle in the large calcite grain from a FIB section of sample A0108-3 (region 3a in Fig. 3A). (**E**) EDS element map of carbon (magenta), oxygen (cyan), and sulfur (yellow) of the area shown in (C). (**F**) EDS element map of carbon (magenta), calcium (green), oxygen (yellow), and sulfur (cyan) of the vesicle shown in (D) showing diffuse organic matter, Fe,Ni-sulfides, and Ca-sulfate. (**G**) Carbon EEL spectra from molecular carbonate incorporated into phyllosilicates, i.e., clay-bound carbon (C0109-11), an aromatic nanoglobule (A0108-39), an IOM-like nanoglobule (C0109-11), and nanodiamonds (A0108-8). Spectra were acquired at 0.02 eV per channel, and are smoothed to 0.4-eV resolution, after power law background subtraction and arbitrary scaling. (**H**) EDS spectra from molecular carbonate clay-bound carbon (C0109-11; green) and an insoluble organic residue (A0106-9; magenta). The asterisk indicates a Cu background peak from the sample support and microscope.

nebula (*37*, *38*). The insoluble carbonaceous residues contain large nanoglobules and fluffy or porous material, comprising demineralized grain coatings, intergranular material, and small nanoglobules. These microstructures are present in samples from both chambers A and C, and they are consistent in size and shape with those in CI and CM chondrites (*28*, *34*).

Organic nanoglobules have previously been found in early Solar System materials, such as primitive carbonaceous chondrites (*39*–*42*), dust particles from Comet Wild 2 (*32*), IDPs (*43*), and AMMs (*33*, *44*). The nanoglobules in Ryugu grains occur in solid and hollow form, typically 50 to 500 nm in diameter, with a few reaching 2000 nm, consistent with nanoglobules in other extraterrestrial materials. The carbon EELS spectra of many of the Ryugu nanoglobules are dominated by an aromatic carbon peak at ~285 eV (Fig. 4G), corresponding to the aromatic-rich carbon-XANES spectra (Fig. 3E). Other prominent peaks are due to aromatic ketone (286.7 eV) and carboxyl (288.5 eV). The fluffy material in the insoluble carbonaceous residues shows these three peaks in varying intensities. The presence of both aromatic- and IOM-like nanoglobules of various sizes indicates that Ryugu experienced heterogeneous aqueous alteration on its parent body. Correlated STEM-NanoSIMS measurements of a 2000-nm nanoglobule (particle A0108-37; figs. S6 and S7) show high abundances of aromatic carbon and isotopically anomalous H and N, indicating preservation of material from the interstellar medium or protoplanetary nebula.

The widespread diffuse carbon mixed into phyllosilicates could have been formed from soluble molecules intercalated into clays through oxidation during aqueous alteration (*34*). Alternatively, the clay-bound diffuse carbon might have been released by hydrolysis of macromolecular organic material during the flow of aqueous fluids (*28*). The EELS spectra show peaks of either aromatic ketones or aliphatic carbon (287 eV) and carbonate (CO_3 at 290.4 eV) along with aromatic carbon (285 eV) (Fig. 4G). These EELS data are consistent with the carbon-XANES spectrum of the diffuse carbon (Fig. 3, B and E). The relative intensities of the 287-eV and 285-eV peaks vary compared with the 290.4-eV peak. This is consistent with clay-bound organics in CI chondrites (*34*) but sometimes is a better match to the ungrouped C2 chondrite Tagish Lake (*34*). In all cases, Mg is detected in the EDS spectra from the clay-bound organic matter (Fig. 4F); however, we cannot determine whether the Mg is associated with the carbonate. We find no evidence for crystalline Mg carbonate in the clay-bound organics, but the CO_3 feature could be associated with molecular CO_3, $MgCO_3$, or a combination of these.

Pockets of organic matter occur in vesicles inside carbonates (Fig. 4D). A STEM-EDS image (Fig. 4F) shows that this vesicle-bound, diffuse organic matter is associated with phyllosilicates and particles of sulfide and Fe-Ni with sizes of ~10 nm, embedded in a larger grain of calcite. This morphology could indicate carbonate formation from diffuse organic matter. The lack of distinct particle boundaries for the organic matter could indicate it is soluble and therefore potentially lost during our sample preparation, which used ultramicrotomy with a water bath.

We obtained AFM-IR maps of organic inclusions and nanoglobule-like matter at lateral resolutions of 25 and 50 nm. AFM-IR measurements map specific vibrational modes; we used the C=O and C=C modes. Samples from chambers A and C were analyzed using AFM-IR in both tapping and contact modes. Figure 5, A and H, shows combined maps of carbonyl C=O (1720 cm^{-1}, 5.81 μm), aromatic C=C (1600 cm^{-1}, 6.25 μm), and Si-O (1020 cm^{-1}, 9.80 μm) modes. The diffuse organic component within the phyllosilicate matrix is evident in both samples. The maps show small (up to ~100 nm) organic nanoglobule-like inclusions

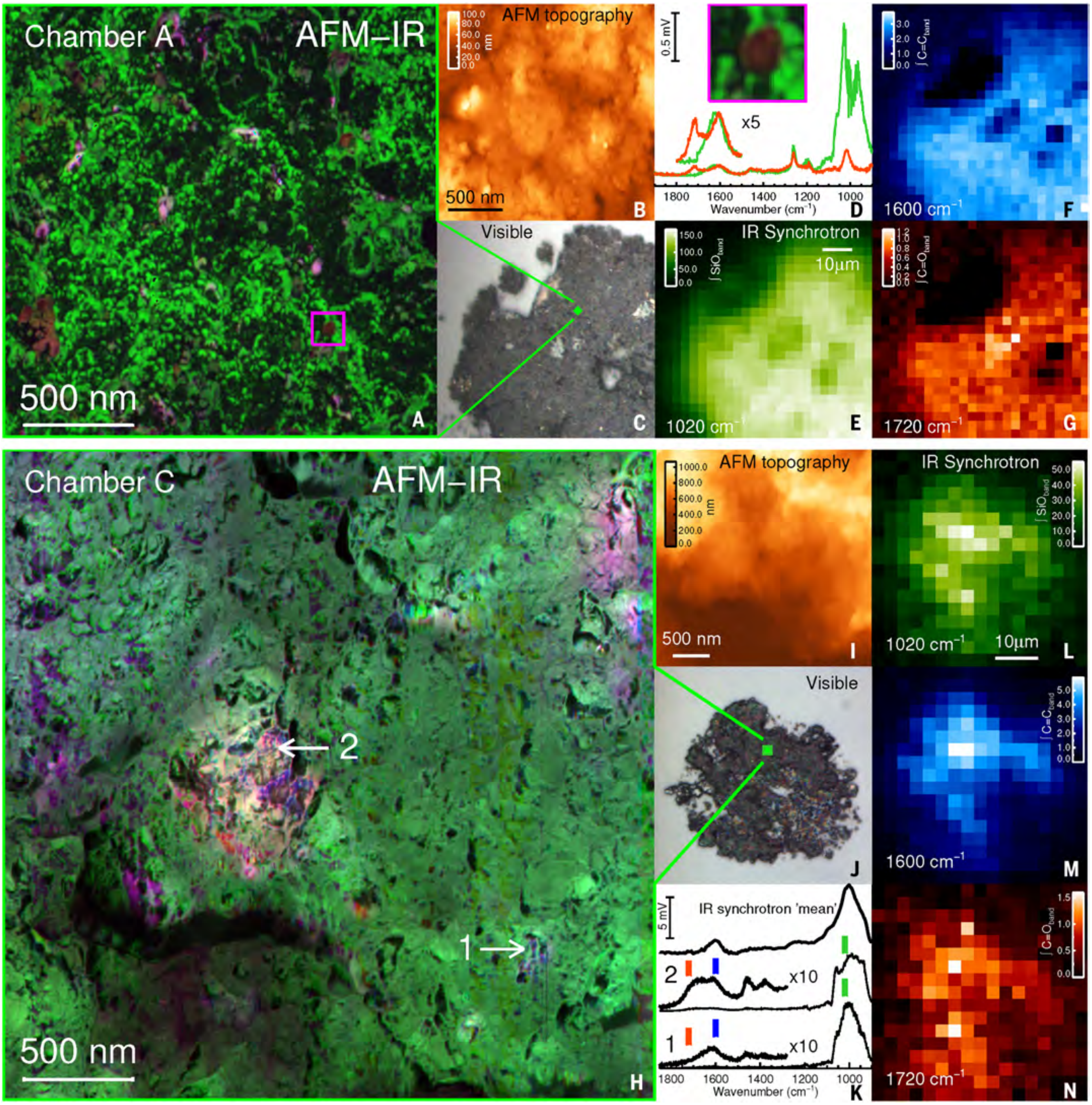

Fig. 5. AFM-IR analysis of intact Ryugu grains A0108 and C0109. (**A** and **H**) Composite AFM-IR images of the intact Ryugu grains A0108-15 in tapping mode, 2 μm by 2 μm (A), and C0109-4 in contact mode, 3 μm by 3 μm (H). Colors indicate the C=O (1720 cm^{-1}, 5.81 μm; red), C=C (1600 cm^{-1}, 6.25 μm; blue), and Si-O (1020 cm^{-1}, 9.80 μm; green) peaks. Each image has been normalized to its maximum peak value. Organic matter is widespread throughout each sample. In (A), small organic globules are visible (red-brown) surrounded by a dominant phyllosilicate. The magenta box indicates the inclusion used for (D). (**B**) AFM topographic map of the 2 μm–by–2 μm area in (A). (**C**) Visible light image (75 μm by 75 μm) showing the location of the AFM-IR map (green square). (**D**) AFM-IR spectrum (red) of the globule indicated in (A) and shown in the inset and background spectrum (green) taken in a region 100 nm away. The AFM-IR signal is shown in millivolts, which is proportional to optical depth (*11*). The C=C and C=O absorptions spectral region is also shown with a ×5 factor for better visibility. (**E** to **G**) Synchrotron FTIR maps of the same 75 μm–by–75 μm area as in (C) of the C=O (1720 cm^{-1}, 5.81 μm; red) (G), C=C (1600 cm^{-1}, 6.25 μm; blue) (F), and Si-O (1020 cm^{-1}, 9.80 μm; green) (E) peaks. Data were acquired with a 6 μm–by–6 μm beam size, sampled with 3-μm steps. Color bars show the integrated optical depths calculated for each band. (H) Organic matter in the Ryugu grain C0109-4 appears as red-purple inclusions standing out from the dominant phyllosilicate signal. Arrows indicate the positions used for the spectra in (K). (**I**) AFM topographic map of the 3 μm–by–3 μm area. (**J**) Visible image (51 μm by 51 μm) showing the location of the AFM-IR map (green square). (**K**) AFM-IR spectra of a C=O–poor region [labeled 1 in (H)] and organic inclusions (labeled 2) compared with the average synchrotron FTIR spectrum. Red, blue, and green tick marks indicate spectral positions corresponding to the AFM-IR images combined in (H). (**L** to **N**) Same as [(E) to (G)] but for the 51 μm–by–51 μm region shown in (J). To aid color-blind readers, another version of this figure with alternatives colors is provided as fig. S5.

in the chamber A sample (Fig. 5A) and organic inclusions in the chamber C samples (Fig. 5H). The abundances of carbonyl and C=C vary between the organic inclusions. These AFM-IR results are consistent with and complimentary to those from STEM-EELS-EDS and STXM-XANES discussed above.

Elemental abundances

The elemental abundances of macromolecular organic matter in meteorites are highly heterogeneous, both between meteorite groups and at the micrometer scale, reflecting the complex histories of these materials (*45*, *46*). We used NanoSIMS to map the H, C, N, O, and S elemental abundances of the Ryugu samples.

The ratios of O/C, N/C, and S/C in the acid-insoluble carbonaceous residues from Ryugu were estimated from NanoSIMS elemental maps of the major isotopes (^{16}O, $^{12}C^{14}N$, and ^{32}S) and were compared between samples taken from chambers A and C. The bulk O/C ratio (0.12 ± 0.03) in chamber A was consistent with those of CI (0.15 to 0.18), CM (0.11 to 0.23), and CR chondrites (0.11 to 0.22) (*45*). The bulk O/C ratio (0.04 ± 0.01) in chamber C was one-third of those values. We cannot determine whether this difference is the result of intrinsic differences between the two sampling sites or heterogeneity within the samples. There are smaller differences in the bulk ratios N/C [0.035 ± 0.006 (A0106); 0.021 ± 0.001 (C0107)] and S/C [0.032 ± 0.001 (A0106); 0.025 ± 0.001 (C0107)] between the two chambers, which are within the ranges of those for CI, CM, and CR chondrites (0.026 < N/C < 0.039 and 0.02 < S/C < 0.06) (*45*).

We also used STEM-EDS to measure N, O, and S abundances, relative to C, at the nano- to micrometer scale. An EDS spectrum from an ~1-μm^2 region of an ultrathin section of carbonaceous residue from chamber A is shown in Fig. 4H. The average compositions measured for carbonaceous residues are $C_{100}N_1O_{10}S_{0.8}$ for chamber A and $C_{100}N_2O_{10}S_{0.8}$ for chamber C. The insoluble carbonaceous residues contain some nanoparticulate minerals, including chromite, with varying Al, Mg, and Fe and sulfides with variable Fe, Ni, and (more rarely) CuS. These particles were excluded from the STEM-EDS measurements when >4 nm in size. These nitrogen abundances are slightly lower than the bulk N/C ratio estimated using NanoSIMS and are consistent with the weak nitrogen-XANES absorption of the Ryugu grains.

Isotopic compositions

NanoSIMS was also used to measure the isotopic compositions of H, C, and N. The resulting maps (Fig. 6, A to C) show bulk enrichments of D (^2H) and/or ^{15}N in most analyzed Ryugu particles from aggregates A0108 and C0109, with a high degree of isotopic heterogeneity at the micrometer scale. The NanoSIMS H measurements are dominated by H from the organic matter but also include H in phyllosilicates and possible contamination by terrestrial water. The isotopic compositions are expressed in delta notation: $\delta R = [(R_{sample}/R_{standard}) - 1] \times 1000$, where R_{sample} is the isotopic ratio of the sample and $R_{standard}$ is the ratio of a terrestrial standard. The average measured H isotopic compositions (δD) of particles range from +254 ± 52 per mil (‰) to +490 ± 100‰ (table S3), consistent with the δD = +252 ± 13‰ measured in an analysis of other Ryugu grains with a different technique (*47*). There is no obvious difference between grains from chambers A and C. The bulk N isotopic compositions $\delta^{15}N$ = +39 ± 5 to +43 ± 4‰ are also within the range reported for other Ryugu grains, measured with different methods [$\delta^{15}N$ = +43.0 ± 9.0‰ (*47*) and $\delta^{15}N$ = 0 to +20‰ (*48*)]. Figure S8 shows that the bulk δD and $\delta^{15}N$ of the Ryugu grains are between the bulk values of CI chondrites [δD = +170 to +300‰ and $\delta^{15}N$ = +39 to +52‰ (*49*)] and IOM in CI chondrites [δD = ~+975‰ and $\delta^{15}N$ = +31‰ (*45*)].

Isotopic ratios determined for individual submicrometer- to micrometer-sized carbonaceous grains within the NanoSIMS maps are similar to those of carbonaceous chondrites and IDPs (*43*, *46*). Most grains are consistent with the bulk average, within the uncertainties, whereas a small fraction of outliers have D and/or ^{15}N enrichments or depletions (Fig. 6, D to F), which we term hotspots and coldspots, respectively. These have a similar range of compositions to those seen in CI (*46*) and CM (*50*) chondrites but smaller than that seen in CR chondrites (*29*). There is no correlation between δD and $\delta^{15}N$ for the hot- or coldspots, and a wide range of compositions occur over small spatial scales (Fig. 6, B and C). The origin(s) of the H and N isotopic anomalies in meteorites are debated; current consensus models propose that they reflect isotopic fractionation at low temperatures in interstellar clouds or the outer protoplanetary nebula (*51*–*54*).

The NanoSIMS measurements show that the bulk Ryugu particles, and almost all C-rich particles within them, have $\delta^{13}C$ values within the range of organic matter in carbonaceous chondrites [$\delta^{13}C$ = −35 to −5‰ (*45*)]. However, ~0.5% of the C-rich particles have ^{13}C enrichments or depletions (Fig. 6G) >2σ above or below the bulk values. These particles have a range of $\delta^{13}C$ and $\delta^{15}N$ values similar to those seen in organic grains with anomalous carbon isotopes in primitive CM chondrites. For the Ryugu samples, ^{13}C-rich particles have a wider range of $\delta^{15}N$ values compared with ^{13}C-poor ones, likely reflecting different origins. Two very small (≤150 nm) regions have much higher ^{13}C enrichments: $\delta^{13}C$ = 700 and 4800‰, which indicates that they are presolar grains that formed in the outflows of previous generations of stars (*55*).

The acid-insoluble carbonaceous residues from the Ryugu samples showed bulk D-enrichments [δD = +306 ± 42‰ (A0106) and +440 ± 52‰ (C0107)] (Fig. 7I) lower than the bulk hydrogen compositions of the IOM in CI chondrites (δD = +972‰ for Orgueil and +978‰ for Ivuna) and CM chondrites (+639‰ < δD < +893‰) (*45*). The distributions of D-rich hotspots [distribution modes δD = +1030‰ (A0106) and +1374‰ (C0107)] were consistent with CI and CM chondrites but not CR chondrites (*56*).

The bulk N isotopic compositions of the insoluble carbonaceous residues from Ryugu samples [$\delta^{15}N$ = +17.4 ± 1.9‰ (A0106) and +30 ± 4.3‰ (C0107)] (Fig. 7J) are consistent with those of IOM in CI chondrites ($\delta^{15}N$ = +30.7‰ for Orgueil and +31.9‰ for Ivuna) (*45*). $\delta^{15}N$ was more heterogeneous in the sample from chamber C than that from chamber A. The ^{15}N-rich hotspots [distribution modes $\delta^{15}N$ = +241‰ (A0106) and +348‰ (C0107)] were within the range of CI and CM carbonaceous chondrites (*57*). ^{15}N-depleted coldspots ($\delta^{15}N$ = −100 to −380‰) were detected. ^{15}N coldspots have previously been reported in the matrices of carbonaceous chondrites (*57*–*59*) and IDPs (*43*) and have been interpreted as indicating organic grains that have been partially equilibrated with protosolar or interstellar N_2 gas (*43*).

Comparison with D-type asteroids and comets

We compare the organic matter of Ryugu (a C-type asteroid) with other primitive small bodies in the early Solar System. Of the carbonaceous chondrites, the Tagish Lake meteorite is thought to be related to dark (D-type) asteroids, which are mainly located in the outer regions of the asteroid belt and among the trojan asteroids of Jupiter (*60*). Tagish Lake contains organic and mineralogical variations between different specimens that reflect variable degrees of alteration on the same parent body (*61*, *62*). The ratios D/H, H/C, and aliphatic carbon to aromatic carbon decrease systematically with increasing alteration of the Tagish Lake meteorite samples (*61*).

We infer that the organic matter in the Ryugu samples has not been heated to temperatures higher than 200°C based on the similarity of its chemical features with primitive carbonaceous CI and CM chondrites. Like the IOM from Orgueil (*63*) and Murchison (*64*), the organic macromolecules in the Ryugu samples likely contain polyaromatic structures that are composed of small numbers of aromatic rings with short, cross-linked aliphatic chains and various oxygen- and nitrogen-bearing functional groups. This macromolecular structure is distinct from graphitic or glassy carbon produced by heating: We did not find any evidence

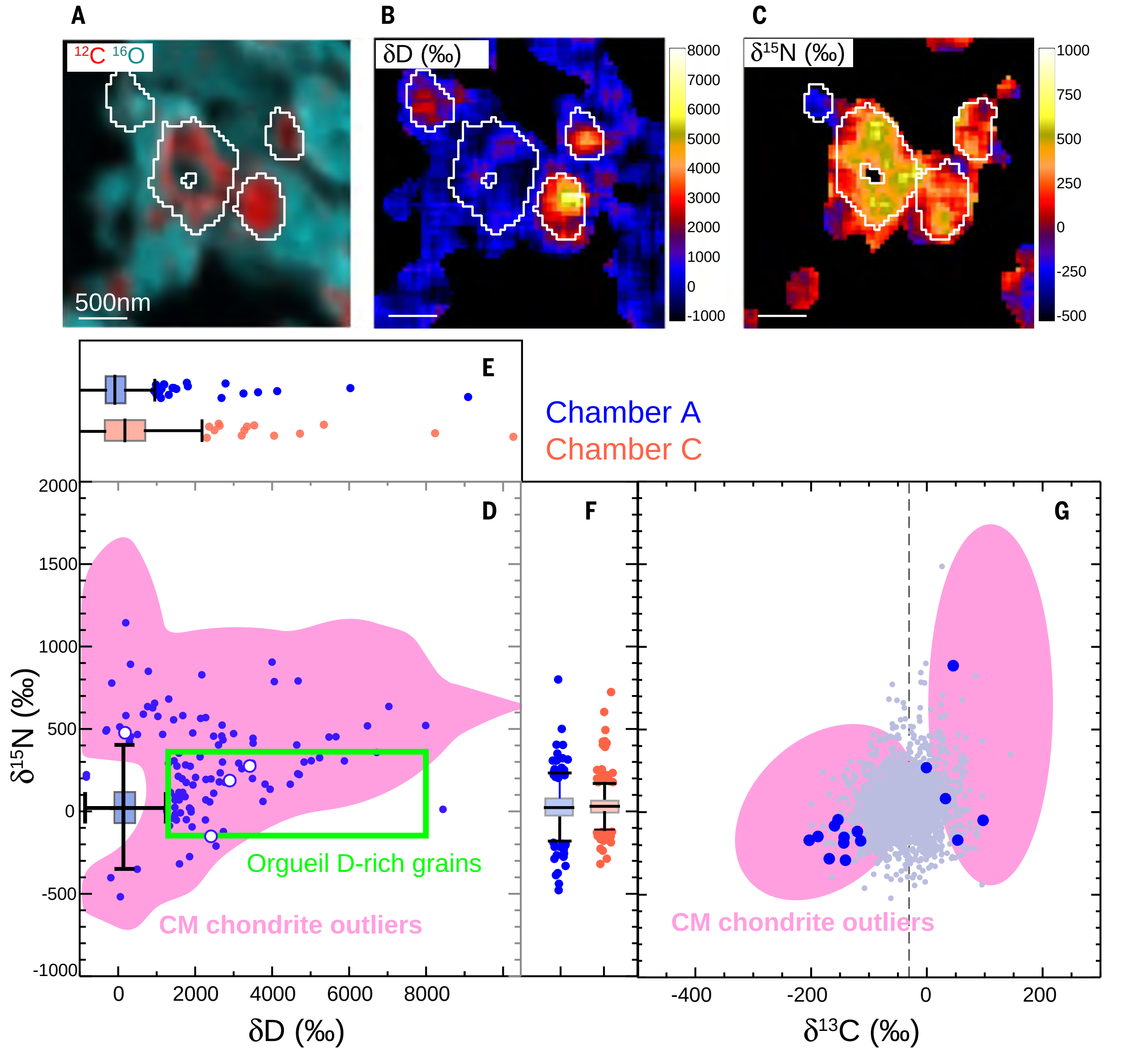

Fig. 6. NanoSIMS analysis of the intact Ryugu grains A0108 and C0109. (**A** to **C**) NanoSIMS images of an ~3 mm–by–3 mm area of a microtome slice from Ryugu grain A0108-11. (A) Map of ^{16}O (cyan) and ^{12}C (red). White outlines indicate four C-rich particles embedded in the silicate matrix. (B and C) Hydrogen (B) and nitrogen (C) isotope abundances of the same region. The ratios vary between the carbonaceous inclusions. (**D** to **F**) H and N isotopic ratios for individual C-rich particles [regions of interest (ROIs)] within Ryugu grains. Most ROIs are consistent (within the uncertainties) with the bulk averages; they are represented by box-and-whisker plots, where the box size represents the inner 50% of data around the median [interquartile range (IQR)] and the whiskers indicate the ±1.5 IQR range beyond that. Dots indicate outliers beyond those ranges (hotspots and coldspots) from A0108 (blue) and C0109 (orange). In (D), white dots indicate the grains shown in (A) to (C), and the error bar is 1σ. The distributions of H and N isotope ratios are consistent between (D) and those in (E) and (F) (acquired in different laboratories) and between the two Ryugu samples. The pink shaded region indicates the ranges of H and N hotspots and coldspots in primitive CM chondrite meteorites (*50*), and the green box indicates the ranges seen in CI chondrite Orgueil (*46*). The Ryugu outliers span a similar range to that of the CI and CM chondrites. (**G**) $\delta^{15}N$ as a function of $\delta^{13}C$ for the Ryugu grain A0109. The gray points indicate all C-rich ROIs, whereas blue circles are outliers (>2σ away from bulk average). The pink region is the same as in (D). The Ryugu outliers span a similar range to that seen in CM chondrites. The dashed vertical line indicates the bulk $\delta^{13}C$ of CI chondrite IOM.

of highly conjugated sp^2 carbon. Laboratory experiments have shown that aliphatic carbon in IOM from primitive carbonaceous chondrites is reduced after hydrous heating at 300°C for 6 days (*65*). Therefore, the higher abundance of aliphatic carbon in the organic residue of Ryugu—compared with that of primitive carbonaceous chondrites—indicates that the Ryugu grains did not experience short heating equivalent to the experimental conditions.

The distribution of organic functional groups present in the Ryugu samples is unlike aqueously altered carbonaceous chondrites, for which organic particles and nanoglobules show predominantly IOM-like XANES spectra with only occasional highly aromatic grains (*28*, *30*, *66*). Ryugu samples contain abundant aromatic-rich particles and nanoglobules, a high abundance of IOM-like diffuse carbon in matrix, and molecular carbonate associated with phyllosilicates. Progressive aqueous alteration in situ causes (i) an increase in the amount of diffuse organic matter associated with matrix phyllosilicates, (ii) an increase in the proportion of aromatic and oxygen-bearing functional groups in discrete organic particles and nanoglobules, and (iii) an increase in the variety of XANES spectral features. On the basis of these trends, much of the internal spectral variation in the Ryugu samples, including carbon grains with

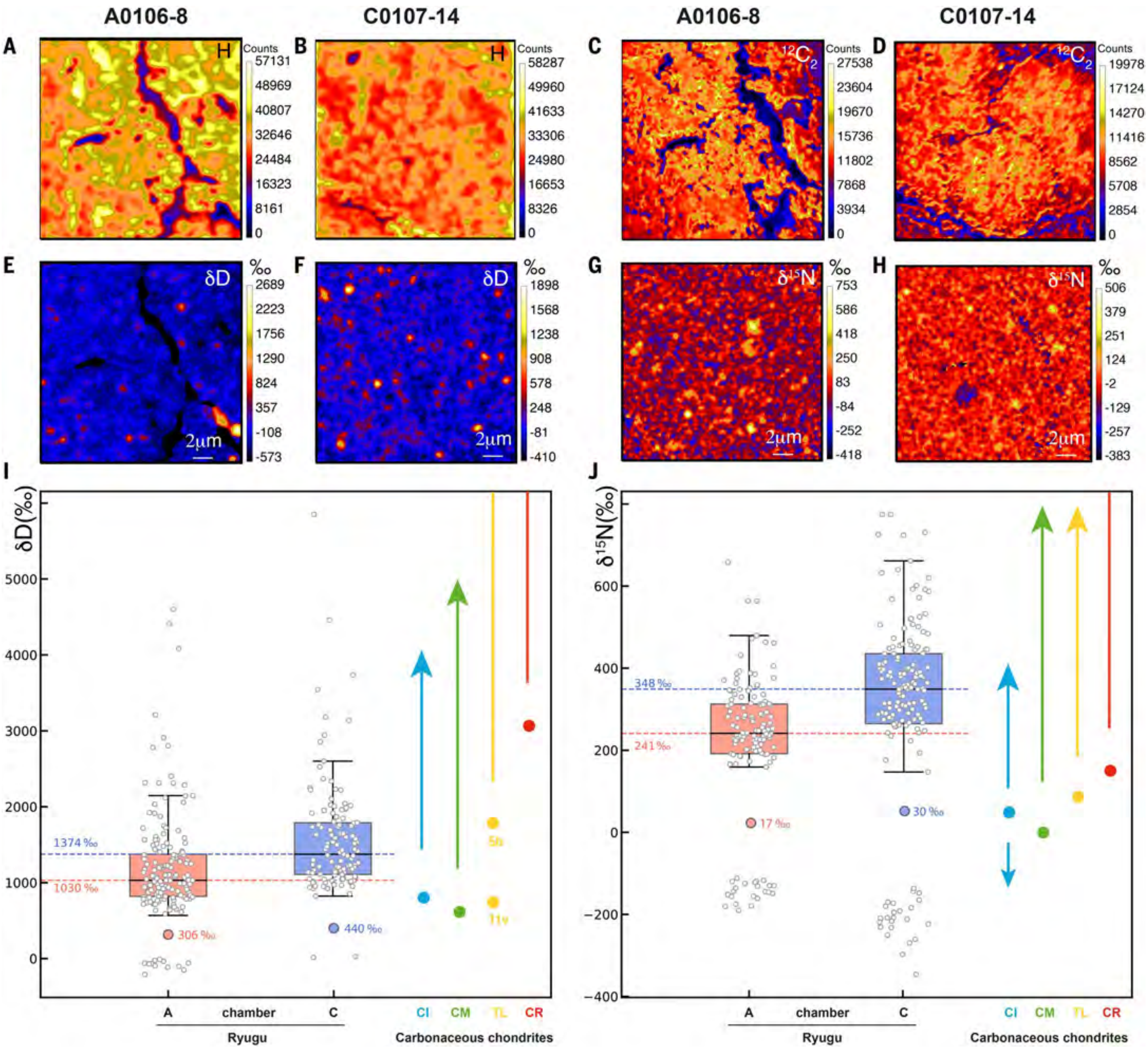

Fig. 7. NanoSIMS analysis of insoluble carbonaceous residues from Ryugu grains A0106 and C0107. (**A** to **D**) Hydrogen [(A) and (B)] and carbon [(C) and (D)] maps for insoluble carbonaceous residues of A0106 and C0107, respectively, acquired at the same locations. (**E** to **H**) The corresponding H [(E) and (F)] and N [(G) and (H)] isotope ratio maps show numerous micrometer-sized D-rich and ^{15}N-rich hotspots. The carbon and hydrogen images indicate that these hotspots consist of organic carbon. (**I** and **J**) Hydrogen (I) and nitrogen (J) box plot diagrams showing the distributions of isotope ratios in the insoluble carbonaceous residues A0106-8 (orange) and C0107-14 (blue). Open gray circles show hotspots (or coldspots), micrometer-sized areas with isotope ratios much higher (or lower) than the average composition. Large orange and blue circles indicate the bulk average value for each residue. Horizontal dashed lines indicate the mode of each distribution of hotspots. Data for the IOM of CI (light blue), CM (green), CR (red), and Tagish Lake (yellow) chondrites are shown for comparison. Filled circles are bulk values (*45*); for Tagish Lake, subsamples 5b (less altered) and 11v (altered) (*61*) are shown separately. Upward-pointing arrows (some extend beyond the plot) indicate the range of hotspots reported for those meteorites (*46*, *56*, *57*). For Orgueil, the downward arrow indicates the extent of ^{15}N-depleted coldspots.

an aromatic XANES spectral shape (Fig. 3E), likely developed through redistribution of organic matter and formation of additional organic molecules during aqueous alteration on the parent body rather than preaccretionary diversity inherited from the protosolar molecular cloud. Carbonaceous grains and nanoglobules with highly aromatic XANES spectra (not aromatic spectra; Fig. 3E) provide a possible exception to this proposal. These highly aromatic grains are more likely to represent original accreted materials because similar XANES spectra have been found in unaltered, petrologic type 3 carbonaceous chondrites (*30*) and in cometary dust particles (*32*). This is consistent with our observation of a large, highly aromatic nanoglobule containing D and ^{15}N isotopic anomalies (figs. S6 and S7).

The δD distributions of the C-rich particles in the Ryugu grains are consistent with those in the Tagish Lake meteorite (*56*) and CI and

CM chondrites (46, 57). The δD distributions of the Ryugu insoluble carbonaceous residues from chambers A and C are within the ranges of IOMs in the most and least altered fragments of Tagish Lake, respectively (61). The hydrogen isotopic variations among the different lithologies of Tagish Lake have previously been explained by depletion of D through hydrogen isotopic exchange or hydrolysis of D-rich structures of IOM during various degrees of planetesimal hydrothermal alteration (65, 67). By contrast, the δD distributions of our Ryugu samples are lower than those of less-altered CR chondrites (56), the most primitive class of IDPs (68), and comet-derived AMMs (33, 69). We therefore propose that Ryugu organic matter is a product of heterogeneous aqueous processing, which occurred on both C- and D-type asteroids, of the common primordial materials formed at an earlier stage of the solar nebula. The $\delta^{15}N$ distributions of the intact grains and insoluble residues from our Ryugu samples were within the ranges of C-rich particles (39, 56) and IOM (bulk) (61) in Tagish Lake and Comet Wild 2 (32) as well as CI and CM chondrites. However, they are lower than the $\delta^{15}N$ distributions of anhydrous IDPs (43, 68) and the IOM from CR chondrites (56). Nitrogen isotopic compositions are less affected than hydrogen isotopes by modification through parent body processes (45, 57, 61, 66), and their variations indicate mixing of different isotopic components from different precursors (53).

Nitrogen content can be an indicator of chemical evolution in the early Solar System. The measured N abundance (N/C = 0.01 to 0.035) of the insoluble carbonaceous residue in Ryugu samples is similar to that in primitive carbonaceous chondrites (45) and consistent with the total bulk N abundance (~0.15 wt %) (47). The N/C ratio of IOM from Tagish Lake (~0.042) is higher than those of the Ryugu samples. By contrast, some cometary materials, such as dust particles from Comet Wild 2, anhydrous AMMs, and ultracarbonaceous AMMs (UCAMMs), contain N-rich organics [N/C = 0.07 to 0.24 (32, 44, 70)]. Those are composed of a variety of nitrogen-bearing functional groups, such as imine, nitrile and/or heterocyclic N, or amide (32, 33, 44, 70, 71). The N contents of Comet 67P/Churyumov-Gerasimenko particles were heterogeneous (N/C = 0.018 to 0.06) (72) but lower than the N/C ratio of the Sun (0.3 ± 0.1) (73). The depletion of N in that comet might be because of the presence of ammonium salts (74, 75). These variations in N/C between different Solar System objects could arise from partitioning between gas and solid phases in the cold interstellar cloud or outer solar nebula or from exposure to the warmer inner Solar System during perihelion passage (74) rather than from processing in the interiors of planetesimals. Experiments simulating parent-body aqueous alteration show the N/C ratios in meteoritic IOMs are not substantially modified (65, 76). We therefore conclude that the N abundance in Ryugu macromolecular organic matter is intrinsic—not the product of extensive parent-body processing.

Conclusions

Our analysis of Ryugu samples indicates a direct link between macromolecular organic matter in C-type asteroids and that in primitive carbonaceous chondrites. The observed similarities and variations in molecular, isotopic, and morphological compositions between the Ryugu samples and other Solar System materials indicate a continuum of source material in the solar nebula, which was incorporated into C-type asteroids, D-type asteroids, and comets in the early Solar System. Macromolecular organic matter in the surface grains of asteroid Ryugu reflects various degrees of parent-body aqueous alteration and localized preservation of inherited nebular or molecular cloud history. The highly variable nature of the material indicates that the Ryugu organic matter is likely derived from material that was not subjected to long-term space weathering and was only recently exposed to the asteroid surface. The macromolecular organic matter shows no record of high-temperature impact heating of Ryugu, despite the asteroid being a rubble-pile body formed from impact debris and geomorphological evidence that it experienced subsequent impact cratering (2, 3). This observation is consistent with the homogeneous reflectance spectra of Ryugu's surface (3).

Ryugu materials are much darker than those from primitive carbonaceous chondrites, despite having similar carbon contents (23, 47), so some other factor (or factors) must determine the albedo. Possibilities include the macromolecular organic matter mixed with phyllosilicates (as discussed in this study) or nanophase sulfides (24), both of which have high light absorption efficiency owing to their small grain sizes. Such major, complex aromatic macromolecules in C- and/or D-type asteroids could have supplied the organic inventory and prebiotic molecules (47) that contributed to making Earth a habitable planet.

REFERENCES AND NOTES

1. S. Tachibana *et al.*, Hayabusa2: Scientific importance of samples returned from C-type near-Earth asteroid (162173) 1999 JU_3. *Geochem. J.* **48**, 571–587 (2014). doi: 10.2343/geochemj.2.0350
2. S. Watanabe *et al.*, Hayabusa2 arrives at the carbonaceous asteroid 162173 Ryugu—A spinning top–shaped rubble pile. *Science* **364**, 268–272 (2019). doi: 10.1126/science.aav8032; pmid: 30890588
3. S. Sugita *et al.*, The geomorphology, color, and thermal properties of Ryugu: Implications for parent-body processes. *Science* **364**, eaaw0422 (2019). doi: 10.1126/science.aaw0422; pmid: 30890587
4. K. Kitazato *et al.*, The surface composition of asteroid 162173 Ryugu from Hayabusa2 near-infrared spectroscopy. *Science* **364**, 272–275 (2019). doi: 10.1126/science.aav7432; pmid: 30890589
5. T. Morota *et al.*, Sample collection from asteroid (162173) Ryugu by Hayabusa2: Implications for surface evolution. *Science* **368**, 654–659 (2020). doi: 10.1126/science.aaz6306; pmid: 32381723
6. N. Sakatani *et al.*, Anomalously porous boulders on (162173) Ryugu as primordial materials from its parent body. *Nat. Astron.* **5**, 766–774 (2021). doi: 10.1038/s41550-021-01371-7
7. E. Tatsumi *et al.*, Spectrally blue hydrated parent body of asteroid (162173) Ryugu. *Nat. Commun.* **12**, 5837 (2021). doi: 10.1038/s41467-021-26071-8; pmid: 34611167
8. E. Tatsumi *et al.*, Collisional history of Ryugu's parent body from bright surface boulders. *Nat. Astron.* **5**, 39–45 (2021). doi: 10.1038/s41550-020-1179-z
9. T. Yada *et al.*, Preliminary analysis of the Hayabusa2 samples returned from C-type asteroid Ryugu. *Nat. Astron.* **6**, 214–220 (2021). doi: 10.1038/s41550-021-01550-6
10. C. Pilorget *et al.*, First compositional analysis of Ryugu samples by the MicrOmega hyperspectral microscope. *Nat. Astron.* **6**, 221–225 (2021). doi: 10.1038/s41550-021-01549-z
11. Materials and methods are available as supplementary materials.
12. S. Tachibana *et al.*, Pebbles and sand on asteroid (162173) Ryugu: In situ observation and particles returned to Earth. *Science* **375**, 1011–1016 (2022). doi: 10.1126/science.abj8624; pmid: 35143255
13. L. Bonal, E. Quirico, M. Bourot-Denise, G. Montagnac, Determination of the petrologic type of CV3 chondrites by Raman spectroscopy of included organic matter. *Geochim. Cosmochim. Acta* **70**, 1849–1863 (2006). doi: 10.1016/j.gca.2005.12.004
14. H. Busemann, C. M. O'D. Alexander, L. R. Nittler, Characterization of insoluble organic matter in primitive meteorites by microRaman spectroscopy. *Meteorit. Planet. Sci.* **42**, 1387–1416 (2007). doi: 10.1111/j.1945-5100.2007.tb00581.x
15. L. Bonal, E. Quirico, L. Flandinet, G. Montagnac, Thermal history of type 3 chondrites from the Antarctic meteorite collection determined by Raman spectroscopy of their polyaromatic carbonaceous matter. *Geochim. Cosmochim. Acta* **189**, 312–337 (2016). doi: 10.1016/j.gca.2016.06.017
16. E. Quirico *et al.*, Prevalence and nature of heating processes in CM and C2-ungrouped chondrites as revealed by insoluble organic matter. *Geochim. Cosmochim. Acta* **241**, 17–37 (2018). doi: 10.1016/j.gca.2018.08.029
17. G. R. Huss, A. E. Rubin, J. N. Grossman, in *Meteorites and the Early Solar System II*, D. S. Lauretta, H. Y. McSween, Eds. (Univ. Arizona Press, 2006), pp. 567–586.
18. T. Nakamura, Yamato 793321 CM chondrite: Dehydrated regolith material of a hydrous asteroid. *Earth Planet. Sci. Lett.* **242**, 26–38 (2006). doi: 10.1016/j.epsl.2005.11.040
19. T. Osawa, H. Kagi, T. Nakamura, T. Noguchi, Infrared spectroscopic taxonomy for carbonaceous chondrites from speciation of hydrous components. *Meteorit. Planet. Sci.* **40**, 71–86 (2005). doi: 10.1111/j.1945-5100.2005.tb00365.x
20. Y. Kebukawa, C. M. O'D. Alexander, G. D. Cody, Comparison of FT-IR spectra of bulk and acid insoluble organic matter in chondritic meteorites: An implication for missing carbon during demineralization. *Meteorit. Planet. Sci.* **54**, 1632–1641 (2019). doi: 10.1111/maps.13302
21. P. Beck *et al.*, Hydrous mineralogy of CM and CI chondrites from infrared spectroscopy and their relationship with low albedo asteroids. *Geochim. Cosmochim. Acta* **74**, 4881–4892 (2010). doi: 10.1016/j.gca.2010.05.020
22. D. Takir *et al.*, Nature and degree of aqueous alteration in CM and CI carbonaceous chondrites. *Meteorit. Planet. Sci.* **48**, 1618–1637 (2013). doi: 10.1111/maps.12171
23. T. Yokoyama *et al.*, Samples returned from the asteroid Ryugu are similar to Ivuna-type carbonaceous meteorites. *Science* **379**, eabn7850 (2023). doi: 10.1126/science.abn7850
24. T. Nakamura *et al.*, Formation and evolution of carbonaceous asteroid Ryugu: Direct evidence from returned samples. *Science* **379**, eabn8671 (2023). doi: 10.1126/science.abn8671
25. M. Gounelle, M. E. Zolensky, The Orgueil meteorite: 150 years of history. *Meteorit. Planet. Sci.* **49**, 1769–1794 (2014). doi: 10.1111/maps.12351
26. Y. Kebukawa, C. M. O'D. Alexander, G. D. Cody, Compositional diversity in insoluble organic matter in type 1, 2 and 3 chondrites as detected by infrared spectroscopy. *Geochim. Cosmochim. Acta* **75**, 3530–3541 (2011). doi: 10.1016/j.gca.2011.03.037

27. F.-R. Orthous-Daunay *et al*., Mid-infrared study of the molecular structure variability of insoluble organic matter from primitive chondrites. *Icarus* **223**, 534–543 (2013). doi: 10.1016/j.icarus.2013.01.003
28. C. Le Guillou, S. Bernard, A. J. Brearley, L. Remusat, Evolution of organic matter in Orgueil, Murchison and Renazzo during parent body aqueous alteration: In situ investigations. *Geochim. Cosmochim. Acta* **131**, 368–392 (2014). doi: 10.1016/j.gca.2013.11.020
29. L. R. Nittler *et al*., A cometary building block in a primitive asteroidal meteorite. *Nat. Astron.* **3**, 659–666 (2019). doi: 10.1038/s41550-019-0737-8
30. B. T. De Gregorio *et al*., Isotopic and chemical variation of organic nanoglobules in primitive meteorites. *Meteorit. Planet. Sci.* **48**, 904–928 (2013). doi: 10.1111/maps.12109
31. L. P. Keller *et al*., The nature of molecular cloud material in interplanetary dust. *Geochim. Cosmochim. Acta* **68**, 2577–2589 (2004). doi: 10.1016/j.gca.2003.10.044
32. B. T. De Gregorio *et al*., Isotopic anomalies in organic nanoglobules from Comet 81P/Wild 2: Comparison to Murchison nanoglobules and isotopic anomalies induced in terrestrial organics by electron irradiation. *Geochim. Cosmochim. Acta* **74**, 4454–4470 (2010). doi: 10.1016/j.gca.2010.05.010
33. T. Noguchi *et al*., Variation of mineralogy and organic material during the early stages of aqueous activity recorded in Antarctic micrometeorites. *Geochim. Cosmochim. Acta* **208**, 119–144 (2017). doi: 10.1016/j.gca.2017.03.034
34. L. A. J. Garvie, P. R. Buseck, Prebiotic carbon in clays from Orgueil and Ivuna (CI), and Tagish Lake (C2 ungrouped) meteorites. *Meteorit. Planet. Sci.* **42**, 2111–2117 (2007). doi: 10.1111/j.1945-5100.2007.tb01011.x
35. G. D. Cody *et al*., Organic thermometry for chondritic parent bodies. *Earth Planet. Sci. Lett.* **272**, 446–455 (2008). doi: 10.1016/j.epsl.2008.05.008
36. C. M. O'D. Alexander, G. D. Cody, B. T. De Gregorio, L. R. Nittler, R. M. Stroud, The nature, origin and modification of insoluble organic matter in chondrites, the major source of Earth's C and N. *Chem. Erde* **77**, 227–256 (2017). doi: 10.1016/j.chemer.2017.01.007; pmid: 31007270
37. D. D. Clayton, Origin of heavy xenon in meteoritic diamonds. *Astrophys. J.* **340**, 613–619 (1989). doi: 10.1086/167422
38. Z. R. Dai *et al*., Possible in situ formation of meteoritic nanodiamonds in the early Solar System. *Nature* **418**, 157–159 (2002). doi: 10.1038/nature00897; pmid: 12110882
39. K. Nakamura-Messenger, S. Messenger, L. P. Keller, S. J. Clemett, M. E. Zolensky, Organic globules in the Tagish Lake meteorite: Remnants of the protosolar disk. *Science* **314**, 1439–1442 (2006). doi: 10.1126/science.1132175; pmid: 17138898
40. T. Matsumoto *et al*., Three-dimensional observation and morphological analysis of organic nanoglobules in a carbonaceous chondrite using X-ray micro-tomography. *Geochim. Cosmochim. Acta* **116**, 84–95 (2013). doi: 10.1016/j.gca.2012.05.007
41. M. Hashiguchi, S. Kobayashi, H. Yurimoto, In situ observation of D-rich carbonaceous globules embedded in NWA 801 CR2 chondrite. *Geochim. Cosmochim. Acta* **122**, 306–323 (2013). doi: 10.1016/j.gca.2013.08.007
42. C. Le Guillou, A. Brearley, Relationships between organics, water and early stages of aqueous alteration in the pristine CR3.0 chondrite MET 00426. *Geochim. Cosmochim. Acta* **131**, 344–367 (2014). doi: 10.1016/j.gca.2013.10.024
43. G. Matrajt, S. Messenger, D. Brownlee, D. Joswiak, Diverse forms of primordial organic matter identified in interplanetary dust particles. *Meteorit. Planet. Sci.* **47**, 525–549 (2012). doi: 10.1111/j.1945-5100.2011.01310.x
44. H. Yabuta *et al*., Formation of an ultracarbonaceous Antarctic micrometeorite through minimal aqueous alteration in a small porous icy body. *Geochim. Cosmochim. Acta* **214**, 172–190 (2017). doi: 10.1016/j.gca.2017.06.047
45. C. M. O'D. Alexander, M. Fogel, H. Yabuta, G. D. Cody, The origin and evolution of chondrites recorded in the elemental and isotopic compositions of their macromolecular organic matter. *Geochim. Cosmochim. Acta* **71**, 4380–4403 (2007). doi: 10.1016/j.gca.2007.06.052
46. L. Remusat, Y. Guan, Y. Wang, J. M. Eiler, Accretion and preservation of D-rich organic particles in carbonaceous chondrites: Evidence for important transport in the early Solar System nebula. *Astrophys. J.* **713**, 1048–1058 (2010). doi: 10.1088/0004-637X/713/2/1048
47. H. Naraoka *et al*., Soluble organic molecules in samples of the carbonaceous asteroid (162173) Ryugu. *Science* **379**, eabn9033 (2023). doi: 10.1126/science.abn9033
48. R. Okazaki *et al*., Noble gases and nitrogen in samples of asteroid Ryugu record its volatile sources and recent surface evolution. *Science* **379**, eabo0431 (2023). doi: 10.1126/science.abo0431
49. J. F. Kerridge, Carbon, hydrogen and nitrogen in carbonaceous chondrites: Abundances and isotopic compositions in bulk samples. *Geochim. Cosmochim. Acta* **49**, 1707–1714 (1985). doi: 10.1016/0016-7037(85)90141-3; pmid: 11539652
50. L. R. Nittler, C. M. O'D. Alexander, M. J. Verdier-Paoletti, paper presented at the 84th Annual Meeting of the Meteoritical Society, Chicago, IL, 15 to 21 August 2021.
51. Y. Aikawa, G. J. van Zadelhoff, E. F. van Dishoeck, E. Herbst, Warm molecular layers in protoplanetary disks. *Astron. Astrophys.* **386**, 622–632 (2002). doi: 10.1051/0004-6361:20020037
52. N. Watanabe, A. Kouchi, Ice surface reactions: A key to chemical evolution in space. *Prog. Surf. Sci.* **83**, 439–489 (2008). doi: 10.1016/j.progsurf.2008.10.001
53. J. Aléon, Multiple origins of nitrogen isotopic anomalies in meteorites and comets. *Astrophys. J.* **722**, 1342–1351 (2010). doi: 10.1088/0004-637X/722/2/1342
54. R. Terzieva, E. Herbst, The possibility of nitrogen isotopic fractionation in interstellar clouds. *Mon. Not. R. Astron. Soc.* **317**, 563–568 (2000). doi: 10.1046/j.1365-8711.2000.03618.x
55. E. K. Zinner, in *Meteorites, Comets, and Planets*, A. M. Davis, Ed. (Elsevier, 2005), pp. 17–39.
56. H. Busemann *et al*., Interstellar chemistry recorded in organic matter from primitive meteorites. *Science* **312**, 727–730 (2006). doi: 10.1126/science.1123878; pmid: 16675696
57. L. Remusat, J.-Y. Bonnet, S. Bernard, A. Buch, E. Quirico, Molecular and isotopic behavior of insoluble organic matter of the Orgueil meteorite upon heating. *Geochim. Cosmochim. Acta* **263**, 235–247 (2019). doi: 10.1016/j.gca.2019.07.013
58. C. Floss, F. Stadermann, Auger nanoprobe analysis of presolar ferromagnesian silicate grains from primitive CR chondrites QUE 99177 and MET 00426. *Geochim. Cosmochim. Acta* **73**, 2415–2440 (2009). doi: 10.1016/j.gca.2009.01.033
59. C. Vollmer *et al*., A primordial ^{15}N-depleted organic component detected within the carbonaceous chondrite Maribo. *Sci. Rep.* **10**, 20251 (2020). doi: 10.1038/s41598-020-77190-z; pmid: 33219224
60. T. Hiroi, M. E. Zolensky, C. M. Pieters, The Tagish Lake meteorite: A possible sample from a D-type asteroid. *Science* **293**, 2234–2236 (2001). doi: 10.1126/science.1063734; pmid: 11520950
61. C. D. K. Herd *et al*., Origin and evolution of prebiotic organic matter as inferred from the Tagish Lake meteorite. *Science* **332**, 1304–1307 (2011). doi: 10.1126/science.1203290; pmid: 21659601
62. C. M. Gilmour, C. D. K. Herd, P. Beck, Water abundance in the Tagish Lake meteorite from TGA and IR spectroscopy: Evaluation of aqueous alteration. *Meteorit. Planet. Sci.* **54**, 1951–1972 (2019). doi: 10.1111/maps.13362
63. A. Gardinier *et al*., Solid state CP/MAS ^{13}C NMR of the insoluble organic matter of the Orgueil and Murchison meteorites: Quantitative study. *Earth Planet. Sci. Lett.* **184**, 9–21 (2000). doi: 10.1016/S0012-821X(00)00300-9
64. G. D. Cody, C. M. O'D. Alexander, F. Tera, Solid-state (^{1}H and ^{13}C) nuclear magnetic resonance spectroscopy of insoluble organic residue in the Murchison meteorite: A self-consistent quantitative analysis. *Geochim. Cosmochim. Acta* **66**, 1851–1865 (2002). doi: 10.1016/S0016-7037(01)00888-2
65. H. Yabuta, L. B. Williams, G. D. Cody, C. M. O'D. Alexander, S. Pizzarello, The insoluble carbonaceous material of CM chondrites: A possible source of discrete organic compounds under hydrothermal conditions. *Meteorit. Planet. Sci.* **42**, 37–48 (2007). doi: 10.1111/j.1945-5100.2007.tb00216.x
66. V. Vinogradoff *et al*., Paris vs. Murchison: Impact of hydrothermal alteration on organic matter in CM chondrites. *Geochim. Cosmochim. Acta* **212**, 234–252 (2017). doi: 10.1016/j.gca.2017.06.009
67. Y. Oba, H. Naraoka, Elemental and isotope behavior of macromolecular organic matter from CM chondrites during hydrous pyrolysis. *Meteorit. Planet. Sci.* **44**, 943–953 (2009). doi: 10.1111/j.1945-5100.2009.tb00779.x
68. S. Messenger, Identification of molecular-cloud material in interplanetary dust particles. *Nature* **404**, 968–971 (2000). doi: 10.1038/35010053; pmid: 10801119
69. J. Duprat *et al*., Extreme deuterium excesses in ultracarbonaceous micrometeorites from central Antarctic snow. *Science* **328**, 742–745 (2010). doi: 10.1126/science.1184832; pmid: 20448182
70. G. D. Cody *et al*., Quantitative organic and light-element analysis of comet 81P/Wild 2 particles using C-, N-, and O-μ-XANES. *Meteorit. Planet. Sci.* **43**, 353–365 (2008). doi: 10.1111/j.1945-5100.2008.tb00627.x
71. E. Dartois *et al*., Ultracarbonaceous Antarctic micrometeorites, probing the Solar System beyond the nitrogen snow-line. *Icarus* **224**, 243–252 (2013). doi: 10.1016/j.icarus.2013.03.002
72. N. Fray *et al*., Nitrogen-to-carbon atomic ratio measured by COSIMA in the particles of comet 67P/Churyumov–Gerasimenko. *Mon. Not. R. Astron. Soc.* **469**, S506–S516 (2017). doi: 10.1093/mnras/stx2002
73. K. Lodders, in *Principles and Perspectives in Cosmochemistry*, A. Goswami, B. E. Reddy, Eds. (Springer, 2010), pp. 379–417.
74. O. Poch *et al*., Ammonium salts are a reservoir of nitrogen on a cometary nucleus and possibly on some asteroids. *Science* **367**, eaaw7462 (2020). doi: 10.1126/science.aaw7462; pmid: 32165559
75. K. Altwegg *et al*., Evidence of ammonium salts in comet 67P as explanation for the nitrogen depletion in cometary comae. *Nat. Astron.* **4**, 533–540 (2020). doi: 10.1038/s41550-019-0991-9
76. H. Naraoka *et al*., A chemical sequence of macromolecular organic matter in the CM chondrites. *Meteorit. Planet. Sci.* **39**, 401–406 (2004). doi: 10.1111/j.1945-5100.2004.tb00101.x

ACKNOWLEDGMENTS

We thank the anonymous reviewers for their helpful comments. The Hayabusa2 spacecraft was developed and built under the leadership of JAXA, with contributions from the German Aerospace Center (DLR) and the Centre National d'Études Spatiales (CNES) and in collaboration with NASA; Nagoya University; University of Tokyo; National Astronomical Observatory of Japan (NAOJ); University of Aizu; Kobe University; and other universities, institutes, and companies in Japan. We thank the many engineers, including N. Inaba at JAXA and T. Masuda, S. Yasuda, K. Matsushima, and T. Ohshima at NEC Corporation for their dedicated work on the Hayabusa2 mission. The STXM data were acquired at beam line 19A of the Photon Factory, High Energy Accelerator Research Organization, and at beam line 5.3.2.2 of the Advanced Light Source (ALS), Lawrence Berkeley National Laboratory. Use of the ALS was supported by the Department of Energy (contract no. DE-AC02-05CH11231). The synchrotron FTIR data were acquired at the SMIS beamline of SOLEIL. The NanoSIMS facility at Muséum National d'Histoire Naturelle (MNHN) in Paris was established by funds from the CNRS, Région Ile de France, Ministère délégué à l'Enseignement supérieur et à la Recherche, and the Muséum National d'Histoire Naturelle. The FIB facility at the University of Tokyo is supported by the Advanced Characterization Nanotechnology Platform in the Nanotechnology Platform Project sponsored by the Ministry of Education, Culture, Sports, Science and Technology (MEXT), Japan. We thank N. Sugimura at Waseda University, Y. Fujioka at Tohoku University, and C. Sandt and F. Borondics at SOLEIL for technical support. We thank S. Kawakami at Gifu Shotoku University, T. Fagan at Waseda University, M. E. Zolensky at NASA Johnson Space Center, MNHN, and B. Fectay and C. Bidaut for providing the meteorite samples used in this study. **Funding:** H.Yab. was supported by KAKENHI from the Japan Society for the Promotion of Science (JSPS) (grant nos. JP20H05846, 19H01954, 18H04461, and 20H04615) and the Astrobiology Center Program of the National Institutes of Natural Sciences (NINS) (grant nos. AB312007, AB022001, and AB032004). Y.Taka., Y.Takeic., Y.K., H.Su., S.Y., and D.W. were supported by KAKENHI from JSPS (grant no. JP17H06458). H.Yab., Y.K., M.Has., and H.Su. were supported by the JSPS Core-to-Core program "International Network of Planetary Sciences." L.Bo. and E.Q. acknowledge funding from the Centre National d'Etudes Spatiales (CNES-France). L.R. acknowledges funding from the European Research Council through the consolidator grant HYDROMA (grant agreement no. 819587). C.E., J.D., E.D., and J.M. acknowledge funding from CNES (MIAMI2), DIM-ACAV+ (C3E), LabEx P2IO, PCMI, and ANR (COMETOR ANR-18-CE31-0011). R.S. and B.D.G. acknowledge funding from NASA awards 80HQTR20T0014 and 80HQTR20T0050. L.N. acknowledges funding from NASA grants NNX16AK72G and 80NSSC20K0340. A.D., A.D.-B., and J.M. acknowledge funding from Paris Ile-de-France Region-DIM "Matériaux anciens et patrimoniaux." Centro de Química Estrutural (Z.M.) acknowledges the financial support of Fundação para a Ciência e Tecnologia (FCT) (grants UIDB/00100/2020, UIDP/00100/2020, and LA/P/0056/2020). **Author contributions:** H.Yab. led the research and wrote the paper with contributions from L.N., B.D.G., R.S., L.R., L.Bo., Y.K., and G.D.C. Sample preparation for the research: H.Yab., B.D.G., T.Oku., M.Has., C.E., L.Bo., M.Matsum., Y.E., K.Kam., and M.S.; Raman analyses: L.Bo., M.K., E.Q., G.M., and Y.K.; FTIR analyses: Y.K., E.Q., E.D., L.Bo., C.E., and J.D.; STXM analyses: B.D.G., H.Yab., Y.K., G.C., D.K., S.Sa.,

R.S., Y.Taka., T.Oh., H.Su., Y.Take., S.Y., D.W., and Y.Tam.; STEM-EELS-EDS analyses: R.S.; AFM-IR analyses: J.M., A.D., A.D.-B., E.D., C.E., J.D., and L.Be.; NanoSIMS analyses: L.R., L.N., M.V.-P., S.M., and J.Ba.; Interpretation and writing: H.Yab., L.N., R.S., B.D.G., R.L., L.B., Y.K., E.D., J.M., E.Q., M.K., G.D.C., C.E., S.Su., T.Oku., M.Has., and S.Tac.; Administration of the initial analysis: S.Tac., H.Yu., T.Na., T.No., R.O., H.Yab., H.Na., K.Sa., H.C.C., and D.S.L.; Sample curation: M.Ab., T.Oka., T.Yad., M.N., K.Yog., A.N., M.Yoshit., A.I., A.Miy., S.F., K.Hata., H.So., Y.H., K.Ku., T.U., T.H., D.Y., and R.F.; Sample collection at Ryugu: Y.Ts., T.S., F.T., S.Tan., M.O., R.T., H.Yan., H.Sa., M.Hay., T.I., S.H., Y.-i.I., A.F., Y.Takei., K.Yoshik., Y.M., G.O., H.T., N.O., S.K., K.S., Y.Ya., H.I., K.Ka., K.Yoshih., T.Yam., H.No., A.Miu., S.Su., K.Ki., Nao.H., R.H., T.Mo., E.T., T.O., N.Sa., N.N., K.M., R.N., K.W., H.Se., K.Ot., Y.Yo., Y.I., Y.S., M.Ya., C.H., T.Mi., M.Matsuo., Nar.H., M.Ar., C.O., M.I., H.Yan., S.Tac., R.O., S.W., T.Na., H.Yab., R.J., J.-P.B., M.G., S.Sc., K.Og., C.P., N.Sc., J.B., T.-M.H., and A.M.-S.; Project management: Y.Ts., S.W., M.Yoshik., M.F., and S.N. All authors discussed the results and commented on the manuscript. **Competing interests:** The authors declare that they have no competing interests. **Data and materials availability:** All images used in this study and machine-readable data files are available at the JAXA Data Archives and Transmission System (DARTS) at https://data.darts.isas.jaxa.jp/pub/hayabusa2/paper/sample/Yabuta_2022/. Data for all Hayabusa2 samples and other data from the mission are available at the DARTS archive at https://www.darts.isas.jaxa.jp/curation/hayabusa2 and https://www.darts.isas.jaxa.jp/planet/project/hayabusa2/, respectively. The samples of Ryugu are curated by the JAXA Astromaterials Science Research Group; distribution for analysis is through an Announcement of Opportunity available at https://jaxa-ryugu-sample-ao.net. The samples we used are listed in table S1.

SUPPLEMENTARY MATERIALS

science.org/doi/10.1126/science.abn9057
Materials and Methods
Supplementary Text
Figs. S1 to S8
Tables S1 to S3
References (*77*–*85*)

Submitted 29 December 2021; accepted 21 December 2022
10.1126/science.abn9057

Macromolecular organic matter in samples of the asteroid (162173) Ryugu

Hikaru Yabuta, George D. Cody, Ccile Engrand, Yoko Kebukawa, Bradley De Gregorio, Lydie Bonal, Laurent Remusat, Rhonda Stroud, Eric Quirico, Larry Nittler, Minako Hashiguchi, Mutsumi Komatsu, Taiga Okumura, Jrmie Mathurin, Emmanuel Dartois, Jean Duprat, Yoshio Takahashi, Yasuo Takeichi, David Kilcoyne, Shohei Yamashita, Alexandre Dazzi, Ariane Deniset-Besseau, Scott Sandford, Zita Martins, Yusuke Tamenori, Takuji Ohigashi, Hiroki Suga, Daisuke Wakabayashi, Maximilien Verdier-Paoletti, Smail Mostefaoui, Gilles Montagnac, Jens Barosch, Kanami Kamide, Miho Shigenaka, Laure Bejach, Megumi Matsumoto, Yuma Enokido, Takaaki Noguchi, Hisayoshi Yurimoto, Tomoki Nakamura, Ryuji Okazaki, Hiroshi Naraoka, Kanako Sakamoto, Harold C. Connolly, Jr., Dante S. Lauretta, Masanao Abe, Tatsuaki Okada, Toru Yada, Masahiro Nishimura, Kasumi Yogata, Aiko Nakato, Miwa Yoshitake, Ayako Iwamae, Shizuho Furuya, Kentaro Hatakeda, Akiko Miyazaki, Hiromichi Soejima, Yuya Hitomi, Kazuya Kumagai, Tomohiro Usui, Tasuku Hayashi, Daiki Yamamoto, Ryota Fukai, Seiji Sugita, Kohei Kitazato, Naru Hirata, Rie Honda, Tomokatsu Morota, Eri Tatsumi, Naoya Sakatani, Noriyuki Namiki, Koji Matsumoto, Rina Noguchi, Koji Wada, Hiroki Senshu, Kazunori Ogawa, Yasuhiro Yokota, Yoshiaki Ishihara, Yuri Shimaki, Manabu Yamada, Chikatoshi Honda, Tatsuhiro Michikami, Moe Matsuoka, Naoyuki Hirata, Masahiko Arakawa, Chisato Okamoto, Masateru Ishiguro, Ralf Jaumann, Jean-Pierre Bibring, Matthias Grott, Stefan Schrder, Katharina Otto, Cedric Pilorget, Nicole Schmitz, Jens Biele, Tra-Mi Ho, Aurlie Moussi-Soffys, Akira Miura, Hirotomo Noda, Tetsuya Yamada, Keisuke Yoshihara, Kosuke Kawahara, Hitoshi Ikeda, Yukio Yamamoto, Kei Shirai, Shota Kikuchi, Naoko Ogawa, Hiroshi Takeuchi, Go Ono, Yuya Mimasu, Kent Yoshikawa, Yuto Takei, Atsushi Fujii, Yu-ichi Iijima, Satoru Nakazawa, Satoshi Hosoda, Takahiro Iwata, Masahiko Hayakawa, Hirotaka Sawada, Hajime Yano, Ryudo Tsukizaki, Masanobu Ozaki, Fuyuto Terui, Satoshi Tanaka, Masaki Fujimoto, Makoto Yoshikawa, Takanao Saiki, Shogo Tachibana, Sei-ichiro Watanabe, and Yuichi Tsuda

Science, **379** (6634), eabn9057.
DOI: 10.1126/science.abn9057

Science

Supplementary Materials for

Macromolecular organic matter in samples of the asteroid (162173) Ryugu

Hikaru Yabuta *et al*.

Corresponding author: Hikaru Yabuta, hyabuta@hiroshima-u.ac.jp

Science **379**, eabn9057 (2023)
DOI: 10.1126/science.abn9057

The PDF file includes:

Materials and Methods

Samples

Aggregate samples of Ryugu grains (A0108 and C0109) were allocated to the Organic Macromolecule sub-team in the Hayabusa2 Initial Analysis Team. The samples were transported from the JAXA Extraterrestrial Samples Curation Center in Sagamihara, Japan, to Hiroshima University for sample preparation and distribution. We carried out a multi-technique study of the A0108 and C0109 samples to reveal the compositional diversities and organics-minerals associations (Fig. S1). Some of the grains were crushed on a diamond window for micro-Fourier transform infrared (FTIR) spectroscopy, micro-Raman spectroscopy, atomic force microscope-based infrared (AFM-IR) spectroscopy, and nanometer-scale secondary ion mass spectrometry (NanoSIMS). Slices of other grains were prepared with a focused ion beam workstation (FIB) and/or an ultramicrotome to obtain ultra-thin sections for scanning transmission X-ray microscopy (STXM), X-ray absorption near edge structure (XANES), scanning transmission electron microscopy (STEM) coupled with electron energy loss spectroscopy (EELS) and energy dispersive X-ray spectroscopy (EDS), AFM-IR, and NanoSIMS. Details on the individual analytical procedures in the analytical protocols (Fig. S1) are described in the following subsections.

In addition to the A0108 and C0109 samples, the residues of other aggregate Ryugu samples (A0106 and C0107), which were yielded after solvent extraction (*47*), were transferred to the Organic Macromolecule sub-team. We used the A0106 and C0107 samples to isolate insoluble carbonaceous residues from the aggregate samples by acid treatment. We analyzed the insoluble carbonaceous residues by micro-FTIR spectroscopy, STXM-XANES, STEM-EELS-EDS, and NanoSIMS to reveal the average compositions of macromolecular organic matter in Ryugu samples. The Ryugu samples used are summarized in Table S1. We assigned a sub-sample number to each grain of aggregate samples and insoluble carbonaceous residues. After the initial analysis was ended on May 31, 2022, all the Ryugu samples used were returned to JAXA.

We analyzed meteorite samples by micro-FTIR spectroscopy and micro-Raman spectroscopy for comparison (Table S2). Insoluble organic matter (IOM) from the Orgueil meteorite and Queen Alexandra Range (QUE) 99177 meteorite were used as standards in the NanoSIMS measurements.

Acid treatment for demineralization

To isolate insoluble carbonaceous residues from the intact Ryugu samples, demineralization of the Ryugu samples were conducted. After the intact Ryugu aggregates (A0106 and C0107) were extracted with solvent and water (*47*), the extracted residues of A0106 (13.08 mg) and C0107 (10.73 mg) in the two Teflon microtubes (1.5 ml) were hand-carried from Kyushu University. The acid treatment was conducted in a custom-made acid resistant clean bench (NSY-8751Ch, AIRTECH) at Hiroshima University. The residues were treated with an 6M HCl solution in high-purity water in Teflon microtubes at room temperature for ~ 48 h with stirring and followed by 9M HF/1M HCl treatment (> 48 h). The process was repeated three times and was followed by 1M HCl rinses, high-purity water rinses, and one last methanol rinse. The acid-insoluble carbonaceous residues in methanol were transferred to a Mini Vial (ACE Glass), dried at ~55°C on a hotplate, and recovered (Fig. S2). The yields of the insoluble residues were not weighed, however approximately 150 μg was obtained from A0106 and larger amounts of the residues were obtained from C0107.

Hydrofluoric acid (HF) (48% solution, guaranteed reagent), hydrochrolic acid (HCl) (38% solution, for amino acid automated analysis), and methanol (99.8+%, super special grade) were purchased from FUJIFILM Wako Chemicals. High-purity water was used for rinses and dilution of acids. Glass mini vials were heated to 500 °C for 4.5 hours in air before use.

Focused ion beam (FIB)

For STXM and TEM analyses, ultra-thin sections of Ryugu intact grains and their isolated acid-insoluble carbonaceous residue were prepared with an FB-2100 focused ion beam (FIB) system (Hitachi) at the University of Tokyo. The sample was pressed into a clean gold disk (~3 mm diameter, 100 μm thickness) using an in-house jig made by diamond glass and SUS304 to obtain flatness for the sample surface. Before the pressing, the gold disk was washed with methanol/dichloromethane and Milli-Q water and then heated at 500 ºC for 3 h. To avoid contamination from the surrounding air, the sample preparation was performed in a clean bench and the sample was stored in a N_2 or Ar gas-filled environment before/after the sample preparation. The samples were locally coated by the deposition of tungsten to prevent beam damage during fabrication and trimmed using a gallium ion beam of 30 kV, and then thinned down to be X-ray-transparent with a low energy beam of 10 kV. The thin sections were processed with a low-energy argon ion milling system (Model 1040 NanoMill, Fischione) operated at 2000, 900, and 500 V as a final process.

Additional ultra-thin sections of Ryugu intact grains were prepared for STXM and TEM analyses with a Thermo Fisher Helios G3 DualBeam FIB at U.S. Naval Research Laboratory. Individual grains were picked up using a freshly made glass needle and deposited on double-sided copper sticky tape on a standard 0.5 inch SEM pin mount. Sample mounts were coated with ~25 nm amorphous carbon to minimize charging. Ultra-thin lamellae were extracted and shaped by sputtering with 30 keV Ga^+ ions using typical FIB liftout protocols, with the exception that no electron imaging was performed on the lamellae after their thickness was less than 1.5 μm to avoid possible radiolysis damage to organic matter by the 5 keV electron beam (*77*). Ion-assisted carbon deposition was used for the protective cover layer. Lamellae were attached to copper half grids with ion-assisted platinum deposition before thinning to a final thickness of <100 nm. Once an adequate sample thickness was achieved, the lamellae were given a final cleaning step of 8 keV Ga+ ions on each side.

Ultramicrotomy

The Ryugu intact grains and their isolated acid-insoluble carbonaceous residue particles were picked up by freshly made glass needles and placed in molten droplets of sulfur kept at 114 °C by a heated glass plate. Needle micromanipulation and monitoring/recording of this operation was done using an EXpressLO ex-situ liftout system. Once the heat source was removed, the sulfur crystallized around the grains, and the entire droplet was attached to an 8 mm epoxy block with a thin layer of cyanoacrylate adhesive. Ultramicrotomy was performed using a diamond knife in a Leica EM UC6 microtome. Sections were created at various thicknesses and substrates depending on the analytical technique. 250 nm sections were placed on 5 × 5 mm diced silicon wafer chips for NanoSIMS measurements. 70 nm sections were placed on lacey carbon support films on 200 mesh copper TEM grids for both STXM and TEM analysis.

Raman spectroscopy

Raman characterization was performed independently by two groups in France and in Japan on distinct Ryugu particles. Raman point analyses were performed on several fragments of six particles from chamber A aggregates (A0108-5, 6, 7, 10, 17, and 18) and six particles from chamber C aggregates (C0109-1, 5, 9, 12, 15, and 16). To combine in situ IR and NanoSIMS measurements on the same samples, fragments of particles were manually selected under a binocular and pressed onto diamond windows. The Raman spectra were acquired with a 532 nm laser in both Japan and France. In France, Raman measurements were performed at the Ecole Normale Supérieure de Lyon (Laboratoire de Géologie de Lyon—Terre, Planètes, Environnement) using a LabRam Raman spectrometer (Horiba Jobin-Yvon) equipped with a 600 grooves per millimeter grating. The laser was focused through a 100× objective to obtain a < 2 µm spot size. The power on the sample was 0.3 mW. Each acquisition comprised six integrations of 15 s that were averaged to make the final spectrum. In Japan, a Renishaw InVia Reflex equipped with a 1800 grooves per millimeter grating at the Materials Characterization Central Laboratory was used at Waseda University. The laser was focused at the sample surface through a 50× objective (spot size ~ 3-4 µm) and its power was set at 0.24 mW and 1 mW. Each acquisition comprised five integrations of 10 s that were combined to produce the final spectrum.

The analytical procedure follows two main steps (i) subtraction of the fluorescence backgrounds assuming a linear shape within the 1000–1700 cm^{-1} range and (ii) fitting the D- and G- Raman bands with models consisting of a Breit–Wigner–Fano and Lorentzian profiles, respectively. The position, maximum intensity, peak intensity and full width at half maximum of the D- and G-bands were determined for each spectrum. For every sample, the mean value and standard deviation of each of these parameters were calculated. The chondritic data shown in Fig. 1 for comparison with Ryugu samples were acquired and processed in the exact same conditions as those applied to Ryugu samples. The analytical procedure we applied for the present work is similar to one used previously (*16*). Due to a higher fluorescence background, the spectral range considered for the analytical procedure was slightly reduced: the numerical values of the considered spectral parameters therefore differ from previous measurements *(16)*. The data shown in Fig. 1 were acquired by the group in France. Because Raman spectroscopy on carbonaceous material is dispersive and because the Raman experimental setup used in France and in Japan are different, the spectral parameters obtained independently cannot be easily merged: the values of the spectral parameters are distinct. However, the data obtained are consistent (fig. S3): the spectral parameters obtained on the intact Ryugu samples in Japan are similar to those from primitive type 1 and type 2 chondrites.

Micro-FTIR spectroscopy

Fourier transform infrared microspectroscopy (micro-FTIR) measurements at Yokohama National University were conducted using the following procedures. Chamber A and Chamber C aggregates (A0108-5, A0108-7, A0108-17, C0109-1, C0109-15, and C0109-16) were hand-carried from Hiroshima University in between hole-glass slides. Each particle (sub-millimeter in diameter) was decomposed by gently crushing between two glass slides, and then the small fragments were pressed between two diamond windows under an optical microscope in a clean hood. For the acid-insoluble carbonaceous residues of Ryugu A0106 and C0107, sample particles were pressed between diamond windows (without pre-crushing). IR absorption spectra were collected from each diamond window with a micro-FTIR (JASCO FT/IR-6100+IRT-5200), equipped with a ceramic IR light source, a germanium-coated KBr beam splitter, a mercury-cadmium-telluride (MCT) detector, and ×16 optical Cassegrain mirrors. The microscope and the FTIR were continuously purged with dry N_2. To remove adsorbed water from the samples, a heating stage (Linkam 10036L) was employed for intact Ryugu aggregates at 60 °C with N_2 flow. At each spot, 128 to 1024 scans of IR transmission spectra were accumulated with a wavenumber resolution of 4 cm^{-1} and with a 20 × 20 to 30 × 30 µm aperture. Typically, spectra from 5 to 20 spots were obtained for each sample and averaged. The Jbilet Winselwan, Murchison, and Ivuna meteorites were analyzed with the same protocol for comparison (except that the spectrum of Jbilet Winselwan was obtained at 80 °C).

Fourier transform infrared microspectroscopy (micro-FTIR) measurements in France were conducted by means of the following procedures. Chamber A and Chamber C aggregates (A0108-15, A0108-19, C0109-4, C0109-10) as well as particles from insoluble acid residues of Ryugu A0106 and C0107 were received by international express shipping from Hiroshima University in between cavity-glass slides. A fragment of each sample (sub-millimeter in size) was gently flattened between two diamond windows in a homemade diamond cell, and the crushing was controlled using an optical/infrared microscope maintained under dry air. Conventional Fourier transform infrared microscopy measurements of chamber A samples (A0108-15 and A0108-19) and chamber C samples (C0109-04 and C0109-10) were performed on the Spectroscopie et Microscopie dans l'Infrarouge avec le Synchrotron (SMIS) beam line at the French national synchrotron facility (Source optimisée de lumière d'énergie intermédiaire du Laboratoire d'Utilisation du Rayonnement Électromagnétique, SOLEIL) during runs in July and October 2021, respectively, to preselect regions to explore with AFM-IR. The synchrotron light source was coupled to a Nicolet continuum infrared microscope equipped with a germanium-coated KBr beam splitter, a liquid-nitrogen-cooled mercury-cadmium-telluride (MCT) detector, and ×32 optical Cassegrain mirrors. Maps covering the entire grain were acquired with an infrared spot size optimized close to the diffraction limit, with 6 × 6 µm beam size, and sampling with 3 µm steps (Nyquist sampling). The intact Ryugu grains A0108 and C0109 as well as the acid-insoluble carbonaceous residues isolated from the Ryugu A0106 and C0107 samples were in addition analyzed in October 2021 with a Nicolet Continuum XL IR microscope located at the Institut des Sciences Moléculaires d'Orsay (ISMO), France, equipped with a silicon carbide globar light source, a germanium-coated KBr beam splitter, a liquid-nitrogen-cooled mercury-cadmium-telluride (MCT) detector, and ×32 optical Cassegrain mirrors. The microscope and the FTIR spectrometer were continuously purged with dry air. For each spot, 512 to 1024 scans of IR transmission spectra were accumulated with a wavenumber resolution of 2 or 4 cm^{-1} and with rectangular apertures of 20 to 100 µm, adapted to cover the entire flattened grain, following its morphology.

Scanning transmission X-ray microscopy (STXM)

STXM measurements were acquired at both beamline 19A at Photon Factory (PF), High Energy Accelerator Research Organization (KEK), Japan and beamline 5.3.2.2 at the Advanced Light Source, Berkeley, CA USA.

The compact STXM at PF beamline 19A employs the APPLE-II type undulator providing synchrotron radiation X-rays with a photon energy range spanning 160-1900 eV. The X-ray intensity at the sample is a flux of 8×10^7 photons per second. The spatial resolution of the STXMs using a Fresnel zone plate (FZP) is typically around 30 nm (*78*). The energy resolution is ~ 5000. Energy calibration was confirmed by measuring highly ordered pyrolytic graphite (HOPG) prior to the measurements.

The soft x-ray STXM at ALS beamline 5.3.2.2 is illuminated by bending magnet radiation. The desired x-ray photon energies from this broadband source are selected with a monochromator grating and focused to a fixed ~35 nm beam spot using a Fresnel zone plate. Entrance slits (V) were set to 60 µm and exit slits (H/V) were adjusted to 30 µm each. Prior to the experiment, the microscope energy control was calibrated against the sharp C and O photoabsorptions of CO_2 gas introduced into the STXM chamber.

X-ray absorption images were acquired at spatial resolutions up to 25 nm per pixel, controlled by motion of the piezo stage scanners. However, hyperspectral data "stacks" were acquired at 50 nm per pixel resolutions to maximize signal-to-noise while minimizing total photon dose. In the near-edge structure region of the energy range, energy steps were set at 0.1 eV resolution for carbon stacks, and 0.2 eV for nitrogen and oxygen stacks. The optical density (OD) of each image in the data stack is calculated by $OD = -\log(I/I_0)$, where I is the x-ray intensity transmitted through the sample and I_0 is the background transmission. XANES spectra of carbonaceous regions of interest are generated by summing pixels in those regions in the optical density datasets. PF STXM data were processed using the Axis2000 software (*79*). ALS STXM data were processed using Axis2000, Mantis (*80*), and custom Python scripts.

<u>Scanning transmission electron microscopy (STEM) coupled with electron energy loss spectroscopy (EELS) and energy dispersive X-ray spectroscopy (EDS)</u>

Bright field TEM images were acquired at the U.S. Naval Research Laboratory with a JEOL 2200FS scanning transmission electron microscope (STEM), operated at 200 kV. Images were recorded with a Gatan OneView camera, with camera constants calibrated with a MagICal Si-Ge superlattice imaging standard. High angle annular dark field STEM images, electron energy loss spectra (EELS) and energy dispersive X-ray spectra (EDS) were obtained with at the Naval Research Laboratory with a Nion UltraSTEM 200-X operated at 60 kV, with a nominal probe size of 0.15 nm and probe currents of 50- 100 pA. Simultaneous EELS-EDS spectrum images were recorded in Digital Micrograph, with a Gatan Enfinium and Bruker Xflash-100 spectrometers. High resolution EDS spectrum images were recorded with the Bruker Espirit 1.92 software. Elemental maps are shown as deconvoluted counts, smoothed over 5 pixels to provide qualitative spatial distributions.

<u>Atomic force microscope based infrared spectroscopy (AFM-IR)</u>

AFM-IR analyses were performed on samples after the FTIR measurements were used for the selection of regions of interest. AFM-IR measurements were acquired on IconIR (Bruker nano, Santa Barbara CA, USA) installed at the Institut de Chimie Physique, Université Paris-Saclay (Orsay, France). This system allows 30 picometer root mean square (pm rms) standard deviation on topography with thermal drift 0.2 nm/min. In this setup, the IR beam was focused on the topside of the sample onto the AFM cantilever. The system was coupled to a multi-chip quantum cascade laser (QCL) source (MIRcat, Daylight Solutions; tunable repetition rates range of 0–2 MHz; spectral resolution of 0.1 cm^{-1}) that covers a portion of the mid-IR range, from 1900 cm^{-1} to 900 cm^{-1}. The data were acquired using the tapping AFM-IR mode (*81*) for chamber A sample (A0108-15), and the contact mode for chamber C sample (C0109-04). The probes used for contact mode (ContGB-G, 13kHz, 0.2 N/m, Budget Sensors) and tapping mode (Multi75GB-G, 75 kHz, 3 N/m, Budget sensor) were both gold-coated to avoid artifact effects due to the silicon IR absorption. The IR-mapping acquisition parameters for tapping mode were 0.4 Hz scan rate with a ~2 nm step size for all wavenumbers. The same acquisition parameters for contact mode were 0.4 Hz scan rate with a ~3 nm step size for all wavenumbers. The AFM-IR maps were recorded at several selected frequencies, targeted to sample organics (1720 and 1600 cm^{-1}) and silicates (1020 cm^{-1}). In addition, spectra were measured by averaging 4 different spectra on the full QCL range acquired at selected positions. Composite RGB color images combining the maps were combined to compare the spatial distribution of organics and silicates. Before combining them, individual images were realigned to compensate for possible small drifts between consecutive AFM-IR map recordings. The realigning was done using an algorithm maximizing the spatial correlation on the topography of the sample. Because the silicate signal dominates in absolute intensity, and thus contrast, each color image was normalized by setting its maximum signal to unity before combining them. From the composite RGB color maps in Fig. 5, it appears that organics are present in two different phases: one is a low level signal in which organics are widespread and intermixed with the silicates whereas the other one corresponds to inclusions that stand out from the low level organic signal.

Nanometer-scale secondary ion mass spectrometry (NanoSIMS)

Intact grains and acid-insoluble carbonaceous residues of Ryugu samples were imaged on the NanoSIMS 50 installed at Museum National d'Histoire Naturelle in Paris, France. Intact particles were either pressed on diamond windows (at Université Grenoble Alpes, France, samples A0108-6, A0108-18, C0109-9 and C0109-12 also analysed by Raman and FTIR) or on clean indium foil (at Université Paris-Saclay, France, samples A0108-15, A0108-19, C0109-4 and C0109-10). Insoluble carbonaceous residues prepared from samples A0106 and C0107 at University of Hiroshima, Japan, were pressed on indium at Université Paris-Saclay, France. All the samples were gold coated (20 nm thick) before NanoSIMS analyses. δD and $\delta^{15}N$ maps were recorded during two separate sessions. We used a 16 keV primary Cs+ beam to collect secondary ions of $^{16}O^-$, $^{12}C_2^-$, $^{26}CN^-$, $^{27}CN^-$ and $^{32}S^-$ for N/C, O/C and S/C ratios as well as for $\delta^{15}N$ images in on session and H^- and D^- to obtain δD images in a second session. We chose to use the ion ratio $^{26}CN^-/^{12}C_2^-$ to lower the topographic effects on the N/C measurements (*82*). The primary beam was set to around 2 pA for N isotope and 12-15 pA for H isotope measurements, leading to a spatial resolution of about 150 nm and 300 nm, respectively. We collected 256×256 pixel images covering 20×20 µm² with a raster speed of 2 milliseconds per pixel. Prior to each analysis, we applied a 25×25 µm² presputtering using a 300 pA primary current during 15 minutes to ensure coating removal, clean the surface, and reach the sputtering steady state. We used Hamamatsu discrete dynode electron multipliers with a dead time of 44 ns in multicollection mode. For H isotopes, we set the mass spectrometer to a mass resolving power of 3000; for N isotopes it was increased to 9000 to be able to resolve interferences like $^{12}C^{15}N^-$ from $^{13}C^{14}N^-$ and $^{32}S^-$ from $^{16}O_2^-$. During the session, the vacuum did not exceed 5×10^{-10} torr.

All the NanoSIMS data were processed with the IDL (L3Harris)-based L'image software (*83*). Each image being a stack of several frames, the first step consists in aligning each frame using a correlation algorithm and applying the same shift in X and Y to all the pixels of a single frame. Then, ratio images could be generated. Each isotopic ratio and the elemental ratios are corrected using calibration lines, determined by measuring known reference samples: terrestrial type 3 kerogens from Virginia, USA, and the Miocene Monterey formation, a charcoal, polystyrene samples of variable D/H ratios as well as the IOM of Orgueil meteorite. All the uncertainties are based on counting statistics uncertainties on each measurement (depending on the total counts in each object).

Isotopic ratios are expressed in delta units, following the relation: $\delta R(‰) = (R_{sample}/R_{standard} - 1) \times 1000$ where R_{sample} is the sample isotopic ratio and $R_{standard}$ is the ratio of a terrestrial standard. Standard Mean Ocean Water (SMOW: D/H= 155.76×10^{-6}) and Air ($^{15}N/^{14}N= 3.67\times10^{-3}$) are used as standards for H and N isotopic measurements, respectively.

The Cameca NanoSIMS 50L at the Carnegie Institution of Washington was used to analyze ultramicrotomed slices of Ryugu particles A0108.

Thick (~250 nm) slices were deposited onto Si wafers and heated to remove elemental S embedding medium and surface contamination. A thin Au coat was applied to avoid surface charging effects in the NanoSIMS. A focused Cs^+ beam was rastered across the particles with simultaneous collection of secondary ions and electrons in multi-collection imaging mode. An intense beam (hundreds of pA) was first used to pre-sputter all particles to remove the Au coat and surface contamination and to reach stable secondary ion currents. Two or three sets of measurements were made on each particle slice. First, a ~0.4-pA beam (<100-nm diameter) was used to collect negative ions of ^{16}O, $^{12}C_2$, $^{12}C^{13}C$, $^{12}C^{14}N$, $^{12}C^{15}N$, ^{28}Si, and $^{24}Mg^{16}O$ and secondary electrons. Second, a ~1.2-pA beam (< 200-nm diameter) was used to detect negative ions of ^{1}H, ^{2}D, and ^{12}C, and secondary electrons. Some particles were re-measured for C and N isotopes (with the same conditions) after the H measurements since it was determined they had been insufficiently pre-sputtered for the first set. Images were divided into either 256 × 256 or 512×512 pixels depending on raster size, and tens of frames collected such that a similar counting time per square micron was used for all measurements. Terrestrial (an organic powder of composition $C_{30}H_{50}O$ and a mixture of powdered SiC and Si_3N_4) and extraterrestrial (IOM from CR2 chondrite QUE 99177) standards were used to tune mass peaks and correct data for instrumental mass fractionation.

NanoSIMS images were analyzed with the L'image software. Images were corrected on a pixel-by-pixel basis for detector deadtime of 44 ns, and image frames were aligned by an auto-correlation algorithm. Isotopic ratio images were generated and carbon-rich sub-grains (ROIs) were defined through a combination of automatic image segmentation and manual inspection. Most ROIs were identified in both the C-N and H-C images allowing H-, N- and C-isotopic data to be directly correlated, although some carbon-rich regions disappeared or appeared as the particles were sputtered under the ion beam.

A total of ten ultramicrotome slices were analyzed for H, C, and N, and from these 2070 correlated carbon-rich ROIs were defined (Figs S6 and 7, Table S3). The vast majority of the ROIs have diameters between 200 nm and 700 nm with an average ~400 nm, with a small number of larger grains extending up to ~2 μm. carbon-rich grains smaller than 200 nm are prevalent in the particles but were not defined as their signals were too low for isotopic measurements. For each particle slice, an average isotopic composition was determined from the total of all defined ROIs. In Fig. S8, we compare the δD and $\delta^{15}N$ values from these 10 bulk carbon-rich measurements to literature data for carbonaceous chondrites. They show a large scatter due to isotopic heterogeneity on the micrometer scale (Figs. 6, S6 and S7), but are mostly between bulk CI and CR chondrites and the IOM from CI chondrites (*45*). Of the total of 2070 ROIs defined, 2026 were found to have sufficient counting statistics for a reliable N-isotope measurement, 1439 for reliable D/H, and 1412 for both H and N. Most of these are consistent with the average bulk isotopic composition of the carbon-rich material. However, a total of 132 ROIs, or almost 10% of the total, have more extreme isotopic enrichments or depletions and termed hot-spots and cold-spots (Fig. 6). About 0.5% of the carbon-rich ROIs have $\delta^{13}C$ values >3σ away from the average value of -30‰ (Fig. 6).

Supplementary Text

In addition to the carbon-rich ROIs described above that are almost certainly composed of organic matter, two highly ^{13}C-enriched grains were also identified in the NanoSIMS images of two slices of the same Ryugu grain (A0108-37g1). These isotopic compositions are too extreme to have been produced in the Solar System and these grains are thus identified as pre-solar circumstellar grains. Pre-solar grains formed in previous generations of stars and were part of the molecular cloud from which the Solar System formed (*55*). The most abundant ^{13}C-rich pre-solar phase in meteorites is SiC, but because our Ryugu slices are deposited on a Si substrate, identifying the mineralogy of the two ^{13}C-rich anomalous grains is difficult, especially since the grains are very small (<150 nm). Nevertheless, one of them has a correlated Si signal and is likely SiC. No such signal was seen for the other grain, so it may be graphite, though SiC cannot be ruled out. Based on the total analyzed area, we estimate the SiC abundance of the Ryugu sample to be 10 to 20 ppm. This is similar to previous estimates of SiC abundances in carbonaceous chondrites (e.g., 34 ppm for Orgueil CI chondrite (*84*)).

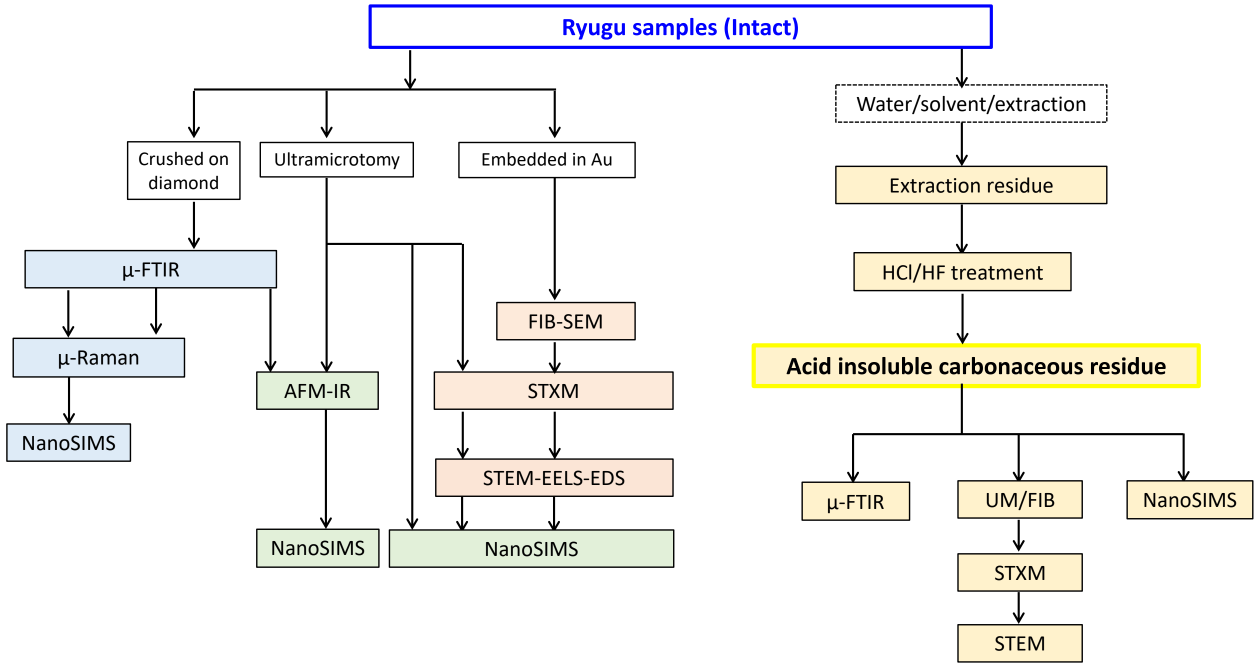

Fig. S1. Analytical protocols applied to our samples. There are two main protocols. The left one is applied to the intact Ryugu samples and the right one is applied for the insoluble carbonaceous residues isolated by acid treatment of the Ryugu samples, respectively. Some of the particles were crushed on a diamond window for micro-FTIR, micro-Raman, AFM-IR and NanoSIMS. Slices of other particles were prepared with a FIB and/or an ultramicrotome to obtain ultra-thin sections for STXM, STEM-EELS-EDS, AFM-IR and NanoSIMS. The water, solvent, and HCl extraction residues of other aggregates of Chamber A (A0106) and Chamber C (C0107) were treated with 6M HCl and 1M HCl/9M HF to yield insoluble carbonaceous residues.

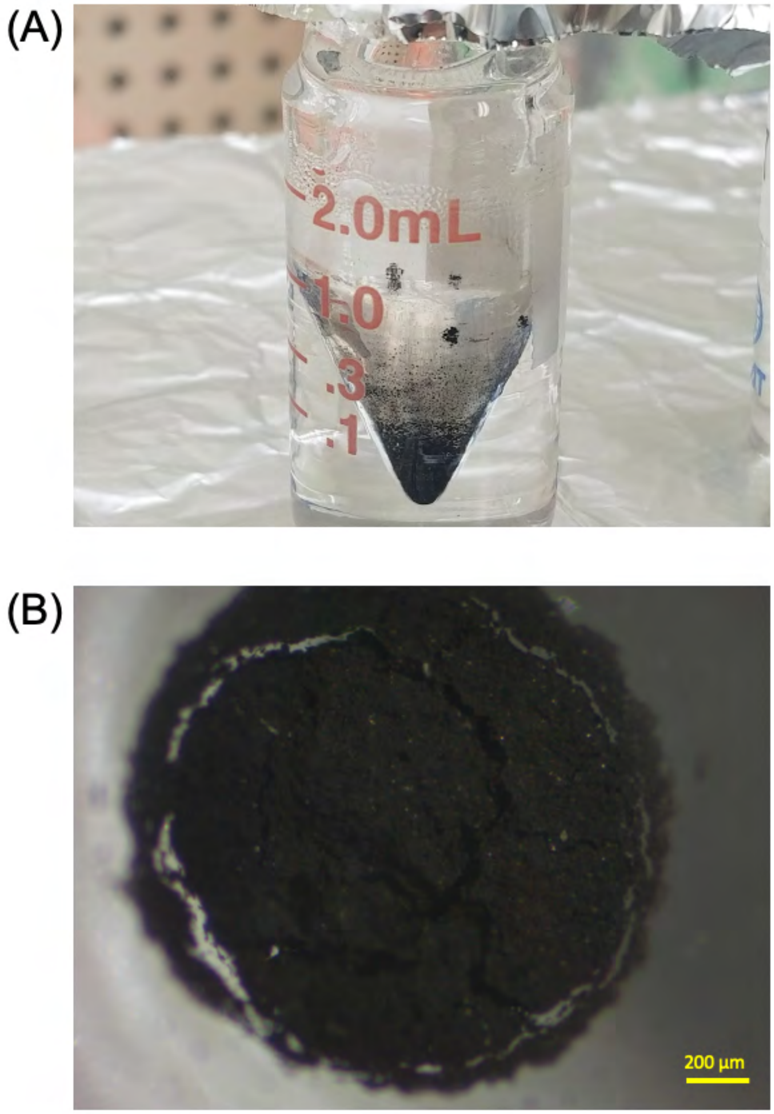

Fig. S2. Images of insoluble carbonaceous residues isolated from the intact Ryugu aggregates (A0106) by HF/HCl treatment. (A) The Ryugu carbonaceous residue in a mini glass vial. (B) An overhead image of the Ryugu carbonaceous residue aliquots transferred in another mini vial.

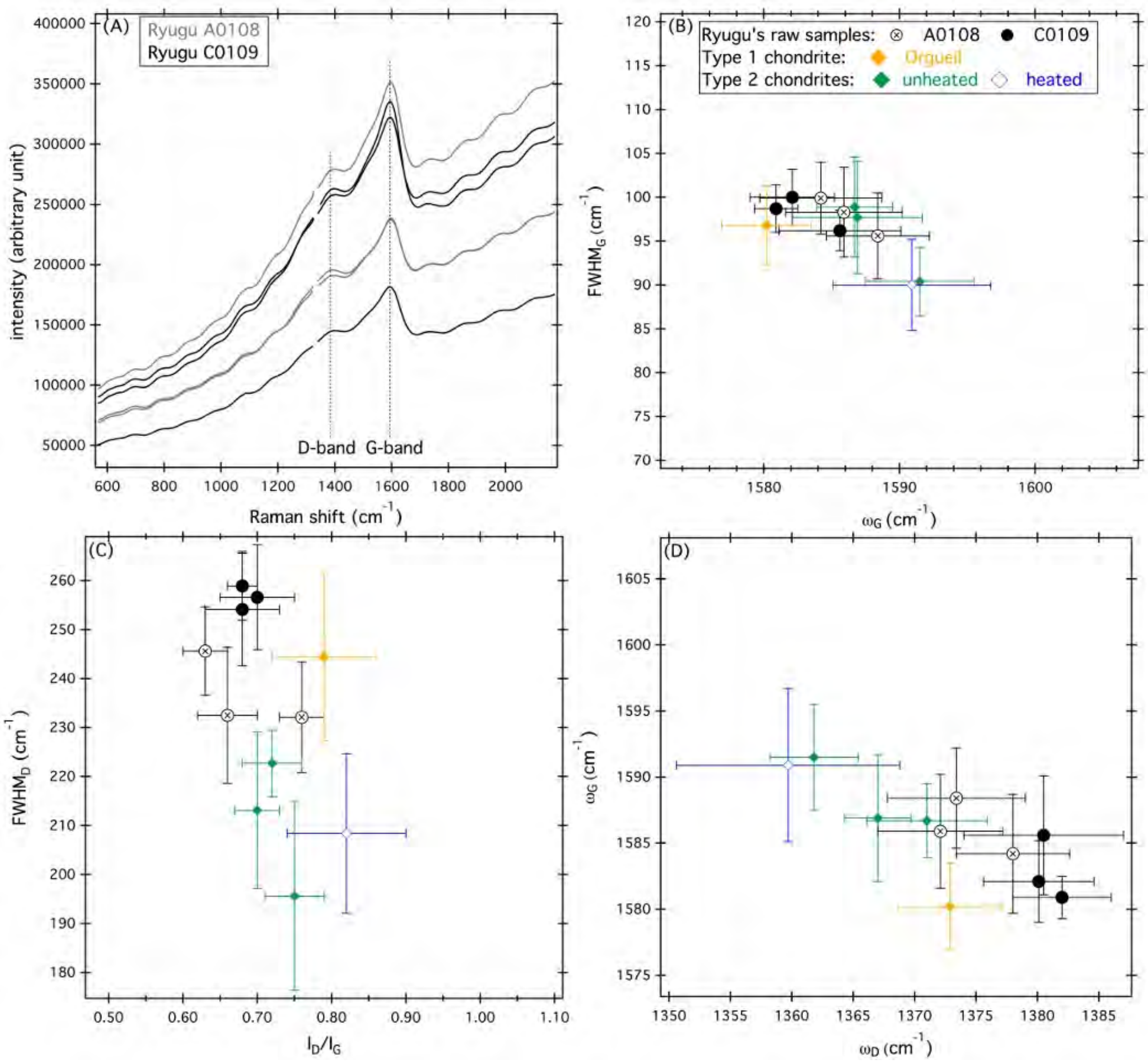

Fig. S3. Same as Figure 1, but for data acquired in a different laboratory (Waseda University, see the main text).

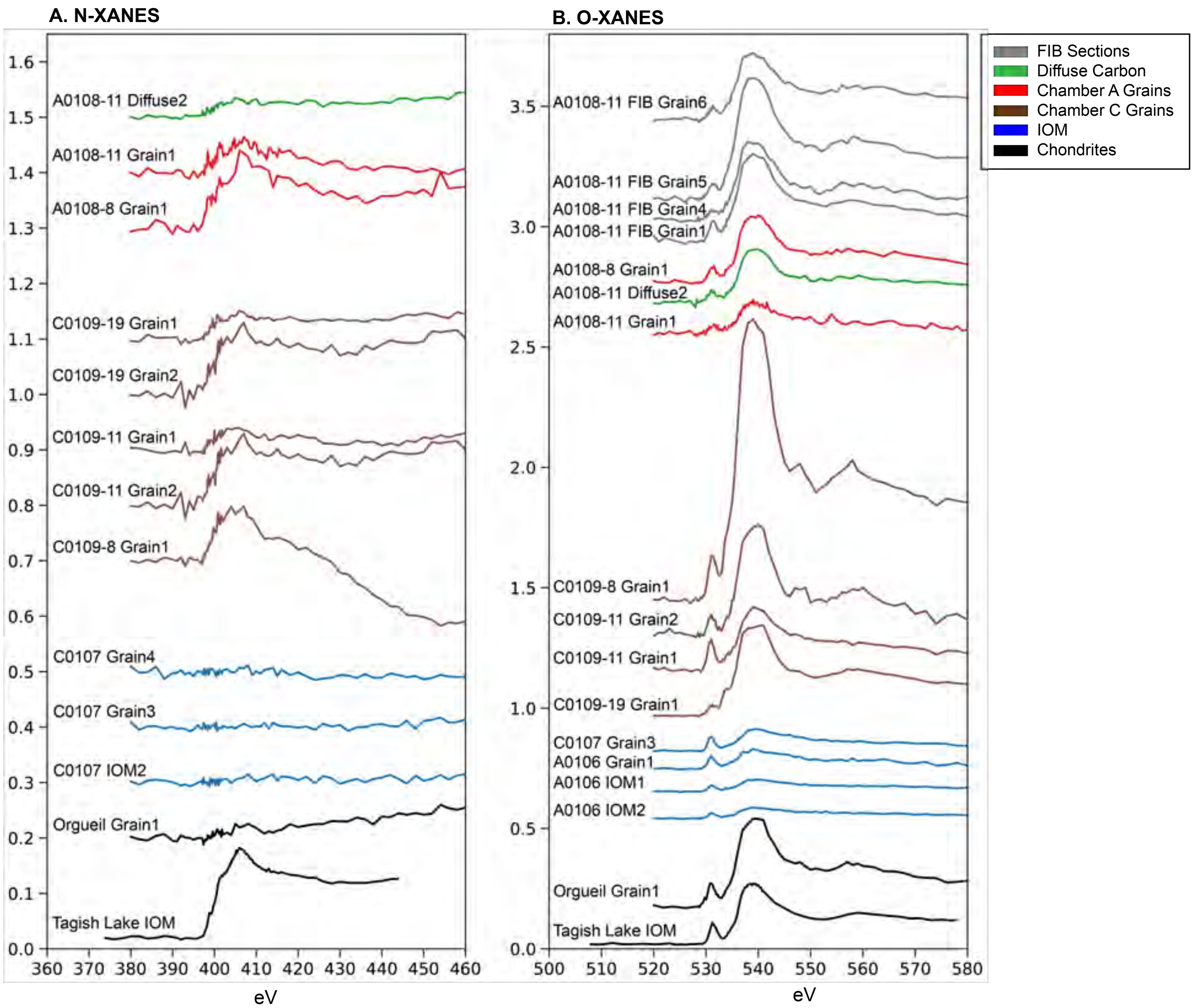

Fig. S4. Nitrogen- and Oxygen-XANES of Ryugu samples compared to chondrites. (A) Nitrogen-XANES spectra for carbonaceous grains (Grain) and matrix regions (Diffuse) from the aggregates A0108 and C0109 and for insoluble carbonaceous residues from C0107. The Orgueil meteorite and IOM from the Tagish Lake meteorite (*45*) are shown for comparison. Nitrogen abundance in insoluble carbonaceous residues from Ryugu samples appears to be extremely low but is detectable in the ultra-thin sections. (B) Oxygen-XANES spectra for carbonaceous grains (Grain) and matrix regions (Diffuse) from the aggregates A0108 and C0109 and for insoluble carbonaceous residues from A0106. The Orgueil meteorite and IOM from the Tagish Lake meteorite (*45*) are shown for comparison. Oxygen abundance in insoluble carbonaceous residues from Ryugu samples is lower than in CI chondrites, but individual grains show a larger C=O peak at 532 eV relative to the main C-O peak centered around 540 eV. It is likely that O-XANES spectra from ultrathin-samples are partly contributed by the surrounding phyllosilicates.

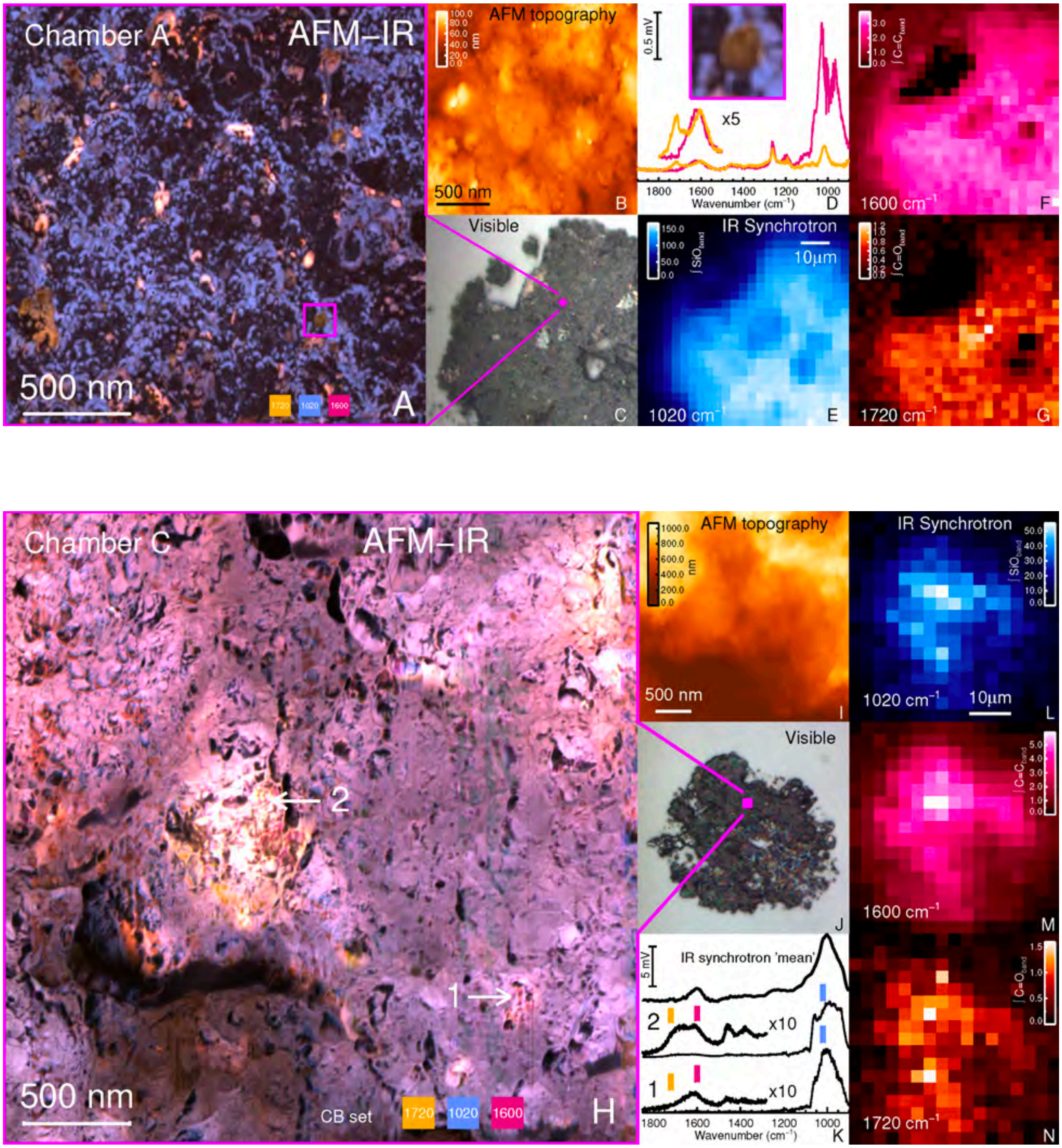

Fig. S5. Same as Figure 5, but for the color-shifted to be color-blind friendly.

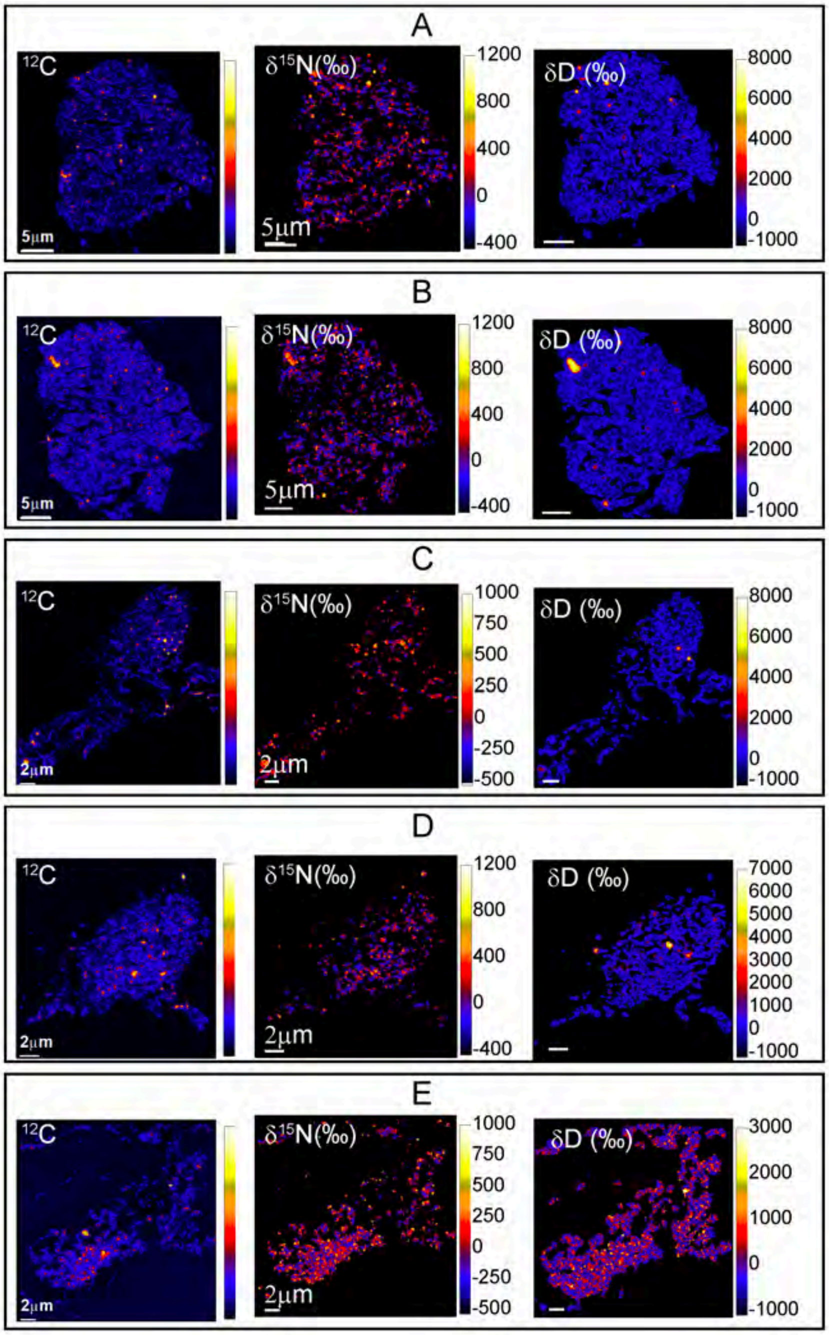

Fig. S6. NanoSIMS images for five ultrathin sections of Ryugu A0108 grains. A) A0108-25-g5a, B) A0108-25-g5b, C) A0108-33-g1a, D) A0108-33-g1b, E) A0108-44-g1d, where the label indicates the grain number (A0108-25) and particular slice label (i.e., "g5a"). For each slice, three images are shown: ^{12}C (arbitrary units), δD, and $\delta^{15}N$. Carbon is present as diffuse background and as distinct sub-mm to mm-sized particles with a wide range of isotopic compositions.

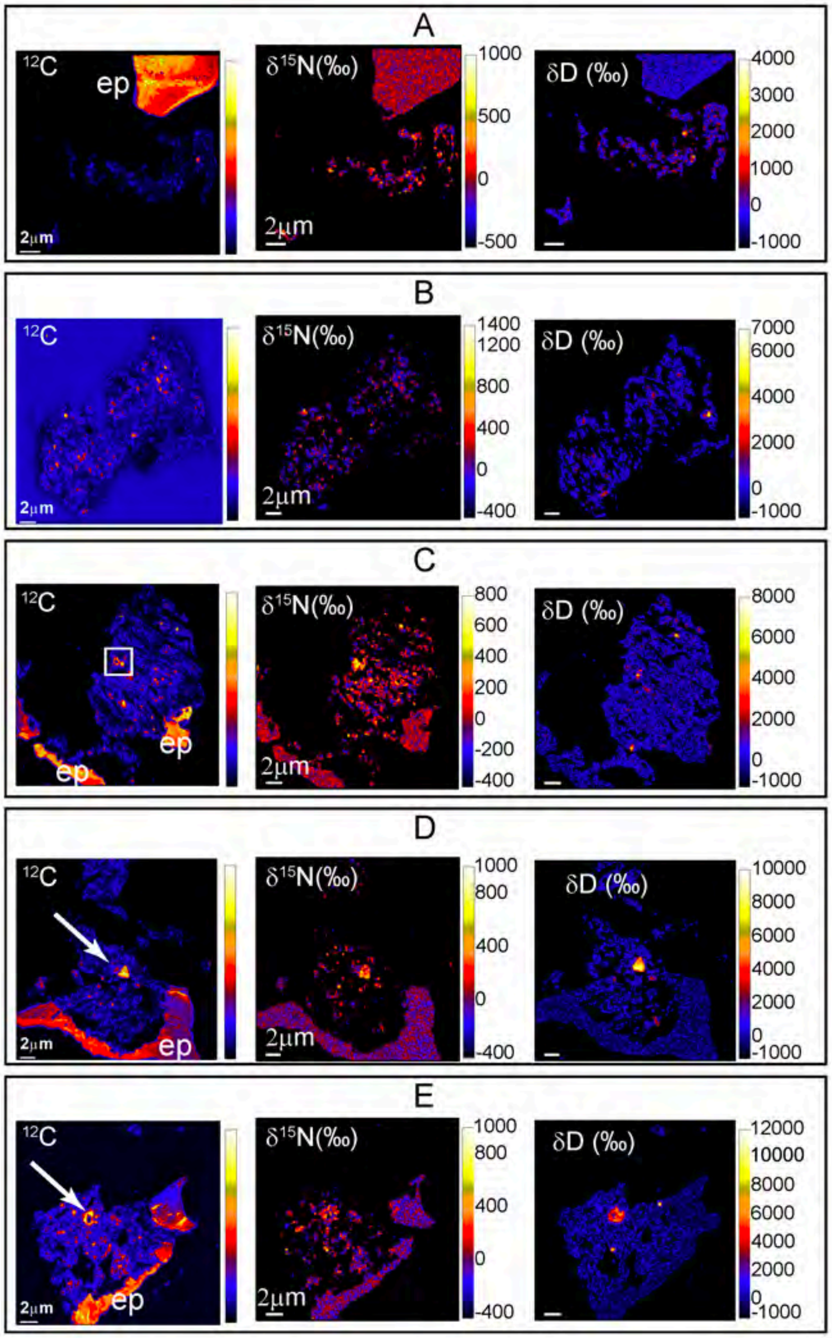

Fig. S7. Same as Figure S6, but for the other five ultrathin sections of Ryugu A0108 grain. A) A0108-25-g1a, B) A0108-25-g1c, C) A0108-37-g1b, D) A0108-37-g1c, E) A0108-37-g1d. The label "ep" indicates regions of residual epoxy from sample preparation. The white box in C indicates the location of images in Fig. 6A-C. The arrows indicate a 2-µm grain visible in two slices of same Ryugu grain and also seen in STEM measurements in an adjacent slice.

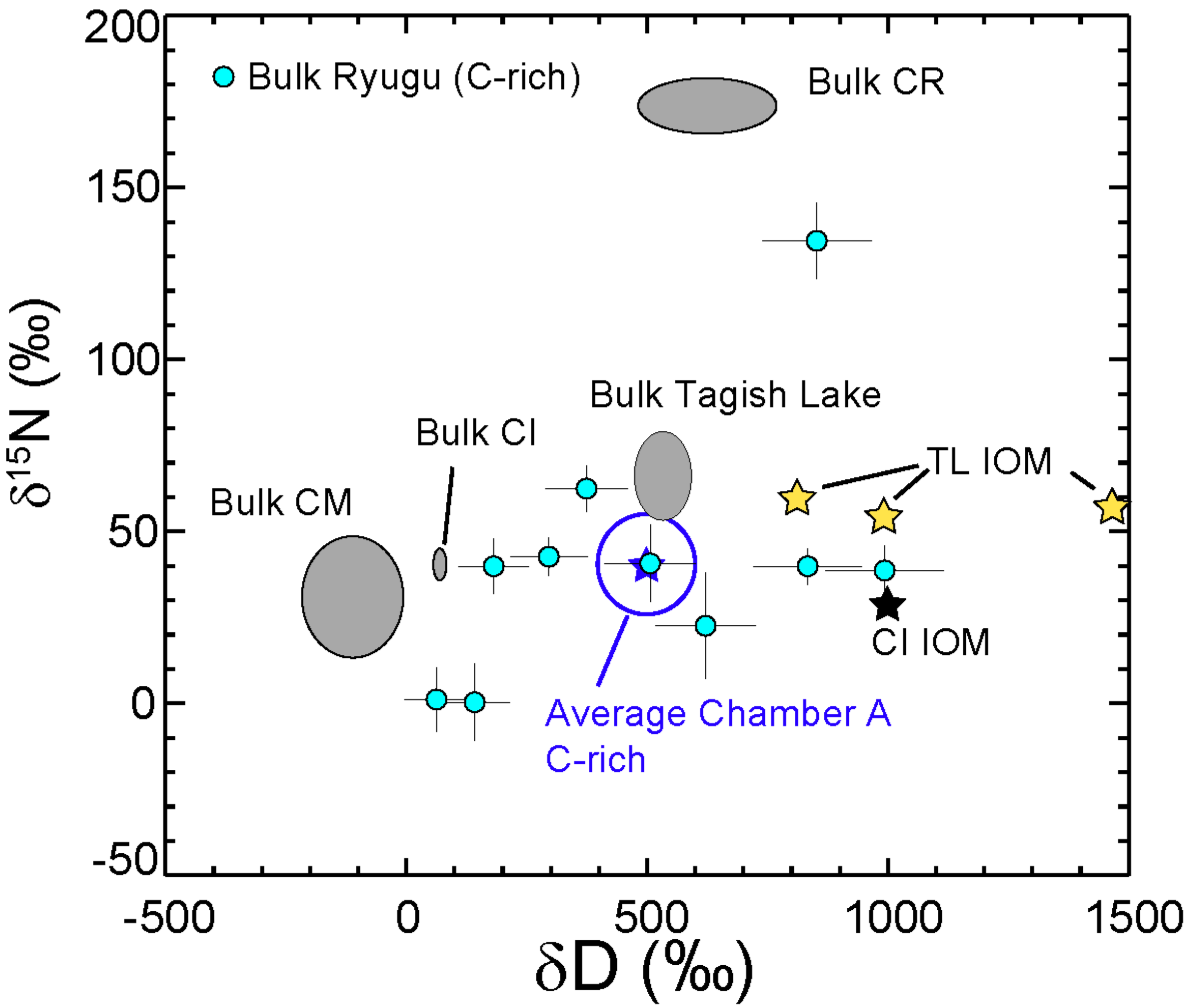

Fig. S8. The δ^{15}N as a function of δD for bulk carbon-rich material in the intact Ryugu grains in comparison with primitive carbonaceous chondrites. Ten ultrathin-sections of Ryugu A0108 (Figs. S6 and S7, cyan filled circles) were compared to bulk CI, CM, CR, and Tagish Lake meteorites (gray ellipse) and IOM from CI chondrites (black star) and different Tagish Lake lithologies (yellow stars) (*46, 61, 85*). The blue star and ellipse show the average and standard error of the mean for the ten samples (Table S3).

Table S1.
The Ryugu samples used.

Sample ID	Sample condition	Sub-sample No.	Preparation	Analysis
A0108	Intact grain	A0108-3	FIB	STXM, STEM-EELS-EDS
		A0108-5	Crushed	μ-FTIR, Raman
		A0108-6	Crushed	μ-FTIR, Raman, NanoSIMS
		A0108-7	Crushed	μ-FTIR, Raman
		A0108-8	Ultramicrotomed	STXM, STEM-EELS-EDS
		A0108-10	Crushed	μ-FTIR, Raman
		A0108-11	Ultramicrotomed	STXM
			FIB	STXM
		A0108-15	Crushed	AFM-IR
		A0108-17	Crushed	μ-FTIR, Raman
		A0108-18	Crushed	μ-FTIR, Raman, NanoSIMS
		A0108-19	Crushed	μ-FTIR
		A0108-25	Ultramicrotomed	NanoSIMS
		A0108-33	Ultramicrotomed	NanoSIMS
		A0108-37	Ultramicrotomed	NanoSIMS
		A0108-39	Ultramicrotomed	STEM-EELS-EDS
		A0108-44	Ultramicrotomed	NanoSIMS
C0109	Intact grain	C0109-1	Crushed	μ-FTIR, Raman
		C0109-4	Crushed	AFM-IR
		C0109-5	Crushed	μ-FTIR, Raman
		C0109-8	Ultramicrotomed	STXM
		C0109-9	Crushed	μ-FTIR, Raman, NanoSIMS
		C0109-10	Crushed	μ-FTIR
		C0109-11	FIB	STEM-EELS-EDS
		C0109-12	Crushed	μ-FTIR, Raman, NanoSIMS
		C0109-15	Crushed	μ-FTIR, Raman
		C0109-16	Crushed	μ-FTIR, Raman
		C0109-19	Ultramicrotomed	STXM
A0106	Acid-insoluble carbonaceous residue	A0106-2	Crushed	μ-FTIR
		A0106-4	Crushed	μ-FTIR
		A0106-8	Crushed	NanoSIMS
		A0106-9	Ultramicrotomed	STXM, STEM-EELS-EDS
C0107	Acid-insoluble carbonaceous residue	C0107-2	Crushed	μ-FTIR
		C0107-8	Crushed	μ-FTIR
		C0107-13	Crushed	μ-FTIR
		C0107-14	Crushed	NanoSIMS
		C0107-15	Crushed	μ-FTIR
		C0107-18	Ultramicrotomed	STXM, STEM-EELS-EDS

Table S2.
The meteorite samples used.

Meteorite name	Meteorite group	Petrologic type	Source	Preparation	Analysis
Orgueil	CI	1	MNHN*	Crushed	μ-FTIR. Raman
			MNHN	Acid treatment (to isolate IOM)	NanoSIMS
Ivuna	CI	1	M. E. Zolensky (NASA JSC**)	Crushed	μ-FTIR
			T. Fagan (Waseda University)	Crushed	Raman
Murchison	CM	2	Chicago Field Museum	Crushed	μ-FTIR
			MNHN	Crushed	Raman
ALH84044	CM	2	MWG***, NASA JSC	Crushed	Raman
Banten	CM	2	MNHN	Crushed	Raman
LEW87022	CM	2	MWG, NASA JSC	Crushed	Raman
MET01070	CM	2	MWG, NASA JSC	Crushed	Raman
Nogoya	CM	2	MNHN	Crushed	Raman
Cold Bokkeveld	CM	2	MNHN	Crushed	Raman
Jbilet Winselwan	CM	2	S. Kawakami (Gifu Shotoku University)	Crushed	μ-FTIR, Raman
MAC88100	CM	2	MWG, NASA JSC	Crushed	Raman
QUE93005	CM	2	MWG, NASA JSC	Crushed	Raman
EET87522	CM	2	MWG, NASA JSC	Crushed	Raman
ALH84033	CM	2	MWG, NASA JSC	Crushed	Raman
EET96029	CM	2	MWG, NASA JSC	Crushed	Raman
PCA91008	CM	2	MWG, NASA JSC	Crushed	Raman
QUE 99177	CR	2	MWG, NASA JSC	Acid treatment (to isolate IOM)	NanoSIMS
Tagish Lake	C2 ungrouped	2	Bruno Fectay and Carine Bidaut	Crushed	Raman
Tarda	C2 ungrouped	2	Bruno Fectay and Carine Bidaut	Crushed	Raman
EET83355	C2 ungrouped	2	MWG, NASA JSC	Crushed	Raman
PCA02012	C2 ungrouped	2	MWG, NASA JSC	Crushed	Raman
WIS91600	C2 ungrouped	2	MWG, NASA JSC	Crushed	Raman
DOM08006	CO	3	MWG, NASA JSC	Crushed	Raman
EET90628	L	3	MWG, NASA JSC	Crushed	Raman
Semarkona	LL	3	MNHN	Crushed	Raman
QUE97008	L	3.05	MWG, NASA JSC	Crushed	Raman
Bishunpur	LL	3.1	MNHN	Crushed	Raman
GRO95502	L	3.1/3.2	MWG, NASA JSC	Crushed	Raman
MET96503	L	3.1/3.2	MWG, NASA JSC	Crushed	Raman
LEW87022	LL	3.2	MNHN	Crushed	Raman
St Mary's County	LL	3.3	MNHN	Crushed	Raman

*Muséum National d'Histoire Naturelle (MNHN), **NASA Johnson Space Center (JSC), ***Meteorite Working Group (MWG)

Table S3.

Average isotopic composition of carbon-rich grains within intact Ryugu particles. The values are based on NanoSIMS measurements at the Carnegie Institution of Washington (CIW) and the National Museum of Natural History, Paris (MNHN).

	δD	Errors	$\delta^{15}N$	Errors	$\delta^{13}C$	Errors	N/C (Atomic)	Errors
Chamber A (CIW)*	490	100	42	14	-32	2	0.029	0.006
Chamber A (MNHN)	254	52	39	5			0.048	0.002
Chamber C (MNHM)	342	69	43	4			0.063	0.001

*Average and standard error of the mean from ten microtomed slices of A0109 fragments (Figs. S6-S8)

References and Notes

1. S. Tachibana, M. Abe, M. Arakawa, M. Fujimoto, Y. Iijima, M. Ishiguro, K. Kitazato, N. Kobayashi, N. Namiki, T. Okada, R. Okazaki, H. Sawada, S. Sugita, Y. Takano, S. Tanaka, S. Watanabe, M. Yoshikawa, H. Kuninaka, Hayabusa2: Scientific importance of samples returned from C-type near-Earth asteroid (162173) 1999 JU_3. *Geochem. J.* **48**, 571–587 (2014). doi:10.2343/geochemj.2.0350

2. S. Watanabe, M. Hirabayashi, N. Hirata, N. Hirata, R. Noguchi, Y. Shimaki, H. Ikeda, E. Tatsumi, M. Yoshikawa, S. Kikuchi, H. Yabuta, T. Nakamura, S. Tachibana, Y. Ishihara, T. Morota, K. Kitazato, N. Sakatani, K. Matsumoto, K. Wada, H. Senshu, C. Honda, T. Michikami, H. Takeuchi, T. Kouyama, R. Honda, S. Kameda, T. Fuse, H. Miyamoto, G. Komatsu, S. Sugita, T. Okada, N. Namiki, M. Arakawa, M. Ishiguro, M. Abe, R. Gaskell, E. Palmer, O. S. Barnouin, P. Michel, A. S. French, J. W. McMahon, D. J. Scheeres, P. A. Abell, Y. Yamamoto, S. Tanaka, K. Shirai, M. Matsuoka, M. Yamada, Y. Yokota, H. Suzuki, K. Yoshioka, Y. Cho, S. Tanaka, N. Nishikawa, T. Sugiyama, H. Kikuchi, R. Hemmi, T. Yamaguchi, N. Ogawa, G. Ono, Y. Mimasu, K. Yoshikawa, T. Takahashi, Y. Takei, A. Fujii, C. Hirose, T. Iwata, M. Hayakawa, S. Hosoda, O. Mori, H. Sawada, T. Shimada, S. Soldini, H. Yano, R. Tsukizaki, M. Ozaki, Y. Iijima, K. Ogawa, M. Fujimoto, T.-M. Ho, A. Moussi, R. Jaumann, J.-P. Bibring, C. Krause, F. Terui, T. Saiki, S. Nakazawa, Y. Tsuda, Hayabusa2 arrives at the carbonaceous asteroid 162173 Ryugu—A spinning top–shaped rubble pile. *Science* **364**, 268–272 (2019). doi:10.1126/science.aav8032 Medline

3. S. Sugita, R. Honda, T. Morota, S. Kameda, H. Sawada, E. Tatsumi, M. Yamada, C. Honda, Y. Yokota, T. Kouyama, N. Sakatani, K. Ogawa, H. Suzuki, T. Okada, N. Namiki, S. Tanaka, Y. Iijima, K. Yoshioka, M. Hayakawa, Y. Cho, M. Matsuoka, N. Hirata, N. Hirata, H. Miyamoto, D. Domingue, M. Hirabayashi, T. Nakamura, T. Hiroi, T. Michikami, P. Michel, R.-L. Ballouz, O. S. Barnouin, C. M. Ernst, S. E. Schröder, H. Kikuchi, R. Hemmi, G. Komatsu, T. Fukuhara, M. Taguchi, T. Arai, H. Senshu, H. Demura, Y. Ogawa, Y. Shimaki, T. Sekiguchi, T. G. Müller, A. Hagermann, T. Mizuno, H. Noda, K. Matsumoto, R. Yamada, Y. Ishihara, H. Ikeda, H. Araki, K. Yamamoto, S. Abe, F. Yoshida, A. Higuchi, S. Sasaki, S. Oshigami, S. Tsuruta, K. Asari, S. Tazawa, M. Shizugami, J. Kimura, T. Otsubo, H. Yabuta, S. Hasegawa, M. Ishiguro, S. Tachibana, E. Palmer, R. Gaskell, L. Le Corre, R. Jaumann, K. Otto, N. Schmitz, P. A. Abell, M. A. Barucci, M. E. Zolensky, F. Vilas, F. Thuillet, C. Sugimoto, N. Takaki, Y. Suzuki, H. Kamiyoshihara, M. Okada, K. Nagata, M. Fujimoto, M. Yoshikawa, Y. Yamamoto, K. Shirai, R. Noguchi, N. Ogawa, F. Terui, S. Kikuchi, T. Yamaguchi, Y. Oki, Y. Takao, H. Takeuchi, G. Ono, Y. Mimasu, K. Yoshikawa, T. Takahashi, Y. Takei, A. Fujii, C. Hirose, S. Nakazawa, S. Hosoda, O. Mori, T. Shimada, S. Soldini, T. Iwata, M. Abe, H. Yano, R. Tsukizaki, M. Ozaki, K. Nishiyama, T. Saiki, S. Watanabe, Y. Tsuda, The geomorphology, color, and thermal properties of Ryugu: Implications for parent-body processes. *Science* **364**, eaaw0422 (2019). doi:10.1126/science.aaw0422 Medline

4. K. Kitazato, R. E. Milliken, T. Iwata, M. Abe, M. Ohtake, S. Matsuura, T. Arai, Y. Nakauchi, T. Nakamura, M. Matsuoka, H. Senshu, N. Hirata, T. Hiroi, C. Pilorget, R. Brunetto, F. Poulet, L. Riu, J. P. Bibring, D. Takir, D. L. Domingue, F. Vilas, M. A. Barucci, D. Perna, E. Palomba, A. Galiano, K. Tsumura, T. Osawa, M. Komatsu, A. Nakato, T. Arai, N. Takato, T. Matsunaga, Y. Takagi, K. Matsumoto, T. Kouyama, Y. Yokota, E.

Tatsumi, N. Sakatani, Y. Yamamoto, T. Okada, S. Sugita, R. Honda, T. Morota, S. Kameda, H. Sawada, C. Honda, M. Yamada, H. Suzuki, K. Yoshioka, M. Hayakawa, K. Ogawa, Y. Cho, K. Shirai, Y. Shimaki, N. Hirata, A. Yamaguchi, N. Ogawa, F. Terui, T. Yamaguchi, Y. Takei, T. Saiki, S. Nakazawa, S. Tanaka, M. Yoshikawa, S. Watanabe, Y. Tsuda, The surface composition of asteroid 162173 Ryugu from Hayabusa2 near-infrared spectroscopy. *Science* **364**, 272–275 (2019). doi:10.1126/science.aav7432 Medline

5. T. Morota, S. Sugita, Y. Cho, M. Kanamaru, E. Tatsumi, N. Sakatani, R. Honda, N. Hirata, H. Kikuchi, M. Yamada, Y. Yokota, S. Kameda, M. Matsuoka, H. Sawada, C. Honda, T. Kouyama, K. Ogawa, H. Suzuki, K. Yoshioka, M. Hayakawa, N. Hirata, M. Hirabayashi, H. Miyamoto, T. Michikami, T. Hiroi, R. Hemmi, O. S. Barnouin, C. M. Ernst, K. Kitazato, T. Nakamura, L. Riu, H. Senshu, H. Kobayashi, S. Sasaki, G. Komatsu, N. Tanabe, Y. Fujii, T. Irie, M. Suemitsu, N. Takaki, C. Sugimoto, K. Yumoto, M. Ishida, H. Kato, K. Moroi, D. Domingue, P. Michel, C. Pilorget, T. Iwata, M. Abe, M. Ohtake, Y. Nakauchi, K. Tsumura, H. Yabuta, Y. Ishihara, R. Noguchi, K. Matsumoto, A. Miura, N. Namiki, S. Tachibana, M. Arakawa, H. Ikeda, K. Wada, T. Mizuno, C. Hirose, S. Hosoda, O. Mori, T. Shimada, S. Soldini, R. Tsukizaki, H. Yano, M. Ozaki, H. Takeuchi, Y. Yamamoto, T. Okada, Y. Shimaki, K. Shirai, Y. Iijima, H. Noda, S. Kikuchi, T. Yamaguchi, N. Ogawa, G. Ono, Y. Mimasu, K. Yoshikawa, T. Takahashi, Y. Takei, A. Fujii, S. Nakazawa, F. Terui, S. Tanaka, M. Yoshikawa, T. Saiki, S. Watanabe, Y. Tsuda, Sample collection from asteroid (162173) Ryugu by Hayabusa2: Implications for surface evolution. *Science* **368**, 654–659 (2020). doi:10.1126/science.aaz6306 Medline

6. N. Sakatani, S. Tanaka, T. Okada, T. Fukuhara, L. Riu, S. Sugita, R. Honda, T. Morota, S. Kameda, Y. Yokota, E. Tatsumi, K. Yumoto, N. Hirata, A. Miura, T. Kouyama, H. Senshu, Y. Shimaki, T. Arai, J. Takita, H. Demura, T. Sekiguchi, T. G. Müller, A. Hagermann, J. Biele, M. Grott, M. Hamm, M. Delbo, W. Neumann, M. Taguchi, Y. Ogawa, T. Matsunaga, T. Wada, S. Hasegawa, J. Helbert, N. Hirata, R. Noguchi, M. Yamada, H. Suzuki, C. Honda, K. Ogawa, M. Hayakawa, K. Yoshioka, M. Matsuoka, Y. Cho, H. Sawada, K. Kitazato, T. Iwata, M. Abe, M. Ohtake, S. Matsuura, K. Matsumoto, H. Noda, Y. Ishihara, K. Yamamoto, A. Higuchi, N. Namiki, G. Ono, T. Saiki, H. Imamura, Y. Takagi, H. Yano, K. Shirai, C. Okamoto, S. Nakazawa, Y. Iijima, M. Arakawa, K. Wada, T. Kadono, K. Ishibashi, F. Terui, S. Kikuchi, T. Yamaguchi, N. Ogawa, Y. Mimasu, K. Yoshikawa, T. Takahashi, Y. Takei, A. Fujii, H. Takeuchi, Y. Yamamoto, C. Hirose, S. Hosoda, O. Mori, T. Shimada, S. Soldini, R. Tsukizaki, M. Ozaki, S. Tachibana, H. Ikeda, M. Ishiguro, H. Yabuta, M. Yoshikawa, S. Watanabe, Y. Tsuda, Anomalously porous boulders on (162173) Ryugu as primordial materials from its parent body. *Nat. Astron.* **5**, 766–774 (2021). doi:10.1038/s41550-021-01371-7

7. E. Tatsumi, N. Sakatani, L. Riu, M. Matsuoka, R. Honda, T. Morota, S. Kameda, T. Nakamura, M. Zolensky, R. Brunetto, T. Hiroi, S. Sasaki, S. Watanabe, S. Tanaka, J. Takita, C. Pilorget, J. de León, M. Popescu, J. L. Rizos, J. Licandro, E. Palomba, D. Domingue, F. Vilas, H. Campins, Y. Cho, K. Yoshioka, H. Sawada, Y. Yokota, M. Hayakawa, M. Yamada, T. Kouyama, H. Suzuki, C. Honda, K. Ogawa, K. Kitazato, N. Hirata, N. Hirata, Y. Tsuda, M. Yoshikawa, T. Saiki, F. Terui, S. Nakazawa, Y. Takei, H. Takeuchi, Y. Yamamoto, T. Okada, Y. Shimaki, K. Shirai, S. Sugita, Spectrally blue hydrated parent body of asteroid (162173) Ryugu. *Nat. Commun.* **12**, 5837 (2021). doi:10.1038/s41467-021-26071-8 Medline

8. E. Tatsumi, C. Sugimoto, L. Riu, S. Sugita, T. Nakamura, T. Hiroi, T. Morota, M. Popescu, T. Michikami, K. Kitazato, M. Matsuoka, S. Kameda, R. Honda, M. Yamada, N. Sakatani, T. Kouyama, Y. Yokota, C. Honda, H. Suzuki, Y. Cho, K. Ogawa, M. Hayakawa, H. Sawada, K. Yoshioka, C. Pilorget, M. Ishida, D. Domingue, N. Hirata, S. Sasaki, J. de León, M. A. Barucci, P. Michel, M. Suemitsu, T. Saiki, S. Tanaka, F. Terui, S. Nakazawa, S. Kikuchi, T. Yamaguchi, N. Ogawa, G. Ono, Y. Mimasu, K. Yoshikawa, T. Takahashi, Y. Takei, A. Fujii, Y. Yamamoto, T. Okada, C. Hirose, S. Hosoda, O. Mori, T. Shimada, S. Soldini, R. Tsukizaki, T. Mizuno, T. Iwata, H. Yano, M. Ozaki, M. Abe, M. Ohtake, N. Namiki, S. Tachibana, M. Arakawa, H. Ikeda, M. Ishiguro, K. Wada, H. Yabuta, H. Takeuchi, Y. Shimaki, K. Shirai, N. Hirata, Y. Iijima, Y. Tsuda, S. Watanabe, M. Yoshikawa, Collisional history of Ryugu's parent body from bright surface boulders. *Nat. Astron.* **5**, 39–45 (2021). doi:10.1038/s41550-020-1179-z

9. T. Yada, M. Abe, T. Okada, A. Nakato, K. Yogata, A. Miyazaki, K. Hatakeda, K. Kumagai, M. Nishimura, Y. Hitomi, H. Soejima, M. Yoshitake, A. Iwamae, S. Furuya, M. Uesugi, Y. Karouji, T. Usui, T. Hayashi, D. Yamamoto, R. Fukai, S. Sugita, Y. Cho, K. Yumoto, Y. Yabe, J.-P. Bibring, C. Pilorget, V. Hamm, R. Brunetto, L. Riu, L. Lourit, D. Loizeau, G. Lequertier, A. Moussi-Soffys, S. Tachibana, H. Sawada, R. Okazaki, Y. Takano, K. Sakamoto, Y. N. Miura, H. Yano, T. R. Ireland, T. Yamada, M. Fujimoto, K. Kitazato, N. Namiki, M. Arakawa, N. Hirata, H. Yurimoto, T. Nakamura, T. Noguchi, H. Yabuta, H. Naraoka, M. Ito, E. Nakamura, K. Uesugi, K. Kobayashi, T. Michikami, H. Kikuchi, N. Hirata, Y. Ishihara, K. Matsumoto, H. Noda, R. Noguchi, Y. Shimaki, K. Shirai, K. Ogawa, K. Wada, H. Senshu, Y. Yamamoto, T. Morota, R. Honda, C. Honda, Y. Yokota, M. Matsuoka, N. Sakatani, E. Tatsumi, A. Miura, M. Yamada, A. Fujii, C. Hirose, S. Hosoda, H. Ikeda, T. Iwata, S. Kikuchi, Y. Mimasu, O. Mori, N. Ogawa, G. Ono, T. Shimada, S. Soldini, T. Takahashi, Y. Takei, H. Takeuchi, R. Tsukizaki, K. Yoshikawa, F. Terui, S. Nakazawa, S. Tanaka, T. Saiki, M. Yoshikawa, S.-I. Watanabe, Y. Tsuda, Preliminary analysis of the Hayabusa2 samples returned from C-type asteroid Ryugu. *Nat. Astron.* **6**, 214–220 (2021). doi:10.1038/s41550-021-01550-6

10. C. Pilorget, T. Okada, V. Hamm, R. Brunetto, T. Yada, D. Loizeau, L. Riu, T. Usui, A. Moussi-Soffys, K. Hatakeda, A. Nakato, K. Yogata, M. Abe, A. Aléon-Toppani, J. Carter, M. Chaigneau, B. Crane, B. Gondet, K. Kumagai, Y. Langevin, C. Lantz, T. Le Pivert-Jolivet, G. Lequertier, L. Lourit, A. Miyazaki, M. Nishimura, F. Poulet, M. Arakawa, N. Hirata, K. Kitazato, S. Nakazawa, N. Namiki, T. Saiki, S. Sugita, S. Tachibana, S. Tanaka, M. Yoshikawa, Y. Tsuda, S. Watanabe, J.-P. Bibring, First compositional analysis of Ryugu samples by the MicrOmega hyperspectral microscope. *Nat. Astron.* **6**, 221–225 (2021). doi:10.1038/s41550-021-01549-z

11. Materials and methods are available as supplementary materials.

12. S. Tachibana, H. Sawada, R. Okazaki, Y. Takano, K. Sakamoto, Y. N. Miura, C. Okamoto, H. Yano, S. Yamanouchi, P. Michel, Y. Zhang, S. Schwartz, F. Thuillet, H. Yurimoto, T. Nakamura, T. Noguchi, H. Yabuta, H. Naraoka, A. Tsuchiyama, N. Imae, K. Kurosawa, A. M. Nakamura, K. Ogawa, S. Sugita, T. Morota, R. Honda, S. Kameda, E. Tatsumi, Y. Cho, K. Yoshioka, Y. Yokota, M. Hayakawa, M. Matsuoka, N. Sakatani, M. Yamada, T. Kouyama, H. Suzuki, C. Honda, T. Yoshimitsu, T. Kubota, H. Demura, T. Yada, M. Nishimura, K. Yogata, A. Nakato, M. Yoshitake, A. I. Suzuki, S. Furuya, K. Hatakeda, A. Miyazaki, K. Kumagai, T. Okada, M. Abe, T. Usui, T. R. Ireland, M. Fujimoto, T. Yamada, M. Arakawa, H. C. Connolly Jr., A. Fujii, S. Hasegawa, N. Hirata, N. Hirata, C.

Hirose, S. Hosoda, Y. Iijima, H. Ikeda, M. Ishiguro, Y. Ishihara, T. Iwata, S. Kikuchi, K. Kitazato, D. S. Lauretta, G. Libourel, B. Marty, K. Matsumoto, T. Michikami, Y. Mimasu, A. Miura, O. Mori, K. Nakamura-Messenger, N. Namiki, A. N. Nguyen, L. R. Nittler, H. Noda, R. Noguchi, N. Ogawa, G. Ono, M. Ozaki, H. Senshu, T. Shimada, Y. Shimaki, K. Shirai, S. Soldini, T. Takahashi, Y. Takei, H. Takeuchi, R. Tsukizaki, K. Wada, Y. Yamamoto, K. Yoshikawa, K. Yumoto, M. E. Zolensky, S. Nakazawa, F. Terui, S. Tanaka, T. Saiki, M. Yoshikawa, S. Watanabe, Y. Tsuda, Pebbles and sand on asteroid (162173) Ryugu: In situ observation and particles returned to Earth. *Science* **375**, 1011–1016 (2022). doi:10.1126/science.abj8624 Medline

13. L. Bonal, E. Quirico, M. Bourot-Denise, G. Montagnac, Determination of the petrologic type of CV3 chondrites by Raman spectroscopy of included organic matter. *Geochim. Cosmochim. Acta* **70**, 1849–1863 (2006). doi:10.1016/j.gca.2005.12.004

14. H. Busemann, C. M. O'D. Alexander, L. R. Nittler, Characterization of insoluble organic matter in primitive meteorites by microRaman spectroscopy. *Meteorit. Planet. Sci.* **42**, 1387–1416 (2007). doi:10.1111/j.1945-5100.2007.tb00581.x

15. L. Bonal, E. Quirico, L. Flandinet, G. Montagnac, Thermal history of type 3 chondrites from the Antarctic meteorite collection determined by Raman spectroscopy of their polyaromatic carbonaceous matter. *Geochim. Cosmochim. Acta* **189**, 312–337 (2016). doi:10.1016/j.gca.2016.06.017

16. E. Quirico, L. Bonal, P. Beck, C. M. O'D. Alexander, H. Yabuta, T. Nakamura, A. Nakato, L. Flandinet, G. Montagnac, P. Schmitt-Kopplin, C. D. K. Herd, Prevalence and nature of heating processes in CM and C2-ungrouped chondrites as revealed by insoluble organic matter. *Geochim. Cosmochim. Acta* **241**, 17–37 (2018). doi:10.1016/j.gca.2018.08.029

17. G. R. Huss, A. E. Rubin, J. N. Grossman, in *Meteorites and the Early Solar System II*, D. S. Lauretta, H. Y. McSween, Eds. (Univ. Arizona Press, 2006), pp. 567–586.

18. T. Nakamura, Yamato 793321 CM chondrite: Dehydrated regolith material of a hydrous asteroid. *Earth Planet. Sci. Lett.* **242**, 26–38 (2006). doi:10.1016/j.epsl.2005.11.040

19. T. Osawa, H. Kagi, T. Nakamura, T. Noguchi, Infrared spectroscopic taxonomy for carbonaceous chondrites from speciation of hydrous components. *Meteorit. Planet. Sci.* **40**, 71–86 (2005). doi:10.1111/j.1945-5100.2005.tb00365.x

20. Y. Kebukawa, C. M. O'D. Alexander, G. D. Cody, Comparison of FT-IR spectra of bulk and acid insoluble organic matter in chondritic meteorites: An implication for missing carbon during demineralization. *Meteorit. Planet. Sci.* **54**, 1632–1641 (2019). doi:10.1111/maps.13302

21. P. Beck, E. Quirico, G. Montes-Hernandez, L. Bonal, J. Bollard, F.-R.Orthous-Daunay, K. T. Howard, B. Schmitt, O. Brissaud, F. Deschamps, B. Wunder, S. Guillot, Hydrous mineralogy of CM and CI chondrites from infrared spectroscopy and their relationship with low albedo asteroids. *Geochim. Cosmochim. Acta* **74**, 4881–4892 (2010). doi:10.1016/j.gca.2010.05.020

22. D. Takir, J. P. Emery, H. Y. Mcsween Jr., C. A. Hibbitts, R. N. Clark, N. Pearson, A. Wang, Nature and degree of aqueous alteration in CM and CI carbonaceous chondrites. *Meteorit. Planet. Sci.* **48**, 1618–1637 (2013). doi:10.1111/maps.12171

23. T. Yokoyama, K. Nagashima, I. Nakai, E. D. Young, Y. Abe, J. Aléon, C. M. O'D. Alexander, S. Amari, Y. Amelin, K. Bajo, M. Bizzarro, A. Bouvier, R. W. Carlson, M. Chaussidon, B.-G. Choi, N. Dauphas, A. M. Davis, T. Di Rocco, W. Fujiya, R. Fukai, I. Gautam, M. K. Haba, Y. Hibiya, H. Hidaka, H. Homma, P. Hoppe, G. R. Huss, K. Ichida, T. Iizuka, T. R. Ireland, A. Ishikawa, M. Ito, S. Itoh, N. Kawasaki, N. T. Kita, K. Kitajima, T. Kleine, S. Komatani, A. N. Krot, M.-C. Liu, Y. Masuda, K. D. McKeegan, M. Morita, K. Motomura, F. Moynier, A. Nguyen, L. Nittler, M. Onose, A. Pack, C. Park, L. Piani, L. Qin, S. S. Russell, N. Sakamoto, M. Schönbächler, L. Tafla, H. Tang, K. Terada, Y. Terada, T. Usui, S. Wada, M. Wadhwa, R. J. Walker, K. Yamashita, Q.-Z. Yin, S. Yoneda, H. Yui, A.-C. Zhang, H. C. Connolly Jr., D. S. Lauretta, T. Nakamura, H. Naraoka, T. Noguchi, R. Okazaki, K. Sakamoto, H. Yabuta, M. Abe, M. Arakawa, A. Fujii, M. Hayakawa, N. Hirata, N. Hirata, R. Honda, C. Honda, S. Hosoda, Y. Iijima, H. Ikeda, M. Ishiguro, Y. Ishihara, T. Iwata, K. Kawahara, S. Kikuchi, K. Kitazato, K. Matsumoto, M. Matsuoka, T. Michikami, Y. Mimasu, A. Miura, T. Morota, S. Nakazawa, N. Namiki, H. Noda, R. Noguchi, N. Ogawa, K. Ogawa, T. Okada, C. Okamoto, G. Ono, M. Ozaki, T. Saiki, N. Sakatani, H. Sawada, H. Senshu, Y. Shimaki, K. Shirai, S. Sugita, Y. Takei, H. Takeuchi, S. Tanaka, E. Tatsumi, F. Terui, Y. Tsuda, R. Tsukizaki, K. Wada, S. Watanabe, M. Yamada, T. Yamada, Y. Yamamoto, H. Yano, Y. Yokota, K. Yoshihara, M. Yoshikawa, K. Yoshikawa, S. Furuya, K. Hatakeda, T. Hayashi, Y. Hitomi, K. Kumagai, A. Miyazaki, A. Nakato, M. Nishimura, H. Soejima, A. Suzuki, T. Yada, D. Yamamoto, K. Yogata, M. Yoshitake, S. Tachibana, H. Yurimoto, Samples returned from the asteroid Ryugu are similar to Ivuna-type carbonaceous meteorites. *Science* **379**, eabn7850 (2023). doi:10.1126/science.abn7850

24. T. Nakamura, M. Matsumoto, K. Amano, Y. Enokido, M. E. Zolensky, T. Mikouchi, H. Genda, S. Tanaka, M. Y. Zolotov, K. Kurosawa, S. Wakita, R. Hyodo, H. Nagano, D. Nakashima, Y. Takahashi, Y. Fujioka, M. Kikuiri, E. Kagawa, M. Matsuoka, A. J. Brearley, A. Tsuchiyama, M. Uesugi, J. Matsuno, Y. Kimura, M. Sato, R. E. Milliken, E. Tatsumi, S. Sugita, T. Hiroi, K. Kitazato, D. Brownlee, D. J. Joswiak, M. Takahashi, K. Ninomiya, T. Takahashi, T. Osawa, K. Terada, F. E. Brenker, B. J. Tkalcec, L. Vincze, R. Brunetto, A. Aléon-Toppani, Q. H. S. Chan, M. Roskosz, J.-C. Viennet, P. Beck, E. E. Alp, T. Michikami, Y. Nagaashi, T. Tsuji, Y. Ino, J. Martinez, J. Han, A. Dolocan, R. J. Bodnar, M. Tanaka, H. Yoshida, K. Sugiyama, A. J. King, K. Fukushi, H. Suga, S. Yamashita, T. Kawai, K. Inoue, A. Nakato, T. Noguchi, F. Vilas, A. R. Hendrix, C. Jaramillo-Correa, D. L. Domingue, G. Dominguez, Z. Gainsforth, C. Engrand, J. Duprat, S. S. Russell, E. Bonato, C. Ma, T. Kawamoto, T. Wada, S. Watanabe, R. Endo, S. Enju, L. Riu, S. Rubino, P. Tack, S. Takeshita, Y. Takeichi, A. Takeuchi, A. Takigawa, D. Takir, T. Tanigaki, A. Taniguchi, K. Tsukamoto, T. Yagi, S. Yamada, K. Yamamoto, Y. Yamashita, M. Yasutake, K. Uesugi, I. Umegaki, I. Chiu, T. Ishizaki, S. Okumura, E. Palomba, C. Pilorget, S. M. Potin, A. Alasli, S. Anada, Y. Araki, N. Sakatani, C. Schultz, O. Sekizawa, S. D. Sitzman, K. Sugiura, M. Sun, E. Dartois, E. De Pauw, Z. Dionnet, Z. Djouadi, G. Falkenberg, R. Fujita, T. Fukuma, I. R. Gearba, K. Hagiya, M. Y. Hu, T. Kato, T. Kawamura, M. Kimura, M. K. Kubo, F. Langenhorst, C. Lantz, B. Lavina, M. Lindner, J. Zhao, B. Vekemans, D. Baklouti, B. Bazi, F. Borondics, S. Nagasawa, G. Nishiyama, K. Nitta, J. Mathurin, T. Matsumoto, I. Mitsukawa, H. Miura, A. Miyake, Y. Miyake, H. Yurimoto, R. Okazaki, H. Yabuta, H. Naraoka, K. Sakamoto, S. Tachibana, H. C. Connolly Jr., D. S. Lauretta, M. Yoshitake, M. Yoshikawa, K. Yoshikawa, K. Yoshihara, Y. Yokota, K. Yogata, H. Yano, Y. Yamamoto, D. Yamamoto, M. Yamada,

T. Yamada, T. Yada, K. Wada, T. Usui, R. Tsukizaki, F. Terui, H. Takeuchi, Y. Takei, A. Iwamae, H. Soejima, K. Shirai, Y. Shimaki, H. Senshu, H. Sawada, T. Saiki, M. Ozaki, G. Ono, T. Okada, N. Ogawa, K. Ogawa, R. Noguchi, H. Noda, M. Nishimura, N. Namiki, S. Nakazawa, T. Morota, A. Miyazaki, A. Miura, Y. Mimasu, K. Matsumoto, K. Kumagai, T. Kouyama, S. Kikuchi, K. Kawahara, S. Kameda, T. Iwata, Y. Ishihara, M. Ishiguro, H. Ikeda, S. Hosoda, R. Honda, C. Honda, Y. Hitomi, N. Hirata, N. Hirata, T. Hayashi, M. Hayakawa, K. Hatakeda, S. Furuya, R. Fukai, A. Fujii, Y. Cho, M. Arakawa, M. Abe, S. Watanabe, Y. Tsuda, Formation and evolution of carbonaceous asteroid Ryugu: Direct evidence from returned samples. *Science* **379**, eabn8671 (2023). doi:10.1126/science.abn8671

25. M. Gounelle, M. E. Zolensky, The Orgueil meteorite: 150 years of history. *Meteorit. Planet. Sci.* **49**, 1769–1794 (2014). doi:10.1111/maps.12351

26. Y. Kebukawa, C. M. O'D. Alexander, G. D. Cody, Compositional diversity in insoluble organic matter in type 1, 2 and 3 chondrites as detected by infrared spectroscopy. *Geochim. Cosmochim. Acta* **75**, 3530–3541 (2011). doi:10.1016/j.gca.2011.03.037

27. F.-R. Orthous-Daunay, E. Quirico, P. Beck, O. Brissaud, E. Dartois, T. Pino, B. Schmitt, Mid-infrared study of the molecular structure variability of insoluble organic matter from primitive chondrites. *Icarus* **223**, 534–543 (2013). doi:10.1016/j.icarus.2013.01.003

28. C. Le Guillou, S. Bernard, A. J. Brearley, L. Remusat, Evolution of organic matter in Orgueil, Murchison and Renazzo during parent body aqueous alteration: In situ investigations. *Geochim. Cosmochim. Acta* **131**, 368–392 (2014). doi:10.1016/j.gca.2013.11.020

29. L. R. Nittler, R. M. Stroud, J. M. Trigo-Rodríguez, B. T. De Gregorio, C. M. O'D. Alexander, J. Davidson, C. E. Moyano-Cambero, S. Tanbakouei, A cometary building block in a primitive asteroidal meteorite. *Nat. Astron.* **3**, 659–666 (2019). doi:10.1038/s41550-019-0737-8

30. B. T. De Gregorio, R. M. Stroud, L. R. Nittler, C. M. O'D. Alexander, N. D. Bassim, G. D. Cody, A. L. D. Kilcoyne, S. A. Sandford, S. N. Milam, M. Nuevo, T. J. Zega, Isotopic and chemical variation of organic nanoglobules in primitive meteorites. *Meteorit. Planet. Sci.* **48**, 904–928 (2013). doi:10.1111/maps.12109

31. L. P. Keller, S. Messenger, G. J. Flynn, S. Clemett, S. Wirick, C. Jacobsen, The nature of molecular cloud material in interplanetary dust. *Geochim. Cosmochim. Acta* **68**, 2577–2589 (2004). doi:10.1016/j.gca.2003.10.044

32. B. T. De Gregorio, R. M. Stroud, L. R. Nittler, C. M. O'D. Alexander, A. L. D. Kilcoyne, T. J. Zega, Isotopic anomalies in organic nanoglobules from Comet 81P/Wild 2: Comparison to Murchison nanoglobules and isotopic anomalies induced in terrestrial organics by electron irradiation. *Geochim. Cosmochim. Acta* **74**, 4454–4470 (2010). doi:10.1016/j.gca.2010.05.010

33. T. Noguchi, H. Yabuta, S. Itoh, N. Sakamoto, T. Mitsunari, A. Okubo, R. Okazaki, T. Nakamura, S. Tachibana, K. Terada, M. Ebihara, N. Imae, M. Kimura, H. Nagahara, Variation of mineralogy and organic material during the early stages of aqueous activity recorded in Antarctic micrometeorites. *Geochim. Cosmochim. Acta* **208**, 119–144 (2017). doi:10.1016/j.gca.2017.03.034

34. L. A. J. Garvie, P. R. Buseck, Prebiotic carbon in clays from Orgueil and Ivuna (CI), and Tagish Lake (C2 ungrouped) meteorites. *Meteorit. Planet. Sci.* **42**, 2111–2117 (2007). doi:10.1111/j.1945-5100.2007.tb01011.x

35. G. D. Cody, C. M. O'D. Alexander, H. Yabuta, A. L. D. Kilcoyne, T. Araki, H. Ade, P. Dera, M. Fogel, B. Militzer, B. O. Mysen, Organic thermometry for chondritic parent bodies. *Earth Planet. Sci. Lett.* **272**, 446–455 (2008). doi:10.1016/j.epsl.2008.05.008

36. C. M. O'D. Alexander, G. D. Cody, B. T. De Gregorio, L. R. Nittler, R. M. Stroud, The nature, origin and modification of insoluble organic matter in chondrites, the major source of Earth's C and N. *Chem. Erde* **77**, 227–256 (2017). doi:10.1016/j.chemer.2017.01.007 Medline

37. D. D. Clayton, Origin of heavy xenon in meteoritic diamonds. *Astrophys. J.* **340**, 613–619 (1989). doi:10.1086/167422

38. Z. R. Dai, J. P. Bradley, D. J. Joswiak, D. E. Brownlee, H. G. M. Hill, M. J. Genge, Possible in situ formation of meteoritic nanodiamonds in the early Solar System. *Nature* **418**, 157–159 (2002). doi:10.1038/nature00897 Medline

39. K. Nakamura-Messenger, S. Messenger, L. P. Keller, S. J. Clemett, M. E. Zolensky, Organic globules in the Tagish Lake meteorite: Remnants of the protosolar disk. *Science* **314**, 1439–1442 (2006). doi:10.1126/science.1132175 Medline

40. T. Matsumoto, A. Tsuchiyama, K. Nakamura-Messenger, T. Nakano, K. Uesugi, A. Takeuchi, M. E. Zolensky, Three-dimensional observation and morphological analysis of organic nanoglobules in a carbonaceous chondrite using X-ray micro-tomography. *Geochim. Cosmochim. Acta* **116**, 84–95 (2013). doi:10.1016/j.gca.2012.05.007

41. M. Hashiguchi, S. Kobayashi, H. Yurimoto, In situ observation of D-rich carbonaceous globules embedded in NWA 801 CR2 chondrite. *Geochim. Cosmochim. Acta* **122**, 306–323 (2013). doi:10.1016/j.gca.2013.08.007

42. C. Le Guillou, A. Brearley, Relationships between organics, water and early stages of aqueous alteration in the pristine CR3.0 chondrite MET 00426. *Geochim. Cosmochim. Acta* **131**, 344–367 (2014). doi:10.1016/j.gca.2013.10.024

43. G. Matrajt, S. Messenger, D. Brownlee, D. Joswiak, Diverse forms of primordial organic matter identified in interplanetary dust particles. *Meteorit. Planet. Sci.* **47**, 525–549 (2012). doi:10.1111/j.1945-5100.2011.01310.x

44. H. Yabuta, T. Noguchi, S. Itoh, T. Nakamura, A. Miyake, S. Tsujimoto, N. Ohashi, N. Sakamoto, M. Hashiguchi, K.-I. Abe, A. Okubo, A. L. D. Kilcoyne, S. Tachibana, R. Okazaki, K. Terada, M. Ebihara, H. Nagahara, Formation of an ultracarbonaceous Antarctic micrometeorite through minimal aqueous alteration in a small porous icy body. *Geochim. Cosmochim. Acta* **214**, 172–190 (2017). doi:10.1016/j.gca.2017.06.047

45. C. M. O'D. Alexander, M. Fogel, H. Yabuta, G. D. Cody, The origin and evolution of chondrites recorded in the elemental and isotopic compositions of their macromolecular organic matter. *Geochim. Cosmochim. Acta* **71**, 4380–4403 (2007). doi:10.1016/j.gca.2007.06.052

46. L. Remusat, Y. Guan, Y. Wang, J. M. Eiler, Accretion and preservation of D-rich organic particles in carbonaceous chondrites: Evidence for important transport in the early Solar

System nebula. *Astrophys. J.* **713**, 1048–1058 (2010). doi:10.1088/0004-637X/713/2/1048

47. H. Naraoka, Y. Takano, J. P. Dworkin, Y. Oba, K. Hamase, A. Furusho, N. O. Ogawa, M. Hashiguchi, K. Fukushima, D. Aoki, P. Schmitt-Kopplin, J. C. Aponte, E. T. Parker, D. P. Glavin, H. L. McLain, J. E. Elsila, H. V. Graham, J. M. Eiler, F.-R. Orthous-Daunay, C. Wolters, J. Isa, V. Vuitton, R. Thissen, S. Sakai, T. Yoshimura, T. Koga, N. Ohkouchi, Y. Chikaraishi, H. Sugahara, H. Mita, Y. Furukawa, N. Hertkorn, A. Ruf, H. Yurimoto, T. Nakamura, T. Noguchi, R. Okazaki, H. Yabuta, K. Sakamoto, S. Tachibana, H. C. Connolly Jr., D. S. Lauretta, M. Abe, T. Yada, M. Nishimura, K. Yogata, A. Nakato, M. Yoshitake, A. Suzuki, A. Miyazaki, S. Furuya, K. Hatakeda, H. Soejima, Y. Hitomi, K. Kumagai, T. Usui, T. Hayashi, D. Yamamoto, R. Fukai, K. Kitazato, S. Sugita, N. Namiki, M. Arakawa, H. Ikeda, M. Ishiguro, N. Hirata, K. Wada, Y. Ishihara, R. Noguchi, T. Morota, N. Sakatani, K. Matsumoto, H. Senshu, R. Honda, E. Tatsumi, Y. Yokota, C. Honda, T. Michikami, M. Matsuoka, A. Miura, H. Noda, T. Yamada, K. Yoshihara, K. Kawahara, M. Ozaki, Y. Iijima, H. Yano, M. Hayakawa, T. Iwata, R. Tsukizaki, H. Sawada, S. Hosoda, K. Ogawa, C. Okamoto, N. Hirata, K. Shirai, Y. Shimaki, M. Yamada, T. Okada, Y. Yamamoto, H. Takeuchi, A. Fujii, Y. Takei, K. Yoshikawa, Y. Mimasu, G. Ono, N. Ogawa, S. Kikuchi, S. Nakazawa, F. Terui, S. Tanaka, T. Saiki, M. Yoshikawa, S. Watanabe, Y. Tsuda, Soluble organic molecules in samples of the carbonaceous asteroid (162173) Ryugu. *Science* **379**, eabn9033 (2023). doi:10.1126/science.abn9033

48. R. Okazaki, B. Marty, H. Busemann, K. Hashizume, J. D. Gilmour, A. Meshik, T. Yada, F. Kitajima, M. W. Broadley, D. Byrne, E. Füri, M. E. I. Riebe, D. Krietsch, C. Maden, A. Ishida, P. Clay, S. A. Crowther, L. Fawcett, T. Lawton, O. Pravdivtseva, Y. N. Miura, J. Park, K. Bajo, Y. Takano, K. Yamada, S. Kawagucci, Y. Matsui, M. Yamamoto, K. Righter, S. Sakai, N. Iwata, N. Shirai, S. Sekimoto, M. Inagaki, M. Ebihara, R. Yokochi, K. Nishiizumi, K. Nagao, J. I. Lee, A. Kano, M. W. Caffee, R. Uemura, T. Nakamura, H. Naraoka, T. Noguchi, H. Yabuta, H. Yurimoto, S. Tachibana, H. Sawada, K. Sakamoto, M. Abe, M. Arakawa, A. Fujii, M. Hayakawa, N. Hirata, N. Hirata, R. Honda, C. Honda, S. Hosoda, Y. Iijima, H. Ikeda, M. Ishiguro, Y. Ishihara, T. Iwata, K. Kawahara, S. Kikuchi, K. Kitazato, K. Matsumoto, M. Matsuoka, T. Michikami, Y. Mimasu, A. Miura, T. Morota, S. Nakazawa, N. Namiki, H. Noda, R. Noguchi, N. Ogawa, K. Ogawa, T. Okada, C. Okamoto, G. Ono, M. Ozaki, T. Saiki, N. Sakatani, H. Senshu, Y. Shimaki, K. Shirai, S. Sugita, Y. Takei, H. Takeuchi, S. Tanaka, E. Tatsumi, F. Terui, R. Tsukizaki, K. Wada, M. Yamada, T. Yamada, Y. Yamamoto, H. Yano, Y. Yokota, K. Yoshihara, M. Yoshikawa, K. Yoshikawa, S. Furuya, K. Hatakeda, T. Hayashi, Y. Hitomi, K. Kumagai, A. Miyazaki, A. Nakato, M. Nishimura, H. Soejima, A. Iwamae, D. Yamamoto, K. Yogata, M. Yoshitake, R. Fukai, T. Usui, H. C. Connolly Jr., D. Lauretta, S. Watanabe, Y. Tsuda, Noble gases and nitrogen in samples of asteroid Ryugu record its volatile sources and recent surface evolution. *Science* **379**, eabo0431 (2023). doi:10.1126/science.abo0431

49. J. F. Kerridge, Carbon, hydrogen and nitrogen in carbonaceous chondrites: Abundances and isotopic compositions in bulk samples. *Geochim. Cosmochim. Acta* **49**, 1707–1714 (1985). doi:10.1016/0016-7037(85)90141-3 Medline

50. L. R. Nittler, C. M. O'D. Alexander, M. J. Verdier-Paoletti, paper presented at the 84th Annual Meeting of the Meteoritical Society, Chicago, IL, 15 to 21 August 2021.

51. Y. Aikawa, G. J. van Zadelhoff, E. F. van Dishoeck, E. Herbst, Warm molecular layers in protoplanetary disks. *Astron. Astrophys.* **386**, 622–632 (2002). doi:10.1051/0004-6361:20020037

52. N. Watanabe, A. Kouchi, Ice surface reactions: A key to chemical evolution in space. *Prog. Surf. Sci.* **83**, 439–489 (2008). doi:10.1016/j.progsurf.2008.10.001

53. J. Aléon, Multiple origins of nitrogen isotopic anomalies in meteorites and comets. *Astrophys. J.* **722**, 1342–1351 (2010). doi:10.1088/0004-637X/722/2/1342

54. R. Terzieva, E. Herbst, The possibility of nitrogen isotopic fractionation in interstellar clouds. *Mon. Not. R. Astron. Soc.* **317**, 563–568 (2000). doi:10.1046/j.1365-8711.2000.03618.x

55. E. K. Zinner, in *Meteorites, Comets, and Planets*, A. M. Davis, Ed. (Elsevier, 2005), pp. 17–39.

56. H. Busemann, A. F. Young, C. M. O'D. Alexander, P. Hoppe, S. Mukhopadhyay, L. R. Nittler, Interstellar chemistry recorded in organic matter from primitive meteorites. *Science* **312**, 727–730 (2006). doi:10.1126/science.1123878 Medline

57. L. Remusat, J.-Y. Bonnet, S. Bernard, A. Buch, E. Quirico, Molecular and isotopic behavior of insoluble organic matter of the Orgueil meteorite upon heating. *Geochim. Cosmochim. Acta* **263**, 235–247 (2019). doi:10.1016/j.gca.2019.07.013

58. C. Floss, F. Stadermann, Auger nanoprobe analysis of presolar ferromagnesian silicate grains from primitive CR chondrites QUE 99177 and MET 00426. *Geochim. Cosmochim. Acta* **73**, 2415–2440 (2009). doi:10.1016/j.gca.2009.01.033

59. C. Vollmer, J. Leitner, D. Kepaptsoglou, Q. M. Ramasse, A. J. King, P. F. Schofield, A. Bischoff, T. Araki, P. Hoppe, A primordial ^{15}N-depleted organic component detected within the carbonaceous chondrite Maribo. *Sci. Rep.* **10**, 20251 (2020). doi:10.1038/s41598-020-77190-z Medline

60. T. Hiroi, M. E. Zolensky, C. M. Pieters, The Tagish Lake meteorite: A possible sample from a D-type asteroid. *Science* **293**, 2234–2236 (2001). doi:10.1126/science.1063734 Medline

61. C. D. K. Herd, A. Blinova, D. N. Simkus, Y. Huang, R. Tarozo, C. M. O'D. Alexander, F. Gyngard, L. R. Nittler, G. D. Cody, M. L. Fogel, Y. Kebukawa, A. L. D. Kilcoyne, R. W. Hilts, G. F. Slater, D. P. Glavin, J. P. Dworkin, M. P. Callahan, J. E. Elsila, B. T. De Gregorio, R. M. Stroud, Origin and evolution of prebiotic organic matter as inferred from the Tagish Lake meteorite. *Science* **332**, 1304–1307 (2011). doi:10.1126/science.1203290 Medline

62. C. M. Gilmour, C. D. K. Herd, P. Beck, Water abundance in the Tagish Lake meteorite from TGA and IR spectroscopy: Evaluation of aqueous alteration. *Meteorit. Planet. Sci.* **54**, 1951–1972 (2019). doi:10.1111/maps.13362

63. A. Gardinier, S. Derenne, F. Robert, F. Behar, C. Largeau, J. Maquet, Solid state CP/MAS ^{13}C NMR of the insoluble organic matter of the Orgueil and Murchison meteorites: Quantitative study. *Earth Planet. Sci. Lett.* **184**, 9–21 (2000). doi:10.1016/S0012-821X(00)00300-9

64. G. D. Cody, C. M. O'D. Alexander, F. Tera, Solid-state (^{1}H and ^{13}C) nuclear magnetic resonance spectroscopy of insoluble organic residue in the Murchison meteorite: A self-

consistent quantitative analysis. *Geochim. Cosmochim. Acta* **66**, 1851–1865 (2002). doi:10.1016/S0016-7037(01)00888-2

65. H. Yabuta, L. B. Williams, G. D. Cody, C. M. O'D. Alexander, S. Pizzarello, The insoluble carbonaceous material of CM chondrites: A possible source of discrete organic compounds under hydrothermal conditions. *Meteorit. Planet. Sci.* **42**, 37–48 (2007). doi:10.1111/j.1945-5100.2007.tb00216.x

66. V. Vinogradoff, C. Le Guillou, S. Bernard, L. Binet, P. Cartigny, A. J. Brearley, L. Remusat, Paris vs. Murchison: Impact of hydrothermal alteration on organic matter in CM chondrites. *Geochim. Cosmochim. Acta* **212**, 234–252 (2017). doi:10.1016/j.gca.2017.06.009

67. Y. Oba, H. Naraoka, Elemental and isotope behavior of macromolecular organic matter from CM chondrites during hydrous pyrolysis. *Meteorit. Planet. Sci.* **44**, 943–953 (2009). doi:10.1111/j.1945-5100.2009.tb00779.x

68. S. Messenger, Identification of molecular-cloud material in interplanetary dust particles. *Nature* **404**, 968–971 (2000). doi:10.1038/35010053 Medline

69. J. Duprat, E. Dobrică, C. Engrand, J. Aléon, Y. Marrocchi, S. Mostefaoui, A. Meibom, H. Leroux, J.-N. Rouzaud, M. Gounelle, F. Robert, Extreme deuterium excesses in ultracarbonaceous micrometeorites from central Antarctic snow. *Science* **328**, 742–745 (2010). doi:10.1126/science.1184832 Medline

70. G. D. Cody, H. Ade, C. M. O'D. Alexander, T. Araki, A. Butterworth, H. Fleckenstein, G. Flynn, M. K. Gilles, C. Jacobsen, A. L. D. Kilcoyne, K. Messenger, S. A. Sandford, T. Tyliszczak, A. J. Westphal, S. Wirick, H. Yabuta, Quantitative organic and light-element analysis of comet 81P/Wild 2 particles using C-, N-, and O-μ-XANES. *Meteorit. Planet. Sci.* **43**, 353–365 (2008). doi:10.1111/j.1945-5100.2008.tb00627.x

71. E. Dartois, C. Engrand, R. Brunetto, J. Duprat, T. Pino, E. Quirico, L. Remusat, N. Bardin, G. Briani, S. Mostefaoui, G. Morinaud, B. Crane, N. Szwec, L. Delauche, F. Jamme, Ch. Sandt, P. Dumas, Ultracarbonaceous Antarctic micrometeorites, probing the Solar System beyond the nitrogen snow-line. *Icarus* **224**, 243–252 (2013). doi:10.1016/j.icarus.2013.03.002

72. N. Fray, A. Bardyn, H. Cottin, D. Baklouti, C. Briois, C. Engrand, H. Fischer, K. Hornung, R. Isnard, Y. Langevin, H. Lehto, L. Le Roy, E. M. Mellado, S. Merouane, P. Modica, F.-R. Orthous-Daunay, J. Paquette, J. Rynö, R. Schulz, J. Silén, S. Siljeström, O. Stenzel, L. Thirkell, K. Varmuza, B. Zaprudin, J. Kissel, M. Hilchenbach, Nitrogen-to-carbon atomic ratio measured by COSIMA in the particles of comet 67P/Churyumov–Gerasimenko. *Mon. Not. R. Astron. Soc.* **469**, S506–S516 (2017). doi:10.1093/mnras/stx2002

73. K. Lodders, in *Principles and Perspectives in Cosmochemistry*, A. Goswami, B. E. Reddy, Eds. (Springer, 2010), pp. 379–417.

74. O. Poch, I. Istiqomah, E. Quirico, P. Beck, B. Schmitt, P. Theulé, A. Faure, P. Hily-Blant, L. Bonal, A. Raponi, M. Ciarniello, B. Rousseau, S. Potin, O. Brissaud, L. Flandinet, G. Filacchione, A. Pommerol, N. Thomas, D. Kappel, V. Mennella, L. Moroz, V. Vinogradoff, G. Arnold, S. Erard, D. Bockelée-Morvan, C. Leyrat, F. Capaccioni, M. C. De Sanctis, A. Longobardo, F. Mancarella, E. Palomba, F. Tosi, Ammonium salts are a

reservoir of nitrogen on a cometary nucleus and possibly on some asteroids. *Science* **367**, eaaw7462 (2020). doi:10.1126/science.aaw7462 Medline

75. K. Altwegg, H. Balsiger, N. Hänni, M. Rubin, M. Schuhmann, I. Schroeder, T. Sémon, S. Wampfler, J.-J. Berthelier, C. Briois, M. Combi, T. I. Gombosi, H. Cottin, J. De Keyser, F. Dhooghe, B. Fiethe, S. A. Fuselier, Evidence of ammonium salts in comet 67P as explanation for the nitrogen depletion in cometary comae. *Nat. Astron.* **4**, 533–540 (2020). doi:10.1038/s41550-019-0991-9

76. H. Naraoka, H. Mita, M. Komiya, S. Yoneda, H. Kojima, A. Shimoyama, A chemical sequence of macromolecular organic matter in the CM chondrites. *Meteorit. Planet. Sci.* **39**, 401–406 (2004). doi:10.1111/j.1945-5100.2004.tb00101.x

77. N. D. Bassim, B. T. De Gregorio, A. L. D. Kilcoyne, K. Scott, T. Chou, S. Wirick, G. Cody, R. M. Stroud, Minimizing damage during FIB sample preparation of soft materials. *J. Microsc.* **245**, 288–301 (2012). doi:10.1111/j.1365-2818.2011.03570.x

78. Y. Takeichi, N. Inami, H. Suga, C. Miyamoto, T. Ueno, K. Mase, Y. Takahashi, K. Ono, Design and performance of a compact scanning transmission X-ray microscope at the Photon Factory. *Rev. Sci. Instrum.* **87**, 013704 (2016). doi:10.1063/1.4940409 Medline

79. A. P. Hitchcock, aXis 2000 - Analysis of X-ray Images and Spectra (2023); http://unicorn.mcmaster.ca/aXis2000.html.

80. M. Lerotic, R. Mak, S. Wirick, F. Meirer, C. Jacobsen, *MANTiS*: A program for the analysis of X-ray spectromicroscopy data. *J. Synchrotron Rad.* **21**, 1206–1212 (2014). doi:10.1107/S1600577514013964 Medline

81. J. Mathurin, E. Dartois, T. Pino, C. Engrand, J. Duprat, A. Deniset-Besseau, F. Borondics, C. Sandt, A. Dazzi, Nanometre-scale infrared chemical imaging of organic matter in ultra-carbonaceous Antarctic micrometeorites (UCAMMs). *Astron. Astrophys.* **622**, A160 (2019). doi:10.1051/0004-6361/201833957

82. A. Thomen, F. Robert, L. Remusat, Determination of the nitrogen abundance in organic materials by NanoSIMS quantitative imaging. *J. Anal. At. Spectrom.* **29**, 512–519 (2014). doi:10.1039/c3ja50313e

83. L. Nittler, L'image: Larry's Image Program; https://sites.google.com/carnegiescience.edu/limagesoftware/.

84. J. Davidson, H. Busemann, L. R. Nittler, C. M. Alexander, F.-R. Orthous-Daunay, I. A. Franchi, P. Hoppe, Abundances of presolar silicon carbide grains in primitive meteorites determined by NanoSIMS. *Geochim. Cosmochim. Acta* **139**, 248–266 (2014). doi:10.1016/j.gca.2014.04.026

85. C. M. O'D. Alexander, R. Bowden, M. L. Fogel, K. T. Howard, C. D. K. Herd, L. R. Nittler, The provenances of asteroids, and their contributions to the volatile inventories of the terrestrial planets. *Science* **337**, 721–723 (2012). doi:10.1126/science.1223474 Medline